Towards Material Modelling within Continuum-Atomistics

vom Fachbereich Maschinenbau und Verfahrenstechnik
der Technischen Universität Kaiserslautern
zur Verleihung des akademischen Grades
Doktor-Ingenieur (Dr.-Ing.)
genehmigte Dissertation

von
M.Sc. Tadesse Abdi

Hauptreferent: Prof. Dr.-Ing. P. Steinmann
Korreferent: JP Dr.-Ing E. Kuhl
Vorsitznder: Prof. Dr.-Ing. habil. D. Eifler

Dekan: Prof. Dr.-Ing. J. C. Aurich

Tag der Einreichung: 28.10.2005
Tag der mündl. Prüfung: 26.05.2006

Kaiserslautern, Mai 2006

D 386

Abstract

Synopsis: With the burgeoning computing power available, multiscale modelling and simulation has these days become increasingly capable of capturing the details of physical processes on different scales. The mechanical behavior of solids is oftentimes the result of interaction between multiple spatial and temporal scales at different levels and hence it is a typical phenomena of interest exhibiting multiscale characteristic. At the most basic level, properties of solids can be attributed to atomic interactions and crystal structure that can be described on nano scale. Mechanical properties at the macro scale are modeled using continuum mechanics for which we mention stresses and strains. Continuum models, however they offer an efficient way of studying material properties they are not accurate enough and lack microstructural information behind the microscopic mechanics that cause the material to behave in a way it does. Atomistic models are concerned with phenomenon at the level of lattice thereby allowing investigation of detailed crystalline and defect structures, and yet the length scales of interest are inevitably far beyond the reach of full atomistic computation and is prohibitively expensive. This makes it necessary the need for multiscale models. The bottom line and a possible avenue to this end is, coupling different length scales, the continuum and the atomistics in accordance with standard procedures. This is done by recourse to the Cauchy-Born rule and in so doing, we aim at a model that is efficient and reasonably accurate in mimicking physical behaviors observed in nature or laboratory.

In this work, we focus on concurrent coupling based on energetic formulations that links the continuum to atomistics. At the atomic scale, we describe deformation of the solid by the displaced positions of atoms that make up the solid and at the continuum level deformation of the solid is described by the displacement field that minimize the total energy. In the coupled model, continuum-atomistic, a continuum formulation is retained as the overall framework of the problem and the atomistic feature is introduced by way of constitutive description, with the Cauchy-Born rule establishing the point of contact. The entire formulation is made in the framework of nonlinear elasticity and all the simulations are carried out within the confines of quasistatic settings. The model gives direct account to measurable features of microstructures developed by crystals through sequential lamination.

Key words: Cauchy-Born rule, ellipticity, hexagonal lattice, material force, microstructure, morphology, rank-one convexity, relaxation, sequential laminate, stability

Zusammenfassung

Mit den heute zur Verfügung stehenden Rechenleistungen ist die Multiskalen-Modellierung und -Berechnung zunehmend in der Lage, detailliert physikalische Prozesse zu simulieren. Das mechanische Verhalten von Festkörpern ist häufig das Ergebnis der Interaktion zwischen vielfachen räumlichen und zeitlichen Skalen auf verschiedenen Stufen und demzufolge ein typisches Phänomen mit Multiskalen-Character. Auf der elementaren Stufe, der Nano-Skala können die Eigenschaften von Festkörpern anhand der atomistischen Wechselwirkung und ihrer Kristallstruktur beschrieben werden. Die mechanischen Eigenschaften auf der Makro-Skala werden oftmals mit Hilfe der Kontinuumsmechanik modelliert. Obwohl Kontinuum-Modelle ein effizienter Weg zur Untersuchung von Materialeigenschaften sind, weisen sie jedoch oftmals eine unzureichende Genauigkeit und einen Mangel an mikrostrukturellen Informationen über die mikroskopische Mechanik auf. Atomistische Modelle andererseits ermöglichen die detaillierte Untersuchung der Kristall- und Defektstruktur. Dennoch sind die Längenskalen, die von Interesse sind, immer noch weit entfernt von den Möglichkeiten einer komplett atomistischen Berechnung und machen diese unerschwinglich teuer. Somit besteht der Bedarf für Multiskalen-Modelle. Die Schlußfolgerung und ein möglicher Zugang zu diesem Ziel ist die Kopplung verschiedener Längenskalen, der kontinuums- und atomistischen Skala, in Übereinstimmung mit Standardverfahren. Mit Zurhilfenahme der Cauchy-Born Regel zielen wir auf ein Modell ab, welches effizient und genügend genau in der Simulation des in der Natur oder im Labor betrachteten physikalischen Verhaltens ist.

In dieser Arbeit konzentrieren wir uns auf eine simultane Kopplung der Kontinuums- mit der atomistischen Formulierung basierend auf energetischen Formulierungen. Auf der atomistischen Skala beschreiben wir die Deformation des Körpers anhand der (verschobenen) Positionen der Atome, die diesen Festkörper bilden. Auf der Kontinuumsebene wird die Deformation des Festkörpers durch den Verschiebungsvektor, der die gesamte freie Energie minimiert, beschrieben. In dem gekoppelten Kontinuum-atomistischen Modell wird eine Kontinuumsformulierung als allgemeiner Rahmen beibehalten. Das atomistische Characteristikum des Modells wird einbezogen mittels einer konstitutiven Beschreibung, wobei die Cauchy-Born Regel als Schnittstelle dient. Die gesamte Formulierung wurde im Rahmen nichtlinearer Elastizität gemacht, wobei quasistatische Zustände angenommen wurden. Das Modell liefert messbare Eigenschaften von Mikrostrukturen, wie sie bei Kristallen durch sequentielle Lamination entstehen.

Acknowledgment

A complete list of every person that has contributed to my understanding of the subject of this work is long. The acquaintances I have made, the discussions I have had with the members of Applied Mechanics have been inspirational and have helped me enormously to have a better insight into the problems and further develop my ideas. I am grateful for having been given the opportunity to experience the conducive atmosphere at the Chair of Applied Mechanics, University of Kaiserslautern. Best words can not express my sincere gratitude to my supervisor Prof. Steinmann, not only for introducing me to continuum mechanics but also for his never ending patience, inspiring advises all the way and above all his relentless support over the years.

Last but not least, it gives me pleasure to thank JP. Kuhl for all her suggestions, reading patiently a continuous stream of drafts and moreover for several hours of joyful discussions and useful ideas.

Contents

Notation

φ	Nonlinear deformation map
$\boldsymbol{F}$	Deformation gradient
$\mathscr{W}_o$	Strain energy density per unit reference volume
$\boldsymbol{Q}$	Proper orthogonal tensor
$SO(n)$	Group of proper orthogonal tensors
$\mathscr{I}$	Energy functional
$\{\varphi_k\}_{k\in\mathbb{N}}$	Sequence of admissible deformations
$\mathcal{B}_0$	Reference configuration
$\partial\mathcal{B}_0$	Reference boundary
$\boldsymbol{K}$	Zero set of energy density

$\mathcal{B}_t$	Current configuration
$\boldsymbol{I}$	Identity tensor
$\boldsymbol{E}_i$	Cartesian basis vector in the reference configuration
$\boldsymbol{e}_i$	Cartesian basis vector in the current configuration
$\mathscr{W}_t$	Strain energy density per unit current volume
$\boldsymbol{X}$	Reference placement
$\boldsymbol{x}$	Current placement
$\boldsymbol{C}$	Left Cauchy-Green deformation tensor
$\boldsymbol{b}$	Distributed body force field per unit mass
$\boldsymbol{\Pi}^t$	First Piola-Kirchhoff stress tensor
ϵ, δ	Parameters of Lennard Jones potential
$\boldsymbol{\sigma}$	Cauchy stress tensor
ρ_0	Reference mass density
ρ	Current mass density
$\boldsymbol{t}$	Surface traction
$\mathscr{A}$	Space of admissible deformations
$\boldsymbol{f}_i^{ext}$	External load on atom i
$d\boldsymbol{X}$	Material line element
$d\boldsymbol{x}$	Spatial line element
dV	Reference volume element
$d\boldsymbol{v}$	Current volume element

ϕ_k	k-atom interaction
E^{int}	Total internal energy
E_i	Energy contribution of site r_i
$\boldsymbol{R}_i$	Reference site
$\boldsymbol{r}_i$	Current site
Ω	Two dimensional domain
$\mathfrak{B}_0$	Finite lattice in reference configuration
r_0	Lattice constant
$\boldsymbol{f}_i$	Net force acting on atom i.
$\boldsymbol{f}_{ij}$	Force on atom i due to interaction with atom j
$\boldsymbol{k}_{ij}$	Atomic level stiffness
E^{tot}	Total energy
$\boldsymbol{u}_i$	Displacement of atom i
$\mathcal{L}$	Set of all lattice sites
$\mathcal{L}_0$	Set of bulk lattice sites

$\boldsymbol{n}$	Unit normal vector in the current configuration
$\boldsymbol{N}$	Unit normal vector in the reference configuration
da	Area element in the current configuration
dA	Area element in the reference configuration
$\mathbb{L}$	Tangent operator
$\mathbb{M}_+^{n \times n}$	Set of orientation preserving tensors of order-n
$\boldsymbol{U}$	Right stretch tensor
$\boldsymbol{q}$	Acoustic tensor
$\boldsymbol{a}$	Amplitude of deformation jump
$\mathcal{G}_n$	Generation of level-n laminate
δ_{ij}	Kronecker delta
$\mathscr{W}_0^Q$	Quasiconvex envelop of $\mathscr{W}_0$
$\mathscr{W}_0^R$	Rank-one convex envelop of $\mathscr{W}_0$
K^{qh}	Quasiconvex hull of K
K^{rh}	Rank-one convex hull of K
ξ	Volume fraction
ξ_i	Local volume fraction
ν_i	Global volume fraction

$\mathfrak{f}_{ij}$	Spatial interaction force
$\boldsymbol{\mathfrak{F}}_{ij}$	Material interaction force
$\boldsymbol{\pi}^t$	Material two-point stress tensor
$\boldsymbol{\Sigma}^t$	Eshelby stress tensor
J	Determinant of deformation gradient

Introduction

Several computational problems in engineering and materials science exhibit predominantly multi-scale behaviors. Examples of practical interest cover crack propagation(e.g. see Fischer et al.(1997) or Rafii-Tabar et al.(1998)), structural analysis of composite materials and crystalline microstructures. Composite materials are generally known to exhibit different behaviors over a range of length scales, consequently the development of modelling techniques for the prediction of the response of such materials to different states of stress and loading conditions goes as far deep a level to the nano-scale.

Why do crystalline materials fracture ? What happens to a crystalline material with initial crack when subjected to external loading ? A comprehensive answer to these deceptively simple questions requires knowledge and understanding of what is happening down to the atomic level. Indeed, one needs to take into account the mechanics of atoms in the material. At the atomic scale empirical potentials are used to describe the interactions between atoms. Furthermore, molecular dynamics which gained popularity in material science research is used to investigate the dynamics of atomic level phenomena that subsumes bond stretching and bond-angle bending. Continuum level(macro-scale) modelling usually applies statistical mechanics to the system as a whole and neglects emphasis on details of the way individual atom behaves, as a result, the corresponding atomistic level computation adheres to quasistatic settings.

Generally, the performance or failure of materials is affected by the mechanics of events at different levels that usually extend down to the atomic scale, hence, some of the problems that deal with material properties are inherently multiscale and therefore inevitably involve processes too complex that one can not describe on a single scale. Consequently, modelling and simulation of material behavior is oftentimes carried out at multiple scales thereby making concurrent simulation necessary. A prototype of such multiscale problems, crack propagation requires integrated simulation of multiple parts at a time. On the one hand, models on the continuum scale are generally known to be efficient but lack accuracy where this drawback arises from the fact that all properties of materials on this scale are described by a constitutive law, usually representing an average behavior of the material as a result of which some specific information on finer scales such as details on an atomic scale is lost. For instance modelling plasticity in this context leads

to representation of the collective action of many dislocations and failure, thereby ignoring the details of individual dislocation interactions. On the other hand, atomistic scale models even if they are accurate in capturing fine-scale features they are computationally not affordable. Insofar as the interatomic force laws accurately describe and appropriately applied to a real material one may conclude that the precise description of material behavior comes from the atomistic models. However, fully atomistic simulation in which each and every atom is explicitly involved and laws of interatomic forces are considered is computationally expensive to be used to model the entire system no matter how essential it might be for capturing the finer scale process in the problem. In recognition of this apparent limitation, the field of multiscale materials modelling whereby atomistic modelling(finer scale model) is used in conjunction with larger scale models and that helps deal with problems over a range of scales has attracted significant attention (for more on this see Arroyo et al.(2002) Broughoton et al.(1999) Dudo et al.(2000) Ghoniem et al.(2003) Friesecke et al.(2000) Hadjiconstantinou(1999) or Kadau et al.(1999, 2002)). For a general model geometry and given boundary conditions, solution of the continuum equations, i.e. the underlying boundary value problem is tackled numerically using approaches such as the finite element method (FEM). For a specific problem and relevant example see e.g. Arnold(2002) Shenoy et al.(1999) Shu et al.(1999) or Gobbert et al.(1999).

Hybrid models directly linking atomistic features to continuum finite element regions have been developed by several people, Tadmor et al.(1996,1999) Sunyk, Steinmann(2001, 2002) . In general, multiscale(continuum-atomistic) computational modelling aims at bridging the scales between atomistic and continuum models. The main mathematical issue in relating continuum models to atomistic systems rests on identifying the appropriate averaging techniques to obtain effective properties at the dominant scales. This marks the point where the Cauchy-Born rule comes into play. In the description of material behavior on continuum scale, one is working with continuum field averages among which one speaks of internal energy, stress, strain etc. Thus, in the framework of continuum the solid is considered as a continuous medium with average properties, where in this average description of material properties every mathematical point in the solid is regarded as a material particle representing a finite sized region on the smaller scales e.g. microscale (Tadmor et al.(1996)). The material property is subsumed into the model through phenomenological constitutive law relating the response of the continuum on a pointwise basis to the local deformation. In view of this, the use of atomistically derived constitutive relations has the advantage of lending the model all the relevant symmetries. The crystal is free to assume any configuration rendered by equilibrium and the resulting structural stability is subject to the fact that particular structures have bond lengths that take advantage of minima in the strain energy density. One of the central missions in the coupled model is to find out the relation between atomistic and continuum perspectives. It is of interest to further examine the correspondence between kinematic notions such as the deformation gradient and the conventional ideas from crystallography where one possible point of contact between these two sets of ideas is provided by the Cauchy-Born rule (Ericksen(1984, 1986)). This rule which mainly serves as a gateway for bringing atomistic features into the realm of continuum basically enables the coupled model deal with problems over range of length scales.

Continuum-atomistic method however it permits the analysis of problems requiring simultaneous resolution of continuum and atomistic features and the associated deformation process, a common difficulty in this field of hybrid modelling is an appropriate description of the transition between atomistic(lattice) and the continuum. Indeed, this problem emanates from the difference in the nature of internal forces that act in the two regions(Kohlhoff et al.(1991)). To be specific, if we consider a fracture mechanics problem and pick the case of crack propagation(a typical example of multiscale system), in order for the crack to grow atomic bonds at the crack tip must be broken and the bond breaking event is obviously followed by a significant deformation of the lattice. In general, in regions surrounding the crack some bonds are totally destroyed and some significantly deformed but not to the extent of debonding. Due to this bond breaking and distortion that is prevalent in the immediate neighborhood of the crack, this regions are dominated by atomistic physics at the nano-scale. Thus, lights that are gleamed from atomistic investigations provide information of paramount significance that give insight into the phenomena controlled by lattice effects. Far from the crack even if the lattice is relatively less deformed, the strain fields persist for longer distances and hence the system is governed by continuum mechanics. In view of this therefore, the continuum-atomistic approach has a viable siginificance for the detailed understanding of the evolution of crack in crystalline solids, see e.g. Kohlhoff et al.(1991) Ortiz, Philips(1999) or Klein, Gao(1998) for examples and further details.

When solids are subjected to deformation, one can observe a structural change in the underlying crystal lattice. For instance, an arrangement of atoms in a highly structured lattice consisting of cubes may change into a tetragonal phase with less symmetry (see Luskin(1997) for details). Such a mechanism leads to the formation of microstructure where different variants of the less symmetric phase occur at the same time on a very small scale (Bartels(2004)) . Continuum models explaining such microstructures as the mixture of these symmetry related states on a fine scale to minimize energy have been studied by a number of people (e.g. Kružík(2003), Lambrecht et al.(1998), Li et al.(1998) or Pedregal(1993)) whereby interesting phenomena like laminate, branching structures etc were observed. A model for the description of such properties has been set out by Ball, James(1987) and Ball(1977). Essentially, the model consists of optimization of an energy functional resulting from nonconvex stored energy density over a space of suitable deformations, often called nonconvex variational problem. The invariance of the energy density with respect to symmetry related states implies that the elastic energy density is nonconvex and must have multiple energy wells. Thus, for various boundary conditions and/or for different external potentials, the gradient of energy minimizing sequence of deformations inevitably oscillate between the energy wells available at its disposal so as to allow the energy get close to the lowest possible value. This naturally paves a way for the material to develop microstructures. A simple and common example of such a microstructure is a laminate in which the deformation gradient oscillates in parallel layers between two homogeneous states.

Microstructure as a feature of crystals with multiple symmetry related energy minimizing states and its importance in the study of materials is known for so long, e.g. *"the austenite-martensite transformation in single crystals is named in honor of the metallurgists Adolf Martens (1850-1914)*

and Sir William Chandler Roberts-Austen (1843-1902)"(Dolzmann(2005)). Elastic properties of a continuum can considerably be affected by the occurrence of different phases at the same time. Modelling materials with multiple phases within the confines of nonlinear elasticity usually involves minimizing the elastic stored energy functional on a class of admissible deformations subject to a given boundary data (see Ball et al.(1987) or Chipot et al.(1988) for an overview). Since symmetry of the underlying lattice is manifested directly through the elastic stored energy density, $\mathscr{W}_0$ can not be convex. Consequently, the convexity condition as required in the direct methods of the calculus of variation is violated. Hence, we can not employ the general theory to investigate existence and uniqueness or explore the degree of regularity of solutions. *'The pioneering work of Morrey established the crucial connection between lower semicontinuity of functionals on Sobolev spaces and quasiconvexity of the integrand'*(Dolzmann(2005)). Roughly speaking, quasiconvexity is sufficient for stability of affine deformations. In other words, if we determine the optimal configuration rendering minimum value of the energy functional by utilizing affine boundary conditions, then such a minimizer is an absolute minimizer.

Quasiconvexity which is an important condition in the calculus of variations has its own demerits. Basically, there are fewer examples of quasiconvex functions to deal with evolving real world problems and furthermore, there are variational problems that can not be analyzed by appeal to the direct method in the calculus of variations that is based on weak lower semicontinuity of the functional, e.g. model problems describing phase transforming materials. A suitable way of analyzing such problems is by considering the largest lower semicontinuous functional that does not exceed the given functional $\mathscr{J}$ and which results from substitution of $\mathscr{W}_0$ by its quasiconvex envelop $\mathscr{W}_0^Q$. This envelop is the largest quasiconvex function just below $\mathscr{W}_0$ and it represents the average energy of the system. Under this circumstance, the material is free to form a microstructure that results in minimum energy state. A prototype of this is relaxation of the minimum of two quadratic energies that was suggested by Kohn(1991)(for further discussion on double well problem see e.g. Carstensen et al.(1997) Dolzmann, Müller(1995) or Gobbert et al.(1999)). In many situations instead of quasiconvexity the stronger condition polyconvexity or the weaker condition rank-one convexity is employed. In this work rank-one convexity is given emphasis and is treated in chapter 4.

Outline of the study

Multiscale modelling of material behavior in general and the framework of continuum-atomistic in particular is well-known. Associated with energy minimization, in some cases change of the external potential leads to significant change in the nature of solution of the whole problem. In particular existence and uniqueness is affected by external potential that may result in an oscillatory behavior of the minimizer whereby the minimizing deformation oscillates between some fixed values, chapter 1 addresses this oscillatory behavior. We then reiterate briefly some of the basic concepts and formulations of boundary value problems that constitute benchmark problems in chapter 2. We commence this chapter by refreshing essentials of atomistic modelling followed

4

by review of continuum modelling of a hyperelastic continua and then visit the coupling as based on the Cauchy-Born rule. We then proceed to numerical examples whereby we employ the model to study a fracture mechanics phenomena with emphasis on the Cauchy-Born rule as a bridge establishing the link between atomistics and continuum.

In chapter 3 we deal with the Cauchy-Born rule in some detail, especially we employ this rule to investigate the response of a crystal lattice subjected to affine deformation on the boundary and thereby test the validity and failure of the rule. In this part, the behavior of equilibrium energy per volume of a finite lattice for increasing system size is studied in the context of lattice statics. A hexagonal lattice model was considered in which the hexagonal unit cell is used to characterize the switching from the Lennard Jones interaction potential to Harmonic potential. Furthermore, using the Cauchy-Born rule in conjunction with the virial stress we compute the stress at the atomic level and compare the result with the established results at a point of a continuum.

On the one hand, minimization of energy functional with non-convex density leads to non-convex variational problems and hence to the appearance of multiple phases associated with different equilibrium states of stored energy in an attempt to achieve the lowest energy possible. On the other hand, phase transition in crystalline solids is accompanied by the development of fine inner structures(microstructures) involving mixtures of phases and the study of these mixtures is usually handled through the minimization of stored energy. Thus, chapter 4 is meant to give a significant account of energy minimization and a procedure that captures the lowest energy density attainable by the material through sequential lamination, i.e. rank-one convexification is discussed. In chapter 5 we see material force method in the context of continuum-atomistics, practically we consider fracture mechanics problems, crack extension and morphology of a void. We give a continuum-atomistic formulation of the relevant problem and close this chapter with finite element implementation of the prototype examples. Finally, chapter 6 sums-up the overall work and closes with discussion.

CHAPTER 1

Motivation

Non-convex variational problems require, in general, a relaxation to ensure existence of their solutions.

Roubićek(1996)

... minimization and relaxation of non-convex energies relevant to the study of equilibria for materials ... Often a starting point for this study directly addresses minimization of the energy, leading to the search for necessary and suffi cient conditions ensuring sequential weak lower semicontinuity ...

Fonseca, Müller(1999)

In what follows we present Rank-one convex envelop and its meaning with respect to oscillatory behavior for non-quasiconvex variational problem. We recall that, by stable configurations of a hyperelastic material with strain energy density $\mathscr{W}_0$ we mean minimizers of the energy functional

$$\mathscr{I}(\boldsymbol{\varphi}) = \int_{\mathcal{B}_0} \mathscr{W}_0(\boldsymbol{F}; \boldsymbol{X}) d\boldsymbol{X} \tag{1.1}$$

As such, the elastic deformation map, $\boldsymbol{\varphi} : \mathcal{B}_0 \to \mathbb{R}^n$, $n \in \{1, 2, 3\}$ needs to meet several restrictions, among which we mention, that under a global condition in place, it is required that $\boldsymbol{\varphi} = \boldsymbol{\varphi}_0$ on the boundary $\partial\mathcal{B}_0$ of the domain $\mathcal{B}_0 \subseteq \mathbb{R}^n$ which is open and bounded. The direct method (see Dacorogna(1989) or Pedregal(1996)) to show optimal solutions of the variational problem

$$M = \inf_{\boldsymbol{\varphi}} \{\mathscr{I}(\boldsymbol{\varphi}) : \boldsymbol{\varphi} \in \mathscr{A}_0\} \tag{1.2}$$

rests basically on the *weak lower semicontinuity* of the energy functional $\mathscr{I}$ (see Dacorogna(1989) Secton 3.1), summarized

$$\lim_{k \to \infty} \boldsymbol{\varphi}_k = \tilde{\boldsymbol{\varphi}} \implies \liminf_{k \to \infty} \mathscr{I}(\boldsymbol{\varphi}_k) \geq \mathscr{I}(\tilde{\boldsymbol{\varphi}}) \tag{1.3}$$

where $\{\boldsymbol{\varphi}_k\}_{k\in\mathbb{N}}$ is a sequence of admissible elastic deformations satisfying the requisite conditions on the boundary and the weak convergence takes place in an appropriate Sobolev space(compare Aranda et al.(2001)). The fact that the convenient property (1.3) is equivalent to quasiconvexity (4.5) of the strain energy density $\mathscr{W}_0$ is well known. However, when a strain energy density $\mathscr{W}_0$ does not satisfy the quasiconvexity property as is evident in many crystalline solids, multiple wells are expected and hence highly oscillatory behavior is exhibited in such circumstances(see Chipot(1991) for further survey). In such a situation, investigation of the corresponding variational problem can be approached by focusing on a relaxed formulation where the integrand $\mathscr{W}_0$ in (1.1) is replaced by its quasiconvex envelop $\mathscr{W}_0^Q$, for an in-depth treatment of lower semicontinuity and lower quasiconvex envelop we refer to Fonseca et al.(2001) Brighi et al.(1994) or Fonseca(1988). For detailed and comprehensive overview of variational models in elasticity see contributions by Müller(2002), Pedregal(1996), Zanzotto(1996) and references therein. Because of the inherent difficulty attached to the description of the quasiconvex envelop (4.8), we incline toward other envelopes that are closely related to quasiconvex envelop, e.g. rank-one convex envelop and then concentrate on rank-one convexity as defined by (4.16).

1.1 Non-uniqueness

It has been verified by many authors that quasiconvexity implies rank-one convexity e.g. Dacorogna et al.(1999), or Dacorogna(1989) and the converse is not true in general except on certain hypersurfaces (see Chaudhuri, Müller(2003) or Šverák(1992)). However, in many examples and models that mimic real problems known thus far, replacing the quasiconvex envelop by its rank-one convex counterpart which is its upper bound in the usual sense, produces reasonably good results. In fact, sequences of minimizers that are associated to rank-one convex envelop of an energy density (i.e. laminate) renders configurations with a reasonable degree of accuracy. Oftentimes, laminate are used as a descriptive term for microstructure, the latter refers to the fine inner structure that materials exhibit in an attempt to achieve the lowest energy available to them so as to accommodate the deformation encountered. For the lamination of microstructures see Bhattacharya et al.(1999) Miehe et al.(2003) or Li(2002) and for rank-one convex envelops we refer to the contribution by Dolzmann(1999). Finally, being familiar with the type of situation that may occur in the study of a given variational problem in nonlinear elasticity which lack weak lower semicontinuity often as a consequence of some specific material symmetry, we proceed to show example with specific energy density.

We consider a variational problem describing the total energy of an elastic body which has the general form,

$$\int_{\mathcal{B}_0} \{\mathscr{W}_0(\boldsymbol{F};\boldsymbol{X}) + \psi(\boldsymbol{\varphi};\boldsymbol{X})\}d\boldsymbol{X} \longrightarrow \inf \ ! \tag{1.4}$$

There is an extensive research work focusing on the pressing problem of existence of minimizers(e.g. Ball(1977), Francfort et al.(2003), Fonseca et al.(1999)) for this class of non-quasiconvex variational problems under constraints on the derivative of elastic deformation map with the nonlinear stored energy density $\mathscr{W}_0$ which is assumed to be objective

$$\mathscr{W}_0(\boldsymbol{F}) = \mathscr{W}_0(\boldsymbol{Q} \cdot \boldsymbol{F}), \quad \forall \boldsymbol{F} \in \mathbb{M}_+^{n \times n} \ \& \ \forall \boldsymbol{Q} \in SO(n) \tag{1.5}$$

and also non-negative $\mathscr{W}_0 \geq 0$.

The zero set of such an energy density has a typical disjoint union of multi-well structure, i.e.

$$\boldsymbol{K} = \{\boldsymbol{F} : \mathscr{W}_0(\boldsymbol{F}) = 0\} = \bigcup_{i=1}^{m} SO(n)\boldsymbol{F}_i = \bigcup_{i=1}^{m}\{\boldsymbol{Q} \cdot \boldsymbol{F}_i : \boldsymbol{Q} \in SO(n)\} \tag{1.6}$$

where $\boldsymbol{F}_i$ is the gradient of admissible deformation preferred for the ith phase, and

$$SO(n) = \{\boldsymbol{Q} \in \mathbb{R}^{n \times n} : det\boldsymbol{Q} = 1, \boldsymbol{Q} \cdot \boldsymbol{Q}^t = \boldsymbol{I} = \boldsymbol{Q}^t \cdot \boldsymbol{Q}\} \tag{1.7}$$

is the group of proper rotations. Furthermore, we assume that(after normalization) $\mathscr{W}_0$ attains its minimum value only on this rotationally invariant set $\boldsymbol{K}$, i.e.

$$\mathscr{W}_0(\boldsymbol{F}) = 0 \quad \text{if and only if} \quad \boldsymbol{F} \in \boldsymbol{K}$$

consequently

$$\mathscr{W}_0(\boldsymbol{F}) > 0, \quad \forall \boldsymbol{F} \in \mathbb{R}^{n \times n} \backslash \boldsymbol{K}.$$

The multi-well property can readily be seen from frame indifference of $\mathscr{W}_0$, that is,

$$\mathscr{W}_0(\boldsymbol{F}) = \mathscr{W}_0(\boldsymbol{Q} \cdot \boldsymbol{F}_1) = \mathscr{W}_0(\boldsymbol{F}_1) = ... = \mathscr{W}_0(\boldsymbol{F}_m), \ \forall \boldsymbol{F} \in \boldsymbol{K}. \tag{1.8}$$

For the sake of demonstration we treat the problem in the model case of 1D and find the favorable energetic configuration for the mixing of phases that reasonably approximates the underlying microstructure of the material. Throughout, we require the derivative of the elastic deformation map satisfies the finite deformation constraint $0 \leq \varphi' \leq 2$, the reference configuration of the 1D body is taken to be the unit interval $\mathcal{B}_0 = [0, 1]$, on the boundary of the domain

$$\varphi(0) = 0, \quad \varphi(1) = \frac{1}{2} \tag{1.9}$$

and ψ is the potential of external forces and the energy density $\mathscr{W}_0$ has the form,

$$\mathscr{W}_0(\boldsymbol{F}) = F^2 \left[2F^2 \left[3F^2 - 5 \right] + 3 \right] + 1 \tag{1.10}$$
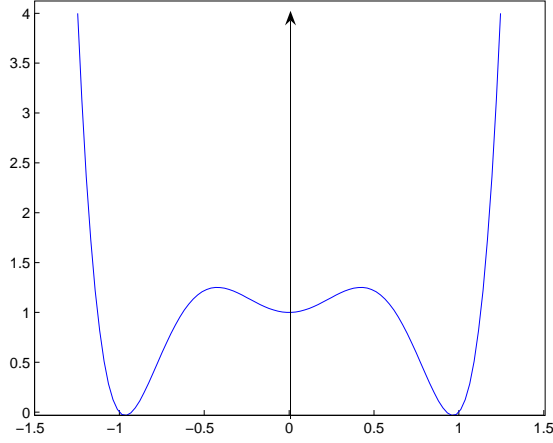
Figure 1.1: Graphical description of the sixth-degree energy density $\mathscr{W}_0$

The energy density $\mathscr{W}_0$ displayed in figure 1.1, is smooth enough to allow operations such as integration by parts, it is also non-negative function with five critical points among which exactly two are stable(global minimum), one is metastable and the remaining two are unstable hill tops. Evidently, the material energetically favors the two stable states corresponding to $\boldsymbol{F} = -1$ and $\boldsymbol{F} = 1$. By metastable state of the crystal we mean one that corresponds to a local minima of the energy functional $\mathscr{I}(\varphi)$ with respect to the space of admissible deformations.

In what follows, we specify the external potential for a given problem of interest and then observe the resulting behavior of energy minimizers.

1.2   External potential and behavior of minimizers

Consider the external force potential of the form

$$\psi(\varphi; X) = \varphi^2(X) \tag{1.11}$$

Our chief objective is to find the solution of (1.4) subject to the boundary data

$$\varphi(0) = 0, \quad \varphi(1) = \frac{1}{2} \tag{1.12}$$

satisfying the general boundedness(finite deformation) requirement

$$0 \leq \varphi' \leq 2. \tag{1.13}$$

Since, both integrands $\mathscr{W}_0$ and ψ are non-negative, it follows that

$$\mathscr{I}(\varphi) \geq 0 \tag{1.14}$$

for all admissible deformations φ, and hence

$$\inf_{\varphi} \mathscr{I}(\varphi) \geq 0. \tag{1.15}$$

The deformation

$$\tilde{\varphi}(X) = \begin{cases} 0 & , \quad 0 \leq X \leq \frac{1}{2} \\ X - \frac{1}{2}, & \frac{1}{2} < X \leq 1 \end{cases}$$

has a non-negative weak derivative, satisfies the boundary conditions and is a minimizer.
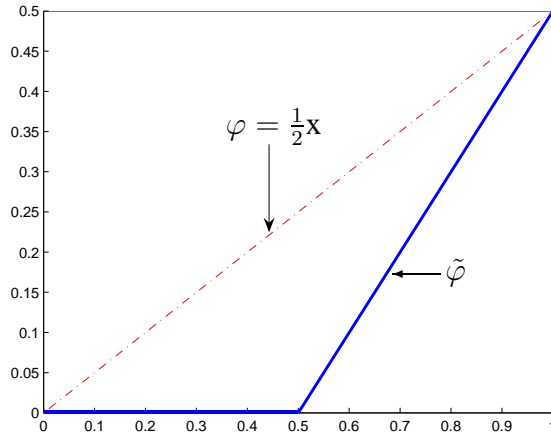

PSfrag replacements

Figure 1.2: The plot of $\tilde{\varphi}$, minimizer of the functional with sixth-degree energy density $\mathscr{W}_0$

Indeed, it is the only deformation with such property, in other words it is a unique minimizer. It can easily be seen that the minimizer $\tilde{\varphi}$ is an absolutely continuous function which is a two-phase[1] deformation. The fact that it is a critical deformation can directly be inferred from the first order variation of the energy functional and that it is a minimizer follows from the second order variation. Verifying this is straightforward, however lengthy.

Now let us modify only the external potential. We solve here again the same variational problem as in the preceeding example except for a change in the external force potential which is given by the expression

$$\psi(\varphi; X) = \varphi(X) - \frac{1}{2}X \tag{1.16}$$

In this case, each of the following deformations satisfy all the premises of the problem and all of them make the energy functional minimum.

$$\varphi_{2^1}(X) = \begin{cases} 0 & , \quad 0 \leq X \leq \frac{1}{2} \\ X - \frac{1}{2}, & \frac{1}{2} < X \leq 1 \end{cases}$$

$$\varphi_{2^2}(X) = \begin{cases} 0 & , \quad 0 \leq X \leq \frac{1}{2^2} \\ X - \frac{1}{2^2}, & \frac{1}{2^2} < X \leq \frac{2}{2^2} \\ \frac{1}{2^2} & , \quad \frac{2}{2^2} < X \leq \frac{3}{2^2} \\ X - \frac{1}{2}, & \frac{3}{2^2} < X \leq 1 \end{cases}$$

$$\varphi_{2^3}(X) = \begin{cases} 0 & , \quad 0 \leq X \leq \frac{1}{2^3} \\ X - \frac{1}{2^3}, & \frac{1}{2^3} < X \leq \frac{2}{2^3} \\ \frac{1}{2^3} & , \quad \frac{1}{2^2} < X \leq \frac{3}{2^3} \\ X - \frac{2}{2^3}, & \frac{3}{2^3} < X \leq \frac{1}{2} \\ \frac{1}{2^2} & , \quad \frac{1}{2} < X \leq \frac{5}{2^3} \\ X - \frac{3}{2^3}, & \frac{5}{2^3} < X \leq \frac{3}{2^2} \\ \frac{3}{2^3} & , \quad \frac{3}{2^2} < X \leq \frac{7}{2^3} \\ X - \frac{1}{2}, & \frac{7}{2^3} < X \leq 1 \end{cases}$$

---

[1]Let $\mathcal{B} \subset \mathbb{R}^{n \times n}$ be an open set, a function $\varphi : \mathcal{B} \to \mathbb{R}^n$ is said to be a two-phase deformation *iff*

$i)\ \varphi \in C^2(\mathcal{B}^0_+ \cup \mathcal{B}^0_- \ , \ \mathbb{R}^n)$
$ii)\nabla\varphi$ and $\nabla\nabla\varphi$ have (at most) jump discontinuities across $\mathcal{K} = \mathcal{B}_+ \cap \mathcal{B}_-$ and $\nabla\varphi(x) \in \mathcal{K} \ \ \forall x \in \mathcal{B}^0$

Here, $\mathcal{B}^0$ is the interior of $\mathcal{B}$ and $\mathcal{B}_\pm$ are such that $\mathcal{B}^0_+ \cap \mathcal{B}^0_- = \emptyset$ and $\mathcal{B}_+ \cup \mathcal{B}_- = \mathcal{B}$

The above deformations are the first three terms of a sequence of deformations with the general term given by the explicit expression

$$
\varphi_{2^n}(X) = \begin{cases}
0 & , & 0 \le X \le \frac{1}{2^n} \\
X - \frac{1}{2^n}, & \frac{1}{2^n} < X \le \frac{1}{2^{n-1}} \\
\frac{1}{2^n} & , & \frac{1}{2^{n-1}} < X \le \frac{3}{2^n} \\
\vdots & \vdots \\
X - \frac{1}{2}, & \frac{2^n - 1}{2^n} < X \le 1
\end{cases}
$$

It can be seen that for any $n \in \mathbb{N}$, the deformation φ_{2^n} satisfies the admissibility condition and is a minimizer. For $n = 1$, it is a deformation with slopes 0 or 1 and for $n > 1$, it is a deformation with slopes alternating between the values 0 and 1. The latter case gives a glimpse at induced microstructures enforced by minimization of total energy with non-quasiconvex energy densities and thereby paves a way for the explanation of oscillatory behaviors of solutions of such problems as visualized in figure 1.3.

PSfrag replacements
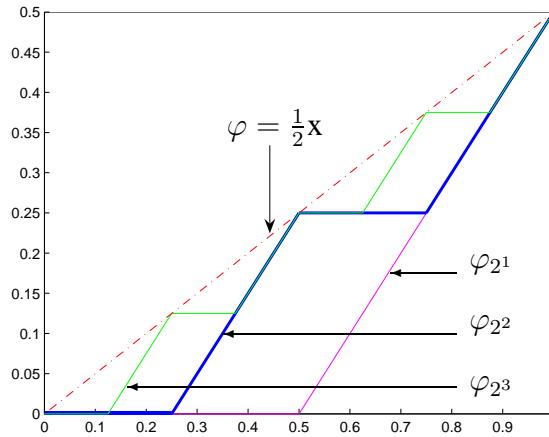
Figure 1.3: Various minimizers(terms of minimizing sequence) of energy functional with sixth-degree non-convex density(1.10) and external potential of the form (1.16) subject to the same boundary conditions

These examples reveal that for the same elastic stored energy density and the same boundary data, modification of the external force potential leads to significant and a complete change in the nature of solution of the variational problem. Indeed, upon modifying only the external force potential the

12

same problem admits infinitely many minimizers thereby violating the uniqueness of solution that was evident from the first example.
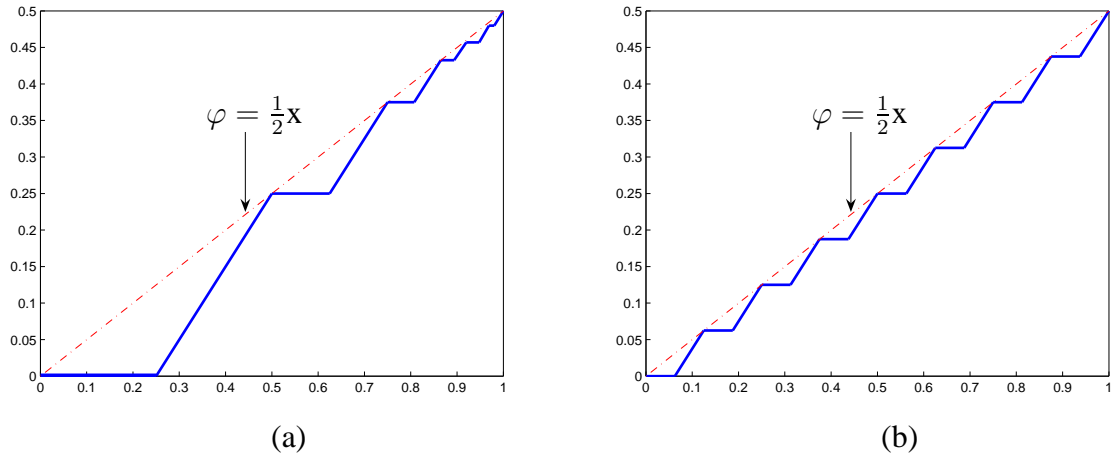
Figure 1.4: Oscillatory minimizers of sixth-degree non-convex density

Apart from giving energetically favorable configurations, figure 1.4 shows the possible mixing of phases related to the underlying microstructure associated with successive reduction of the elastic stored energy.

CHAPTER 2

Mixed continuum atomistic constitutive modelling

I seem to have been only like a boy playing on the seashore, and diverting myself in now and then finding a smoother pebble or a prettier shell than ordinary, whilst the great ocean of truth lay all undiscovered before me.

Newton, Sir Isaac

Mechanical behavior of solids and the associated physical processes are the result of interaction between multiple spatial and temporal scales(cf. Ortiz et al.(1999)). At the fundamental level, everything about solids can be attributed to the electronic structures which obey the Schrödinger equation. However, focusing only on fundamental processes instead of specific details, one may freeze the electronic degrees of freedom and work with nuclear coordinates(see e.g. Tadmor et al.(1996) and references therein). In view of this, interactions and crystal structures can be described at the atomic scale. Mechanical properties at the scale of the continuum are modeled using continuum mechanics for which one speaks of stresses and strains. These effective material properties on continuum scale are averages of material properties at finer scales. Continuum models, however they offer an efficient way of studying average material properties, they usually suffer from inadequate accuracy and lack of microstructural details that help us understand the microscopic mechanics influencing the material to behave in the way it does(see the monograph Phillips(2001) for further survey and examples) . Atomistic models, on the other hand, allow us gain insight and probe the detailed crystal lattice and defect structure. Thus, by coupling continuum models with atomistics we intend to develop a model that have accuracy which is comparable to the atomistic model and efficiency that is reasonably close to the continuum model(see Tadmor et al.(1999) on finite elements and atomistics for complex crystals). To this end, we concentrate on *concurrent* coupling that links different scales on the fly. In a broader sense, we may group concurrent coupling method into two major classes, one based on dynamic formulations and the other based on energetics. In this work, the latter is employed.

2.1 Atomistic modelling

Atomistic modelling is established on the fundamental assumption that associated with every property observed at the macroscopic scale there is a set of microscopic processes on the background, the understanding of which clarify the observed macroscopic behavior(see e.g. Grabowski et al.(2002) Lilleodden et al.(2003) Olmsted et al.(2005) or Moriarty(1998) for application to specific problems). A recurring centerpiece in the study of materials is the connection between structure and properties. Whether our description of structure is made at the level of the crystal lattice or the defect arrangements that pervades the material or even at the level of continuum deformation fields, a crucial prerequisite which precedes the detail study of connection of structure and properties is the ability to describe the total energy of the system of interest(Phillips(2001)). In this regard, one seeks for a functional such that given a description for the geometry of the system, the energy of that system can be obtained on the basis of the kinematic measures that have been used to characterize the underlying geometry.

2.1.1 Description of total energy

We assume that there is a reference configuration consisting of N atomic nuclei described by lattice, and the computation of total energy adheres to description in terms of these atomic positions. In the framework of standard lattice statics employing empirical potentials, there is a well defined total internal energy functional E^{int} that might be determined from the relative positions of all atoms in the aggregate. In many empirical models such a functional has the general format,

$$E^{\text{int}} = \sum_k \left\{ \frac{1}{k!} \sum_{i_1,\ldots,i_k \in I} \phi_k(\boldsymbol{r}_{i_1},\ldots,\boldsymbol{r}_{i_k}) \right\} \tag{2.1}$$

where

$$E_k = \frac{1}{k!} \sum_{i_1,\ldots,i_k \in I} \phi_k(\boldsymbol{r}_{i_1},\ldots,\boldsymbol{r}_{i_k})$$

is the k-atom energy contribution with $\phi_k(\boldsymbol{r}_{i_1},\ldots,\boldsymbol{r}_{i_k})$ characterizing the k-atom interaction and I is an indexing set (cf. Ortiz et al.(1999)).
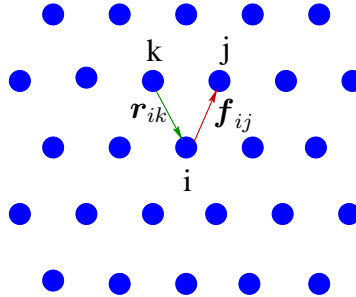

Figure 2.1: Schematics of a crystal lattice, interaction force and separation

For a finite energy, with the assumption that the series converges fast, we truncate the series and thereby concentrate only on two-body interactions. But then the total internal energy reduces to

$$E^{int} = \sum_{i=1}^{N} E_i \quad \text{where} \quad E_i = \frac{1}{2} \sum_{j \neq i} \phi(r_{ij}) \tag{2.2}$$

is the energy contribution from site $\boldsymbol{r}_i$ and $\phi(r_{ij})$ is a pair-potential such that $r_{ij} = \|\boldsymbol{r}_{ij}\| = \|\boldsymbol{r}_i - \boldsymbol{r}_j\|$ with the quantity r_{ij} interpreted as the separation between atoms i and j. From basic vector calculus, the distance function measuring the separation between vectors is a function of the vectors themselves, thus, through the relative placements of the atoms in the deformed configuration, the energy contribution of atom i, E_i becomes a function of the positions $\boldsymbol{r}_j$ of all the atoms in the collection,

$$E^{int} := E^{int}(\boldsymbol{r}_1, \boldsymbol{r}_2, ..., \boldsymbol{r}_N)$$

In the process of search for optimal configuration, we are looking for stationary atomic positions, and therefore, observation of such a description of E^{int} as a function of atomic positions instead of interatomic separation proves to be important.

2.1.2 Kinematics and atomic level constitutive law

The total energy often serves as a gateway for the analysis of material behavior. Though, our primary emphasis will center on the calculation of energies, it is also worth remembering that the total energy serves as the basis for the determination of forces as well. In many instances (e.g. relaxation or molecular dynamics) the calculation of forces is a prerequisite to the performance of structural relaxation. Recent advances in the understanding and modelling of the energetics and interatomic interactions in materials coupled with advances in computational techniques make atomistics a powerful candidate for the analysis of complex materials phenomena(e.g. see the contribution by Phillips et al.(2002) or Fried, Gurtin(1999)).

In describing kinematics, we commence by a brief review of the direct atomistic modelling, the discussion is restricted to classical lattice statics (cf. Sunyk, Steinmann(2001) or Ortiz et al.(1999)). Consider a crystalline material consisting of N interacting atoms as visualized in figure 2.2.
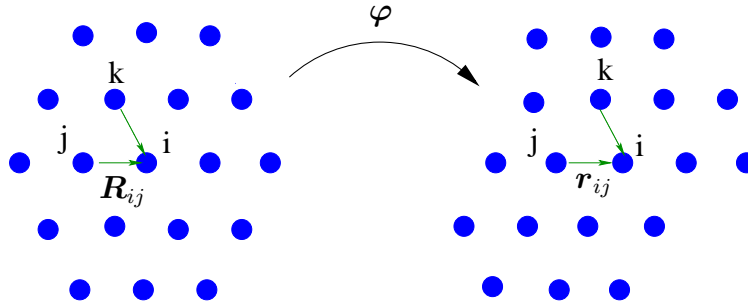

Figure 2.2: Graphical representation of deformation of a crystalline material.

16

The kinematics are then described in terms of the interatomic distance vectors $\boldsymbol{R}_{ij} = \boldsymbol{R}_i - \boldsymbol{R}_j$ between the atoms labeled i and j respectively. The discrete map φ relates the reference configuration to the current configuration via $\boldsymbol{r}_{ij} = \varphi(\boldsymbol{R}_{ij})$. The interatomic interactions are described using empirical potentials. Whereas there are many well known pair-potentials to the material modeler (e.g. Morse, Buckingham), for the sake of transparency we will use the simplest of its kind, namely the Lennard-Jones[1] 6-12 pair-potential which takes the format

$$\phi(r) = 4\,\epsilon \left[\left(\frac{\sigma}{r} \right)^{12} - \left(\frac{\sigma}{r} \right)^{6} \right] \tag{2.3}$$

with the atomic separation $r = r_{ij} = \|\boldsymbol{r}_{ij}\|$ and parameters σ and ϵ. Once the pair potential has been identified, the next task is to give a description of the total energy of the system, find its radial derivative which is straightforward and then determine the corresponding force fields. This force fields, in turn, provide the basis for lattice statics or molecular dynamics analysis of the problem of interest. To this end, using the energy contribution of the atom i which is given by

$$E_i = \frac{1}{2} \sum_{j \neq i} \phi(r_{ij}) = 2\,\epsilon \sum_{j \neq i} \left[\left(\frac{\sigma}{r_{ij}} \right)^{12} - \left(\frac{\sigma}{r_{ij}} \right)^{6} \right] \tag{2.4}$$

the total potential energy is then represented by

$$E^{tot} = \sum_i E_i = 2\,\epsilon \sum_i \sum_{j \neq i} \left[\left(\frac{\sigma}{r_{ij}} \right)^{12} - \left(\frac{\sigma}{r_{ij}} \right)^{6} \right] \tag{2.5}$$

The force $\boldsymbol{f}_i$ acting on an atom i due to the interactions with all the remaining atoms in the collection is given by the radial derivative of the total energy

$$\boldsymbol{f}_i = -\nabla_{\boldsymbol{r}_i} E^{tot} = \sum_{j \neq i} \boldsymbol{f}_{ij} \tag{2.6}$$

with

$$\boldsymbol{f}_{ij} = -\nabla_{\boldsymbol{r}_i} \phi(r_{ij}) = -\frac{\phi'_{ij}}{r_{ij}} \boldsymbol{r}_{ij} \tag{2.7}$$

rendering the underlying constitutive law in the context of lattice statics.

---

[1]The Lennard-Jones $m-n$ interaction potential has the format $E_{m,n} = \dfrac{n\epsilon}{n-m} \left(\dfrac{n}{m} \right)^{\frac{m}{n-m}} \left[\left(\dfrac{\sigma}{r} \right)^n - \left(\dfrac{\sigma}{r} \right)^m \right]$ where the pair (m,n) of parameters is usually of the type $(6,n)$ such that $8 \leq n \leq 20$. Setting $\mathscr{N}_{m,n} = \frac{n\epsilon}{n-m} \left(\frac{n}{m} \right)^{\frac{m}{n-m}}$ renders $\mathscr{N}_{6,12} = 4\epsilon$ leading to Lennard-Jones 6-12 interaction potential

The second derivative of E^{tot} with respect to $\boldsymbol{r}_j$ yields a second order tensor, the symmetric atomic level stiffness which is needed in the iterative solution strategy (see Sunyk, Steinmann(2001) for details)

$$\boldsymbol{k}_{ij} = -\frac{\partial^2 E^{tot}}{\partial \boldsymbol{r}_i \otimes \partial \boldsymbol{r}_j} = \frac{\phi'_{ij}}{r_{ij}} \boldsymbol{I} + \left[\frac{\phi''_{ij}}{r_{ij}^2} - \frac{\phi'_{ij}}{r_{ij}^3} \right] \boldsymbol{r}_{ij} \otimes \boldsymbol{r}_{ij}. \tag{2.8}$$

Please note that, symmetry of the stiffness tensor is a consequence of the equality of mixed partial derivatives with the assumption of continuity on the energy functional.

It is also worth noting that the diagonal component is the sum over off-diagonal components

$$\boldsymbol{k}_{ii} = -\frac{\partial^2 E^{tot}}{\partial \boldsymbol{r}_i \otimes \partial \boldsymbol{r}_i} = -\sum_{j \neq i} \boldsymbol{k}_{ij} \tag{2.9}$$

2.1.3 Energy and external load

The ensemble of atoms may experience a force due to an external agent, in this circumstance where our concern is to find a configuration with minimal energy, in addition to the interatomic potential energy there is an energy due to an external load applied to the atoms. In this case, the total potential energy of the system of atoms consists of the potential energy due to the interaction of the atoms and the energy due to the applied load, and can be written as

$$E^{tot} = E^{int}(\boldsymbol{r}_1, \boldsymbol{r}_2, ..., \boldsymbol{r}_N) - \sum_{i=1}^{N} f(\boldsymbol{r}_i) \tag{2.10}$$

Here, $\boldsymbol{r}_i$ denotes the position of the atom i after deformation and the series term describes the energy due to applied loads. As pointed out earlier, the dependence of E^{int} on $\boldsymbol{r}_i$ is through the relative positions of atoms in the deformed configuration. In the sequel, we seek a function $E^{tot}(\boldsymbol{r}_i, i = 1, 2..., N)$ where $\boldsymbol{r}_i$ refers to nuclear coordinate, and then in the context of lattice statics we seek the placement $\boldsymbol{r}_i$ such that the total energy is minimum. Thus far, the description is in terms of atomic positions, but if one is interested in the description of behavior of the system in terms of displacement fields, taking $\boldsymbol{R}_i$ to be the position of the ith atom in the reference configuration, the displacement it experiences due to deformation can be given by the vector $\boldsymbol{u}_i = \boldsymbol{r}_i - \boldsymbol{R}_i$. This allows us to rewrite the total energy in terms of atomic displacement as,

$$E^{tot} = E^{int}(\boldsymbol{u}_1, \boldsymbol{u}_2, ..., \boldsymbol{u}_N) - \sum_{i=1}^{N} \boldsymbol{f}_i^{ext} \cdot \boldsymbol{u}_i \tag{2.11}$$

where $\boldsymbol{f}_i^{ext} \cdot \boldsymbol{u}_i$ is the potential energy of the applied load $\boldsymbol{f}_i^{ext}$ on the atom i.

2.2 Continuum modelling

By way of contrast, formulation and treatment of material properties on macro scales through continuum models oftentimes leads to phenomenological description of the total energy whereby the entropy is assumed to vary in accordance with some functional of relevant strain measures. Thus, we seek a functional $E^{tot}(\boldsymbol{F})$ which relates the spatially varying deformation field and the corresponding energy.
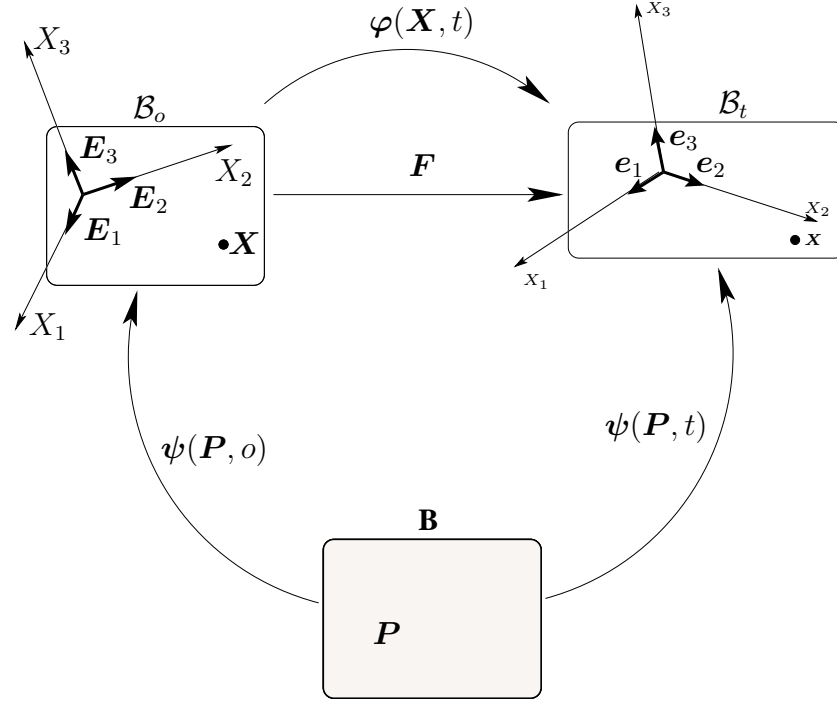
Figure 2.3: Non-linear motion, linear tangent map and configurations

2.2.1 Deformation and motion of hyperelastic continua

A body **B** (see figure 2.3) regarded a set whose elements are referred to as particles (material points) is set into one-to-one correspondence with points of a region $\mathcal{B}_t$ contained in Euclidean space which we call *configuration* of the body. Practically speaking, we have an invertible map

$$\boldsymbol{\psi} : \mathbf{B} \times [0, \infty) \to \mathcal{B}_t \subset \mathbb{R}^3 \tag{2.12}$$

which assigns to each element $\boldsymbol{P} \in \mathbf{B}$ and $t \in [0, \infty)$, a point $\boldsymbol{\psi}(\boldsymbol{P}, t) \in \mathcal{B}_t$. In order to render a natural description of the motion undergone by the body, on the one hand a fixed configuration

corresponding to $t = 0$ is chosen as *reference configuration* denoted $\mathcal{B}_0$, i.e $\mathcal{B}_0 := \boldsymbol{\psi}(\mathbf{B}, 0)$ and on the other hand, the deformation of the body at $t > 0$ termed *current configuration* is denoted by $\mathcal{B}_t$ in other words $\mathcal{B}_t := \boldsymbol{\psi}(\mathbf{B}, t)$. By setting,

$$\boldsymbol{X} := \boldsymbol{\psi}(\boldsymbol{P}, 0) \quad \text{and} \quad \boldsymbol{x} := \boldsymbol{\psi}(\boldsymbol{P}, t) \tag{2.13}$$

one can then get rid of the material point $\boldsymbol{P}$, and write the next expression

$$\boldsymbol{x} = \boldsymbol{\psi}(\boldsymbol{\psi}^{-1}(\boldsymbol{X}, 0), t) = \boldsymbol{\varphi}(\boldsymbol{X}, t) \tag{2.14}$$

To facilitate understanding of the kinematics of $\mathbf{B}$, we introduce relevant systems of coordinates both in the reference and current configurations. We use a fixed Cartesian coordinate system with origin $\boldsymbol{O}$ and basis vectors $\{\boldsymbol{E}_i : i = 1, 2, 3\}$ in the reference configuration, and a Cartesian frame with basis vectors $\{\mathbf{e}_i : i = 1, 2, 3\}$ and origin $\boldsymbol{o}$ in the current configuration, thereby equipping a continuum body with two different configurations, material and spatial. Consequently, the deformation gradient which is a tensor valued quantity results from the derivative of the deformation map $\boldsymbol{\varphi}$

$$\boldsymbol{F} = \nabla_X \otimes \boldsymbol{\varphi} \tag{2.15}$$

At each point $\boldsymbol{X} \in \mathcal{B}_0$ the deformation gradient $\boldsymbol{F}$ is linear and maps infinitesimal material line elements to infinitesimal spatial line elements,

$$d\boldsymbol{x} = \boldsymbol{F} \cdot d\boldsymbol{X}. \tag{2.16}$$

In the context of differential geometry, the deformation gradient is called the *tangent map of $\boldsymbol{\varphi}$* and it maps the reference tangent space (infinitesimal neighborhoods of $\boldsymbol{X}$) to the spatial tangent space (infinitesimal neighborhoods of $\boldsymbol{x}$). As a result, it takes the following representation in component form,

$$\boldsymbol{F} = F_{ij}\mathbf{e}_i \otimes \boldsymbol{E}_j \quad \text{with} \quad F_{ij} = x_{i,j} = \frac{\partial x_i}{\partial X_j}. \tag{2.17}$$

Since the deformation gradient is invertible, we require its determinant to be nonzero

$$J = det(\boldsymbol{F}) \neq 0 \tag{2.18}$$

Besides being non-zero, for orientation preserving deformation the determinant satisfies,

$$J = det(\boldsymbol{F}) > 0 \tag{2.19}$$

For hyperelastic material response, the scalar valued strain energy function $\mathscr{W}_0$ per unit reference volume at a placement $\boldsymbol{X}$ depends in general on the deformation gradient $\boldsymbol{F}$(for in-depth on hyperelasticity see the monograph by Marsden et al.(1994) or the contribution by Chipot(1990) for the notion of hyperelasticity in crystals),

$$\mathscr{W}_0 = \mathscr{W}_0(\boldsymbol{F}; \boldsymbol{X}) \tag{2.20}$$

Moreover, the elastic constitutive law is furnished by the first Piola-Kirchhoff stress tensor which results from the derivative of the strain energy $\mathscr{W}_0$ with respect to the deformation gradient $\boldsymbol{F}$

$$\boldsymbol{\Pi}^t = \nabla_{\boldsymbol{F}} \mathscr{W}_0 \tag{2.21}$$

Finally, the fourth order tangent operator $\mathbb{L}$, which in general results from linearization of the constitutive stress function, is given by

$$\mathbb{L} = \frac{\partial^2 \mathscr{W}_0(\boldsymbol{F}; \boldsymbol{X})}{\partial \boldsymbol{F} \otimes \partial \boldsymbol{F}} . \tag{2.22}$$

2.2.2 Measures of deformation

In an effort to describe the constitutive response of an elastic continuum, we encounter measures of deformation in the immediate neighborhood of a point in the continuum. In view of this therefore, the Lagrangian measure of deformation, the right Cauchy-Green deformation tensor $\boldsymbol{C} = \boldsymbol{F}^t \cdot \boldsymbol{F}$, resolved into components in Cartesian frame is given by

$$\boldsymbol{C} = C_{ij}\boldsymbol{E}_i \otimes \boldsymbol{E}_j \quad \text{with} \quad C_{ij} = x_{k,i}x_{k,j} = F_{ki}F_{kj} \tag{2.23}$$

In the same spirit, the Eulerian measure of deformation, the Finger deformation tensor $\boldsymbol{b} = \boldsymbol{F} \cdot \boldsymbol{F}^t$ is expressed as

$$\boldsymbol{b} = b_{ij}\mathbf{e}_i \otimes \mathbf{e}_j \quad \text{with} \quad b_{ij} = x_{i,k}x_{j,k} = F_{ik}F_{jk} \tag{2.24}$$

The aforementioned Cauchy-Green tensors are both symmetric and positive definite. Consequently, their eigenvalues are real and positive.

In what follows, we observe how the element of area and the element of volume changes during the deformation process.
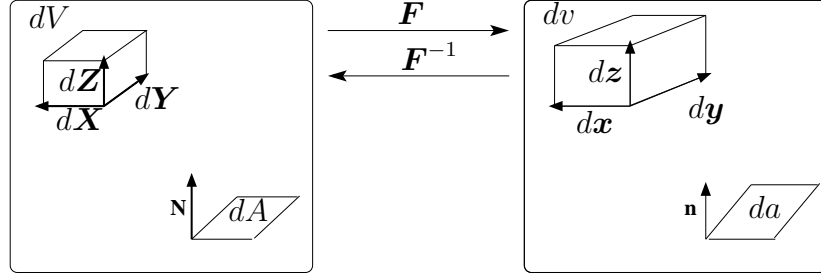
Figure 2.4: Schematics of volume and area elements in the reference and current configurations

The referential element of volume[2] dV is defined by

$$dV = d\boldsymbol{X} \cdot (d\boldsymbol{Y} \wedge d\boldsymbol{Z}) \tag{2.25}$$

and is carried onto an element of volume dv during the motion, their relation is established as,

$$
\begin{aligned}
dv &= d\boldsymbol{x} \cdot (d\boldsymbol{y} \wedge d\boldsymbol{z}) \\
&= \boldsymbol{F} \cdot d\boldsymbol{X} \cdot (\boldsymbol{F} \cdot d\boldsymbol{Y} \wedge \boldsymbol{F} \cdot d\boldsymbol{Z}) \\
&= J dV
\end{aligned}
$$

If $\boldsymbol{n}$ is a unit vector normal to the area element da in the current configuration then

$$
\begin{aligned}
\boldsymbol{n} da &= d\boldsymbol{x} \wedge d\boldsymbol{y} \\
&= \boldsymbol{F} \cdot d\boldsymbol{X} \wedge \boldsymbol{F} \cdot d\boldsymbol{Y} \\
&= det\boldsymbol{F}(\boldsymbol{F}^{-t}(d\boldsymbol{X} \wedge d\boldsymbol{Y})) \\
&= J\boldsymbol{F}^{-t} \cdot \boldsymbol{N} dA
\end{aligned}
$$

where $\boldsymbol{N}$ is the corresponding unit normal to the area element in the reference configuration. This expression is oftentimes referred to as Nanson's formula.

2.3 Coupling the atomistic core to the surrounding continuum

In the context of concurrent coupling based on energetic formulation(cf. Sunyk Steinmann(2001)), though description of the mechanics of materials on the continuum level is founded on the assumption that the spatial variations in a given field variable are sufficiently slow so as to allow the smearing out of the atomic degrees of freedom upon which they are founded, a common difficulty in multiscale modelling is the proper handling of the transition between lattice and the continuum(see the cotribution by Rudd et al.(2000) and references therein for an overview on a seamless coupling of quatum to statistical to continuum). Indeed, this problem arises from different nature of the internal forces which act in the two regimes. Investigation of these forces basically lies on the description of internal energy. Hence, the central idea in this part is to establish a connection between the phenomenological macroscopic energy density $\mathscr{W}_0$ and the atomic potential of interest.

---

[2]$d\boldsymbol{Y} \wedge d\boldsymbol{Z}$ is the vector product in the usual sense and $J = det\boldsymbol{F}$.

2.3.1 Macroscopic energy and interaction potential

The link between atomistic and continuum material properties requires a procedure for determining the nonlinear elastic continuum response of crystal with a particular atomistic structure. The continuum response rests on the results produced by discrete formulation at the atomistic scales based on discrete lattice statics. The procedure of determining the continuum response involves computing the changes in the stored energy of a crystallite under the action of continuum deformation measures. Thus, deformation is applied to lattice using the standard Cauchy-Born rule(Ericksen(1984)) which prescribes the atomic positions in the strained lattice by application of the local deformation gradient $\boldsymbol{F}$.
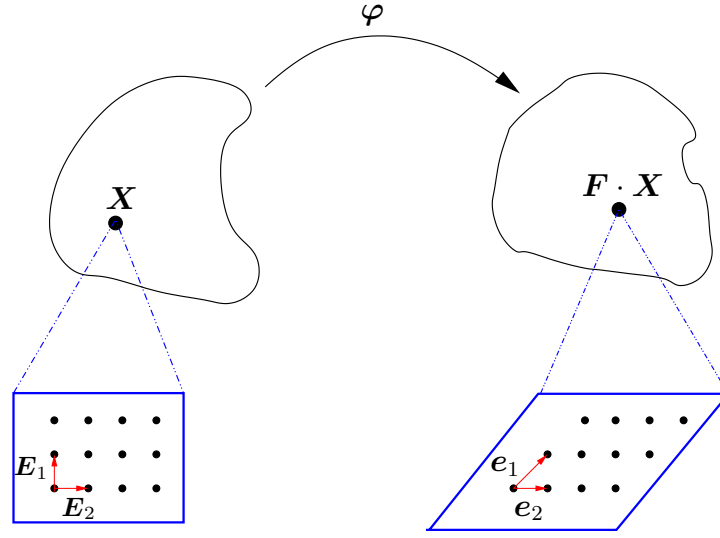
Figure 2.5: Illustration of the Cauchy-Born rule in the model case of 2D

Supposing that underlying each point of a continuum there is a bravais lattice generated by basis vectors $\boldsymbol{E}_1$, $\boldsymbol{E}_2$ and $\boldsymbol{E}_3$, if the continuum is subjected to a deformation φ with corresponding deformation gradient $\boldsymbol{F}$ the Cauchy-Born hypotheses states that $\boldsymbol{e}_1 = \boldsymbol{F} \cdot \boldsymbol{E}_1$, $\boldsymbol{e}_2 = \boldsymbol{F} \cdot \boldsymbol{E}_2$ and $\boldsymbol{e}_3 = \boldsymbol{F} \cdot \boldsymbol{E}_3$ constitutes a basis of the deformed lattice, i.e. a lattice vector behaves like a material filament. To give a brief account of this, we start with a homogeneous deformation of an infinite representative crystallite body. Since lattice vectors are assumed to deform as would material line elements, it follows that the position vectors $\boldsymbol{r}_i$ in the spatial configuration would be obtained from the corresponding vectors $\boldsymbol{R}_i$ in the material configuration by applying the deformation gradient $\boldsymbol{F}$, which is possible by recourse to relative atomic positions. Consequently, the lattice vector $\boldsymbol{r}_{ij}$ is given by

$$\boldsymbol{r}_{ij} = \boldsymbol{F} \cdot \boldsymbol{R}_{ij}. \tag{2.26}$$

Furthermore, the site energy which depends only on relative distances $\boldsymbol{r}_{ij}$ becomes a function of the deformation gradient $\boldsymbol{F}$ and the lattice vectors $\boldsymbol{R}_{ij}$, that is,

$$E_i = \frac{1}{2} \sum_{j \neq i} \phi(r_{ij}) = \frac{1}{2} \sum_{j \neq i} \phi(\|\boldsymbol{F} \cdot \boldsymbol{R}_{ij}\|) \,. \tag{2.27}$$

Assuming that the energy of each atom is uniformly distributed over the volume V of its Voronoi polyhedron, an important relation between the site energy (discrete atomistic quantity) and the strain energy density (continuum quantity), which we were looking for is given by

$$\mathscr{W}_0(\boldsymbol{F}; \boldsymbol{X}) = \frac{E_i}{V} = \frac{1}{2V} \sum_{j \neq i} \phi(\|\boldsymbol{F} \cdot \boldsymbol{R}_{ij}\|) \,. \quad (2.28)$$
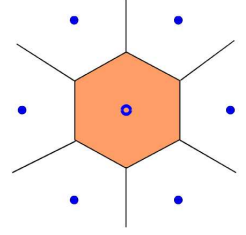

Figure 2.6: Voronoi polyhedron

2.3.2   Elastic constitutive law

The two-point second order tensor field, the Piola-Kirchhoff stress tensor $\boldsymbol{\Pi}^t$ which results from the derivative of the strain energy density has the physical meaning that its components are the forces acting on the deformed configuration per unit undeformed area. In other words, they are thought of as acting on the undeformed solid . Plugging (2.28) in to the expression in (2.21) yields the corresponding constitutive law,

$$\boldsymbol{\Pi}^t = \frac{\partial \mathscr{W}_0(\boldsymbol{F}; \boldsymbol{X})}{\partial \boldsymbol{F}} = \frac{1}{2V} \sum_{j \neq i} \boldsymbol{f}_{ji} \otimes \boldsymbol{R}_{ij} \,. \tag{2.29}$$

Ultimately, the tangent operator takes the form

$$\mathbb{L} = \frac{1}{2V} \sum_{j \neq i} \boldsymbol{k}_{ij} \,\overline{\otimes}\, [\,\boldsymbol{R}_{ij} \otimes \boldsymbol{R}_{ij}\,] \tag{2.30}$$

with, $\boldsymbol{k}_{ij}$ as defined in (2.8) and $[\,\boldsymbol{a}\,\overline{\otimes}\,\boldsymbol{b}\,]_{ijkl} = [\,\boldsymbol{a}\,]_{ik}\,[\,\boldsymbol{b}\,]_{jl}$.

Referring to the expression in (2.26), the modulus of the spatial lattice vector $\boldsymbol{r}_{ij}$ may be computed by appealing to the Cauchy-Green tensor $\boldsymbol{C} = \boldsymbol{F}^t \cdot \boldsymbol{F}$ as,

$$r_{ij} = \|\boldsymbol{r}_{ij}\| = \sqrt{\boldsymbol{R}_{ij} \cdot \boldsymbol{C} \cdot \boldsymbol{R}_{ij}} \tag{2.31}$$

24

or Green-Lagrange tensor $\boldsymbol{E}$,

$$r_{ij} = \sqrt{\boldsymbol{R}_{ij} \cdot \boldsymbol{R}_{ij} + 2\boldsymbol{R}_{ij} \cdot \boldsymbol{E} \cdot \boldsymbol{R}_{ij}} \qquad (2.32)$$

where the Green-Lagrange deformation tensor

$$\boldsymbol{E} = \frac{1}{2}[\boldsymbol{F}^t \cdot \boldsymbol{F} - \boldsymbol{I}] \qquad (2.33)$$

is a symmetric one-point tensor with the component representation

$$\boldsymbol{E} = \frac{1}{2}[C_{ij} - \delta_{ij}]\boldsymbol{E}_i \otimes \boldsymbol{E}_j \qquad (2.34)$$

In general, the deformation can not assumed to be uniform at scales approaching atomistic dimensions, even for infinitesimal deformations. However, in that case one can handle the problem by recourse to averaging techniques such as homogenization. The coupling procedure introduces atomistic degrees of freedom into expressions for the stored energy which modify the computed constitutive properties to give better agreement with experimental results as desired.

For an orientation preserving deformation $\boldsymbol{F}$, the material frame indifference property of the strain energy density allow us to reduce the dependence of $\mathscr{W}_0$ on such $\boldsymbol{F}$ to a dependence only on the corresponding stretch tensors as can be seen from the following observation. Any second order tensor

$$\boldsymbol{F} \in \mathbb{M}^{3\times3}_+, \text{ where } \mathbb{M}^{3\times3}_+ = \{\boldsymbol{F} \in \mathbb{M}^{3\times3} : det(\boldsymbol{F}) > 0\}$$

admits the polar decomposition, Gurtin(1983),

$$\boldsymbol{F} = \boldsymbol{R} \cdot \boldsymbol{U} \qquad (2.35)$$

whereby $\boldsymbol{R}$ is proper orthogonal and $\boldsymbol{U}$ is the right stretch tensor which is symmetric and positive definite. For this class of deformations, we have

$$\begin{aligned} \mathscr{W}_0(\boldsymbol{R}^t \cdot \boldsymbol{F}; \boldsymbol{X}) &= \mathscr{W}_0(\boldsymbol{R}^t \cdot \boldsymbol{R} \cdot \boldsymbol{U}; \boldsymbol{X}) \\ &= \mathscr{W}_0(\boldsymbol{U}; \boldsymbol{X}) \end{aligned}$$

and thus from the objectivity of $\mathscr{W}_0$ it follows that

$$\begin{aligned} \mathscr{W}_0(\boldsymbol{F}; \boldsymbol{X}) &= \mathscr{W}_0(\boldsymbol{U}; \boldsymbol{X}) \\ &= \mathscr{W}_0(\boldsymbol{C}; \boldsymbol{X}) \end{aligned}$$

2.4 Equilibrium equation

After an excursion to the direct atomistic modelling with the discussion restricted to classical lattice statics settings and having reviewed the deformation and motion of a hyperelastic continua, we took a glimpse at the coupling paradigm(see Knap, Ortiz(2001) among others) that is meant to permit analysis of problems requiring simultaneous resolution of the continuum and atomistic features and the associated deformation process by establishing a connection between the phenomenological macroscopic energy density $\mathscr{W}_0$ and the atomic potential of interest by recourse to the Cauchy-Born rule. With this at the background, we shall now proceed to formulate the relevant equilibrium equation and subsequently the corresponding boundary value problem of interest.
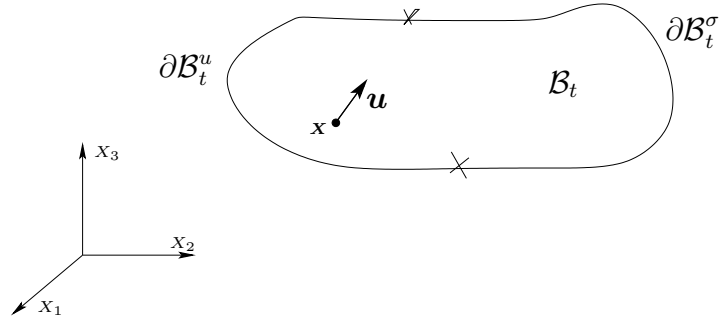
PSfrag replacements

Figure 2.7: Illustration of a continuum positioned in Cartesian co-ordinate sytstem

The set of spatial points $\boldsymbol{x}$ defines the configuration $\mathcal{B}_t$ with the boundary $\partial\mathcal{B}_t$ composed of Dirichlet $\partial\mathcal{B}_t^u$ and Neumann $\partial\mathcal{B}_t^\sigma$ type, and the unknown $\boldsymbol{u}$, i.e, the dependent variable $\boldsymbol{u}$ is a vector valued displacement and in general it depends on $\boldsymbol{x} \in \mathcal{B}_t$. A basic assumption underlying our formulation of equilibrium field equations is that a body is acted upon by a system of forces, a distributed body force field per unit mass $\boldsymbol{b}$ and a force due to an external agent in the form of surface traction $\boldsymbol{t}$. These comprises the resultant force acting on the continuum body given by

$$\boldsymbol{F}(\mathcal{B}_t) = \int_{\mathcal{B}_t} \rho\boldsymbol{b}dV + \int_{\partial\mathcal{B}_t} \boldsymbol{t}da. \tag{2.36}$$

The balance of linear momentum leads to

$$\int_{\mathcal{B}_t} \rho\boldsymbol{b}dV + \int_{\partial\mathcal{B}_t} \boldsymbol{t}da = \int_{\mathcal{B}_t} \rho\boldsymbol{a}da. \tag{2.37}$$

If inertial effects are neglected in the equilibrium equation (2.37) then the underlying problem specification will change considerably and this is realized by employing quasistatic assumption

26

which leads to zero acceleration field, consequently equation (2.37) reduces to

$$\int_{\mathcal{B}_t} \rho \boldsymbol{b} dV + \int_{\partial \mathcal{B}_t} \boldsymbol{t} da = \boldsymbol{0}. \tag{2.38}$$

Applying the Cauchy stress theorem $\boldsymbol{t} = \boldsymbol{\sigma} \cdot \boldsymbol{n}$, we may write

$$\int_{\mathcal{B}_t} \rho \boldsymbol{b} dV + \int_{\partial \mathcal{B}_t} \boldsymbol{\sigma} \cdot \boldsymbol{n} da = \boldsymbol{0}. \tag{2.39}$$

Piola transformation facilitates the passage from $\boldsymbol{\sigma}$ to $\boldsymbol{\Pi}^t$ through

$$\boldsymbol{\sigma} = \frac{1}{J} \boldsymbol{\Pi}^t \cdot \boldsymbol{F}^t \tag{2.40}$$

Using this, the expression in (2.39) can be written as

$$\int_{\mathcal{B}_t} \rho \boldsymbol{b} dV + \int_{\partial \mathcal{B}_t} \frac{1}{J} [\boldsymbol{\Pi}^t \cdot \boldsymbol{F}^t] \cdot \boldsymbol{n} da = \boldsymbol{0}. \tag{2.41}$$

Nanson's formula

$$\boldsymbol{n} da = J \boldsymbol{F}^{-t} \cdot \boldsymbol{N} dA$$

together with the volume ratio $dV = J dV_0$ augmented with the relation between the reference and current mass densities $\rho = \frac{1}{J} \rho_0$ transforms equation (2.41) to

$$\int_{\mathcal{B}_0} \rho_0 \boldsymbol{b} dV_0 + \int_{\partial \mathcal{B}_0} \boldsymbol{\Pi}^t \cdot \boldsymbol{N} dA = \boldsymbol{0}. \tag{2.42}$$

Eventually, applying Divergence theorem to the surface integral in (2.42), the balance equation further reduces to

$$\int_{\mathcal{B}_0} \rho_0 \boldsymbol{b} dV_0 + \int_{\mathcal{B}_0} \text{Div} \boldsymbol{\Pi}^t dV_0 = \int_{\mathcal{B}_0} [\, \rho_0 \boldsymbol{b} + \text{Div} \boldsymbol{\Pi}^t \,] dV_0 = \boldsymbol{0}. \tag{2.43}$$

Consequently, the local form (pointwise in $\mathcal{B}_0$) of the *equilibrium equation* is given by

$$\text{Div} \boldsymbol{\Pi}^t + \rho_0 \boldsymbol{b} = \boldsymbol{0}. \tag{2.44}$$

In the absence of body forces we simply have

$$\text{Div} \boldsymbol{\Pi}^t = \boldsymbol{0}. \tag{2.45}$$

27

2.4.1 Boundary value problem

Consider a hyperelastic continuum body with reference configuration $\mathcal{B}_0$. The total potential energy of the crystal is given by

$$E^{tot} = \int_{\mathcal{B}_0} \mathscr{W}_0(\boldsymbol{F}; \boldsymbol{X}) dV_0 - \int_{\mathcal{B}_0} \rho_0 \boldsymbol{b} \cdot \boldsymbol{\varphi} dV_0 - \int_{\partial \mathcal{B}_0} \boldsymbol{T} \cdot \boldsymbol{\varphi} dA \qquad (2.46)$$

Where $\mathscr{W}_0$ is the strain energy density that depends in general on the deformation gradient $\boldsymbol{F}$ and is parameterized by reference placement $\boldsymbol{X}$. The stable configuration of the crystal is identified with the minimizers of the potential energy,

$$E^{tot} \longrightarrow \inf ! \qquad (2.47)$$

A necessary condition for the energy functional E^{tot} to reach an extreme value is the stationary condition in terms of vanishing first order variation,

$$\delta E^{tot}(\boldsymbol{\varphi}) = \delta \int_{\mathcal{B}_0} \mathscr{W}_0(\nabla \boldsymbol{\varphi}; \boldsymbol{X}) dV_0 - \delta \{ \int_{\mathcal{B}_0} \rho_0 \boldsymbol{b} \cdot \boldsymbol{\varphi} dV_0 - \int_{\partial \mathcal{B}_0} \boldsymbol{T} \cdot \boldsymbol{\varphi} dA \} = 0. \qquad (2.48)$$

The above expression (2.48) which is often called virtual displacement principle can also be expressed as,

$$\int_{\mathcal{B}_0} \nabla_{\boldsymbol{F}} \mathscr{W}_0 : \nabla_{\boldsymbol{X}} \delta \boldsymbol{\varphi} dV_0 - \int_{\mathcal{B}_0} \rho_0 \boldsymbol{b} \cdot \delta \boldsymbol{\varphi} dV_0 - \int_{\partial \mathcal{B}_0} \boldsymbol{T} \cdot \delta \boldsymbol{\varphi} dA = 0. \qquad (2.49)$$

Since

$$\nabla_{\boldsymbol{F}} \mathscr{W}_0 = \boldsymbol{\Pi}^t \qquad (2.50)$$

which is referred to as the elastic *constitutive law*, substituting this into (2.49) yields

$$\int_{\mathcal{B}_0} \boldsymbol{\Pi}^t : \nabla_{\boldsymbol{X}} \delta \boldsymbol{\varphi} dV_0 - \int_{\mathcal{B}_0} \rho_0 \boldsymbol{b} \cdot \delta \boldsymbol{\varphi} dV_0 - \int_{\partial \mathcal{B}_0} \boldsymbol{T} \cdot \delta \boldsymbol{\varphi} dA = 0. \qquad (2.51)$$

We recall, from the product property of vector differential calculus that

$$\mathrm{Div}(\delta \boldsymbol{\varphi} \cdot \boldsymbol{\Pi}^t) = \delta \boldsymbol{\varphi} \cdot \mathrm{Div} \boldsymbol{\Pi}^t + \boldsymbol{\Pi}^t : \nabla_{\boldsymbol{X}} \delta \boldsymbol{\varphi} \qquad (2.52)$$

This leads us to write

$$\int_{\mathcal{B}_0} \boldsymbol{\Pi}^t : \nabla_{\boldsymbol{X}} \delta \boldsymbol{\varphi} dV_0 = \int_{\mathcal{B}_0} \mathrm{Div}(\delta \boldsymbol{\varphi} \cdot \boldsymbol{\Pi}^t) dV_0 - \int_{\mathcal{B}_0} \delta \boldsymbol{\varphi} \cdot \mathrm{Div} \boldsymbol{\Pi}^t dV_0 \qquad (2.53)$$

Plugging this into (2.51) we have,

$$\int_{\mathcal{B}_0} \mathrm{Div}(\delta \boldsymbol{\varphi} \cdot \boldsymbol{\Pi}^t) dV_0 - \int_{\mathcal{B}_0} [\delta \boldsymbol{\varphi} \cdot \mathrm{Div} \boldsymbol{\Pi}^t + \rho_0 \boldsymbol{b} \cdot \delta \boldsymbol{\varphi}] dV_0 - \int_{\partial \mathcal{B}_0} \boldsymbol{T} \cdot \delta \boldsymbol{\varphi} dA = 0. \qquad (2.54)$$

Next, employing Divergence theorem , we bring the integral from volume to surface

$$\int_{\mathcal{B}_0} \text{Div}(\delta\boldsymbol{\varphi} \cdot \boldsymbol{\Pi}^t) dV_0 \;\; = \int_{\partial\mathcal{B}_0} \delta\boldsymbol{\varphi} \cdot \boldsymbol{\Pi}^t \cdot \boldsymbol{N} dA \tag{2.55}$$

Consequently, the expression in (2.54) reduces to

$$\int_{\mathcal{B}_0} \delta\boldsymbol{\varphi} \cdot [\text{Div}\boldsymbol{\Pi}^t + \rho_0 \boldsymbol{b}] dV_0 - \int_{\partial\mathcal{B}_0} \delta\boldsymbol{\varphi} \cdot [\boldsymbol{\Pi}^t \cdot \boldsymbol{N} - \boldsymbol{T}] dA = 0. \tag{2.56}$$

Comparing the expressions in (2.56) with the local equilibrium equation (2.44) renders

$$\boldsymbol{T} = \boldsymbol{\Pi}^t \cdot \boldsymbol{N} \;\; \text{on} \;\; \partial\mathcal{B}_0. \tag{2.57}$$

Subsequently we have the boundary value problem

$$\text{Div}\boldsymbol{\Pi}^t + \rho_0 \boldsymbol{b} = \boldsymbol{0} \;\; \text{in} \;\; \mathcal{B}_0 \tag{2.58}$$
$$\boldsymbol{T} = \boldsymbol{\Pi}^t \cdot \boldsymbol{N} \;\; \text{on} \;\; \partial\mathcal{B}_0$$

Consider now general boundary data, i.e. the case in which the boundary $\partial\mathcal{B}_0$ is subdivided into two regions Γ_0^u and Γ_0^σ corresponding to Dirichlet and Neumann boundary data obeying the following conditions

$$\Gamma_0^u \cup \Gamma_0^\sigma = \partial\mathcal{B}_0 \;, \quad \Gamma_0^u \cap \Gamma_0^\sigma = \varnothing$$

Thus, if the continuum is subjected to boundary conditions of the mixed type, that is,

$$\boldsymbol{\varphi}(\boldsymbol{X}) = \boldsymbol{u}_0, \;\; \forall \boldsymbol{X} \in \Gamma_0^u \;\; \text{and} \;\; \boldsymbol{T} = \boldsymbol{\Pi}^t \cdot \boldsymbol{N}, \;\; \forall \boldsymbol{X} \in \Gamma_0^\sigma \tag{2.59}$$

where the displacement boundary condition ensures the variational principle, because it is a constraint on the primary variable $\boldsymbol{u}$ and the space of trial functions. A trial function $\boldsymbol{\varphi} \in \mathscr{A}$, where

$$\mathscr{A} = \{\boldsymbol{\varphi} | \boldsymbol{\varphi}(\boldsymbol{X}) \in H^1(\mathcal{B}_0), \; \boldsymbol{\varphi}(\boldsymbol{X}) = \boldsymbol{u}_0 \;\; \forall \boldsymbol{X} \in \Gamma_0^u\} \tag{2.60}$$

is called kinematically admissible and the set[3] $\mathscr{A}$ constitutes the space of admissible deformations.

$$\int_{\partial\mathcal{B}_0} \delta\boldsymbol{\varphi} \cdot \boldsymbol{\Pi}^t \cdot \boldsymbol{N} dA = \int_{\Gamma_0^u} \delta\boldsymbol{\varphi} \cdot \boldsymbol{\Pi}^t \cdot \boldsymbol{N} dA + \int_{\Gamma_0^\sigma} \delta\boldsymbol{\varphi} \cdot \boldsymbol{\Pi}^t \cdot \boldsymbol{N} dA \tag{2.61}$$

But since $\delta\boldsymbol{\varphi} = 0$ along the Dirichlet boundary, hence

$$\int_{\partial\mathcal{B}_0} \delta\boldsymbol{\varphi} \cdot \boldsymbol{\Pi}^t \cdot \boldsymbol{N} dA \;\; = \int_{\Gamma_0^\sigma} \delta\boldsymbol{\varphi} \cdot \boldsymbol{\Pi}^t \cdot \boldsymbol{N} dA \tag{2.62}$$

Consequently, the boundary value problem (2.58) is recovered with the familiar Neumann type boundary conditions

$$\text{Div}\boldsymbol{\Pi}^t + \rho_0 \boldsymbol{b} \;\; = \boldsymbol{0}, \;\text{in} \;\; \mathcal{B}_0 \tag{2.63}$$
$$\boldsymbol{T} = \boldsymbol{\Pi}^t \cdot \boldsymbol{N}, \;\text{on} \;\; \Gamma_0^\sigma$$

---

[3]$H^1(\mathcal{B}_0) = W^{1,2} = \{\varphi \in L_2 \mid \partial^\alpha\varphi \in L_2(\mathcal{B}_0), \; \forall\alpha \; \text{a multi-index with} \; \|\alpha\| \leq 1 \}$

2.4.2 Extremum variational principle for elastic continuum

Any φ that satisfies the virtual displacement principle (2.49) is an equilibrium solution and the perturbation of the potential energy ΔE^{tot} around such an equilibrium configuration can be examined to yield

$$\Delta E^{tot} = E^{tot}(\varphi + \delta\varphi) - E^{tot}(\varphi)$$

$$= \int_{\mathcal{B}_0} \mathscr{W}_0(\nabla\varphi + \nabla\delta\varphi)dV_0 - \int_{\mathcal{B}_0} \mathscr{W}_0(\nabla\varphi)dV_0 - \int_{\mathcal{B}_0} \rho_0\boldsymbol{b}\cdot\delta\varphi dV_0 - \int_{\Gamma_0^\sigma} \boldsymbol{T}\cdot\delta\varphi dA \quad (2.64)$$

Upon replacing the integrand in the first term on the right hand side of the above equation by its second order Taylor approximation the whole expression reduces to

$$\Delta E^{tot} = \int_{\mathcal{B}_0} \nabla_{\boldsymbol{F}}\mathscr{W}_0 : \nabla\delta\varphi dV_0 - \int_{\mathcal{B}_0} \rho_0\boldsymbol{b}\cdot\delta\varphi dV_0 - \int_{\Gamma_0^\sigma} \boldsymbol{T}\cdot\delta\varphi dA + \int_{\mathcal{B}_0} \nabla\delta\varphi : \mathbb{L} : \nabla\delta\varphi dV_0$$

$$= \delta E^{tot} + \delta^2 E^{tot}. \quad (2.65)$$

where $\mathbb{L}$ is a fourth order two point tensor defined symbolically by

$$\mathbb{L} = \nabla_{\boldsymbol{F}} \otimes \boldsymbol{\Pi}^t \quad (2.66)$$

From equilibrium condition we have $\delta E^{tot} = 0$, as a result of which we have

$$\Delta E^{tot} = \delta^2 E^{tot} = \int_{\mathcal{B}_0} \nabla\delta\varphi : \mathbb{L} : \nabla\delta\varphi dV_0. \quad (2.67)$$

And hence, with this and the condition of strong ellipticity requirement on $\mathbb{L}$, we end up with the following second order variational inequality,

$$\Delta E^{tot} = \delta^2 E^{tot} > 0 \quad (2.68)$$

This in turn implies that for all kinematically admissible deformations $\varphi \in \mathscr{A}$ the equilibrium solution is a minimizer of the total potential energy of the crystal, as a result of this the corresponding configuration of the crystal is said to be stable. The pointwise form of the second order variational inequality which is given by

$$\nabla\delta\varphi : \mathbb{L} : \nabla\delta\varphi > 0 \quad (2.69)$$

30

characterizes the local phenomena. In the context of incremental elastic deformations, for a special case of $\nabla \delta \boldsymbol{\varphi}$ the expression in (2.69) reduces to

$$\boldsymbol{m} \otimes \boldsymbol{N} : \mathbb{L} : \boldsymbol{m} \otimes \boldsymbol{N} > 0, \quad \forall \boldsymbol{m} \otimes \boldsymbol{N} \neq \boldsymbol{0} \tag{2.70}$$

where $\boldsymbol{m}$ is an Eulerian and $\boldsymbol{N}$ is a Lagrangean tensor. But then, in view of the monograph by Ogden(1984) this allows interpretation connected to classification of the underlying equilibrium equations as elliptic systems where the use of the term is in accordance with the usual terminology of the theory of partial differential equations (Ellipticity will be revisited in chapter 4). In other words, among all kinematically admissible deformation fields which are also statically admissible there is a deformation $\tilde{\boldsymbol{\varphi}}$ such that

$$E^{tot}(\tilde{\boldsymbol{\varphi}}) \leq E^{tot}(\boldsymbol{\varphi}), \quad \forall \boldsymbol{\varphi} \in \mathscr{A} \tag{2.71}$$

The principle of minimum potential energy then reads as

$$E^{tot}(\tilde{\boldsymbol{\varphi}}) = \inf_{\boldsymbol{\varphi} \in \mathscr{A}} E^{tot}(\boldsymbol{\varphi}) \tag{2.72}$$

2.4.3 Localized convexity

In general, the strain energy density as a function of atomic positions can never be convex, see Appendix C for a quick survey. In this part, we shall see under what conditions one may speak about convexity of such densities. Essentially we shall establish sufficient condition for local convexity of the strain energy density $\mathscr{W}_0$. To this end, if $\boldsymbol{\varphi}$ and $\boldsymbol{\varphi}'$ are two kinematically admissible deformations with corresponding deformation gradients $\boldsymbol{F}$, $\boldsymbol{F}'$, nominal stresses $\boldsymbol{\Pi}^t$, $\boldsymbol{\Pi}^{t'}$ and body forces $\mathbf{b}$, $\mathbf{b}$' respectively, then (2.49) leads to

$$\int_{\mathcal{B}_0} [\boldsymbol{\Pi}^{t'} - \boldsymbol{\Pi}^t] : [\delta \boldsymbol{F}' - \delta \boldsymbol{F}] dV_0 \quad = \int_{\mathcal{B}_0} \rho_0 [\mathbf{b}' - \mathbf{b}].[\delta \boldsymbol{\varphi}' - \delta \boldsymbol{\varphi}] dV_0 \tag{2.73}$$
$$+ \int_{\Gamma_0^\sigma} [\boldsymbol{T}' - \boldsymbol{T}].[\delta \boldsymbol{\varphi}' - \delta \boldsymbol{\varphi}] dV_0.$$

If, in particular the body force is independent of $\boldsymbol{\varphi}$ and there is a *dead load* surface traction, the two integrals on the right hand side are identically zero, it then follows that

$$\int\limits_{\mathcal{B}_0} [\boldsymbol{\Pi}^{t'} - \boldsymbol{\Pi}^t] : [\delta \boldsymbol{F}' - \delta \boldsymbol{F}] dV_0 = 0 \tag{2.74}$$

and the corresponding local form is given by

$$[\boldsymbol{\Pi}^{t'} - \boldsymbol{\Pi}^t] : \delta[\boldsymbol{F}' - \boldsymbol{F}] = 0 \tag{2.75}$$

for all *variations* of $\boldsymbol{F}' - \boldsymbol{F}$ leading to

$$\boldsymbol{\Pi}^{t'} : \delta[\boldsymbol{F}' - \boldsymbol{F}] = \boldsymbol{\Pi}^t : \delta[\boldsymbol{F}' - \boldsymbol{F}]. \tag{2.76}$$

Now, if we assume that $\boldsymbol{F}'$ arises due to a small perturbation of $\boldsymbol{F}$, on the one hand we can write

$$\mathscr{W}_0(\boldsymbol{F}') = \mathscr{W}_0(\boldsymbol{F}) + \boldsymbol{\Pi}^t : \delta[\boldsymbol{F}' - \boldsymbol{F}] \tag{2.77}$$

and on the other hand from the first order Taylor approximation of $\mathscr{W}_0$ about $\boldsymbol{F}$ we have

$$\mathscr{W}_0(\boldsymbol{F}') = \mathscr{W}_0(\boldsymbol{F}) + \boldsymbol{\Pi}^t : [\boldsymbol{F}' - \boldsymbol{F}]. \tag{2.78}$$

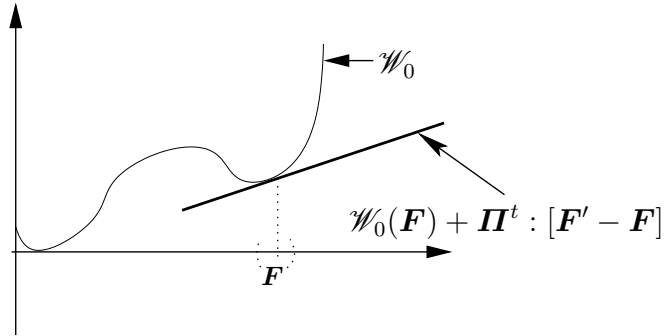Figure 2.8: Local (infinitesimal) convexity of $\mathscr{W}_0$

Since the characterization (2.75) is a pointwise condition, furthermore, $\mathscr{W}_0(\boldsymbol{F}) + \boldsymbol{\Pi}^t : \delta[\boldsymbol{F}' - \boldsymbol{F}]$ corresponds to a point on a hyperplane (tangent), thus, for a homogeneous stress field in the context of linearized theory superimposed on finite deformation the inequality

$$\mathscr{W}_0(\boldsymbol{F}') - \mathscr{W}_0(\boldsymbol{F}) - \boldsymbol{\Pi}^t : \delta[\boldsymbol{F}' - \boldsymbol{F}] > 0 \qquad (2.79)$$

has the meaning that in an infinitesimal neighborhood of the equilibrium deformation the epigraph of the elastic stored energy density $\mathscr{W}_0$ lies above the hyperplane (see figure 2.8). Evidently, for hyperelastic material with strain energy density $\mathscr{W}_0$, this states that $\mathscr{W}_0$ is strictly convex scalar function in an infinitesimal neighborhood of the equilibrium deformation $\boldsymbol{F}$ (cf. Ogden(1984) Sec. 6.2.2). Consequently, we state the sufficient condition for local (infinitesimal) convexity as

> **A strain energy density $\mathscr{W}_0$ of a hyperelastic continuum, which is assumed to be a scalar valued $C^2(\mathcal{B}_0)$ function is said to be infinitesimally convex provided that $\mathscr{W}_0(\boldsymbol{F}') - \mathscr{W}_0(\boldsymbol{F}) - \boldsymbol{\Pi}^t : \delta[\boldsymbol{F}' - \boldsymbol{F}] > 0$.**

2.5 Numerical investigation

The coupled model developed thus far is used to simulate an edge-crack in a rectangular specimen under tension. Uniform external loading is applied on the boundary of the specimen and the material is assumed to be homogeneous. As long as we are restricted to the quasistatic fracture problem, it is natural to presume that the initial state of the body is stable where the notion of stabilizer we employ here is that of a minimizer, i.e. the deformation φ of a body is said to be stable if it minimizes the total energy functional in the class of admissible deformations.
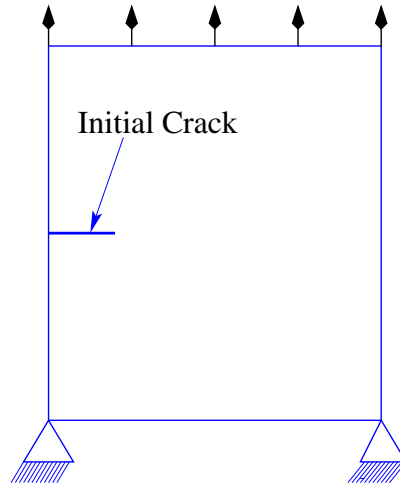

Figure 2.9: Model geometry of a homogeneous material with initial crack and loading conditions

In the context of standard finite element discretization procedures, the specimen is partitioned into constant-strain triangular elements with the crack aligned between elements such that the tip coincides with an element node. Furthermore, a one-point integration rule is used with the quadrature point made to coincide with the element centroid (see figure 2.10).

PSfrag replacements
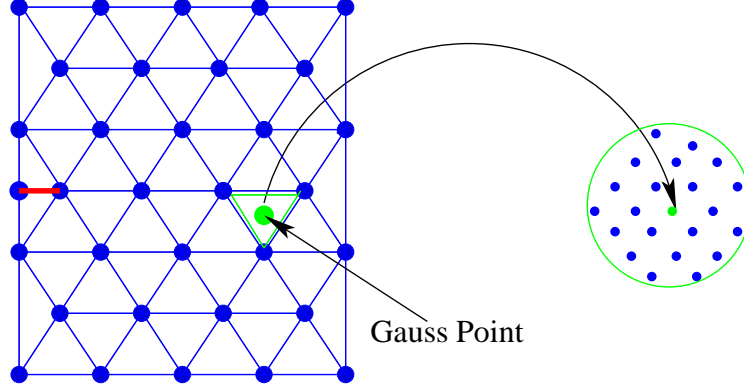
Gauss Point

FE node / Lattice atom

Figure 2.10: Schematic of Continuum-Atomistics

The deformation in the continuum is represented by the displacement at the element nodes and the nodal displacements are obtained by minimizing the total energy of the system subject to linear boundary conditions. Employing the expression given in (2.28), the strain energy density of each element is evaluated at quadrature point. Consequently, the element energy is obtained directly from an atomistic crystal computation, and for the purpose of this lattice based computation we attach the continuum to an imagined underlying crystal lattice as shown in figure 2.10 and then for each element we select an atom from the lattice which is closest or possibly coincides with the element centroid to serve as a representative atom. The energy of the selected atom is computed by considering a lattice of neighbors lying within a circle of radius r_c (cut-off circle).

2.5.1 Continuum deformation and crystallite

The energy extracted from atomistics (employing 2.28) is incorporated into the elastic constitutive law as described by the expression in (2.29). Since the constitutive equation as it stands in (2.29) defines a two-point tensor, for the solution strategy one may replace it by either its push-forward or pull-back depending on which configuration (reference or current) the problem is intended to be solved. In view of this, for the implementation of the boundary value problem (2.63) we use the push-forward of the constitutive equation (2.29) which renders the following expression

$$\boldsymbol{\sigma}^t = \frac{1}{2V} \sum_{j \neq i} \frac{\phi'}{r_{ij}} \boldsymbol{r}_{ij} \otimes \boldsymbol{r}_{ij}. \tag{2.80}$$

34

Herein $\boldsymbol{r}_{ij} = \boldsymbol{F} \cdot \boldsymbol{R}_{ij}$ is the lattice vector deformed according to the local deformation gradient $\boldsymbol{F}$ which is induced to the underlying lattice at each Gauss point that coincides with the element centroid in the finite element triangulation.
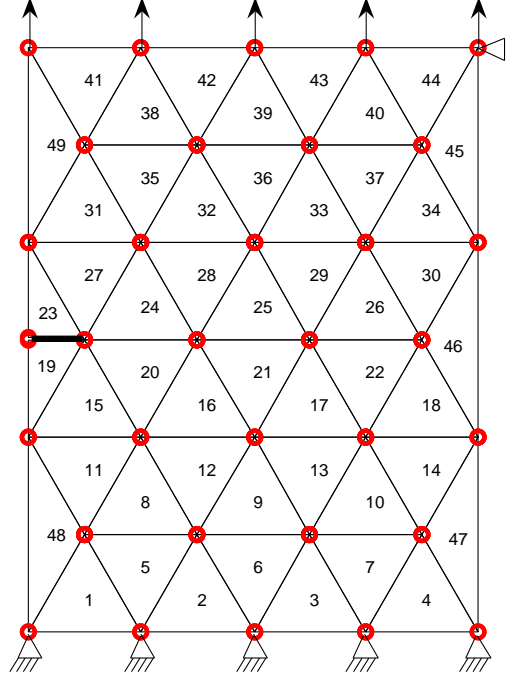

Figure 2.11: Finite element discretization of continuum with crack

In the computation of the stress tensor (2.80) or generally in the process of extracting element energy from atomistics, the interatomic separation which is essentially the length of the lattice vector in the deformed crystallite is computed by using the Cauchy-Born rule. Thus, based on the implementation of the boundary value problem formulated in (2.63), this section is devoted to the investigation of the Cauchy-Born rule.

Since this rule (2.26) states that crystal vectors deform in accordance with the local deformation gradient, the crystallite which represents an assumed collection of atoms which is attached to the continuum is distorted according to the local continuum deformation field $\boldsymbol{F}$ at the corresponding quadrature point of each element. For the one-point integration rule the quadrature point coincides with the element centroid and hence the continuum deformation is elaborated to the underlying crystal lattice at the element centroid.

In what follows, the boundary value problem (2.63) is subjected to uniform loading on the upper boundary. Zero displacement boundary conditions are applied on the lower boundary as indicated in figure 2.11. Subsequently, the crystal lattice in the deformed configuration is visualized and compared for those elements with node coincident with the crack tip (see figure 2.11).

35

In the finite element solution process, the continuum with crack (see figure 2.9) which is discretized into elements is subjected to uniform loading and zero displacement boundary condition is applied as shown in figure 2.11. Related to this opening-mode crack problem, figure 2.12 shows the deformed lattice corresponding to those elements with a common node coincident with the crack tip resulting from the computation based on the Cauchy-Born rule.
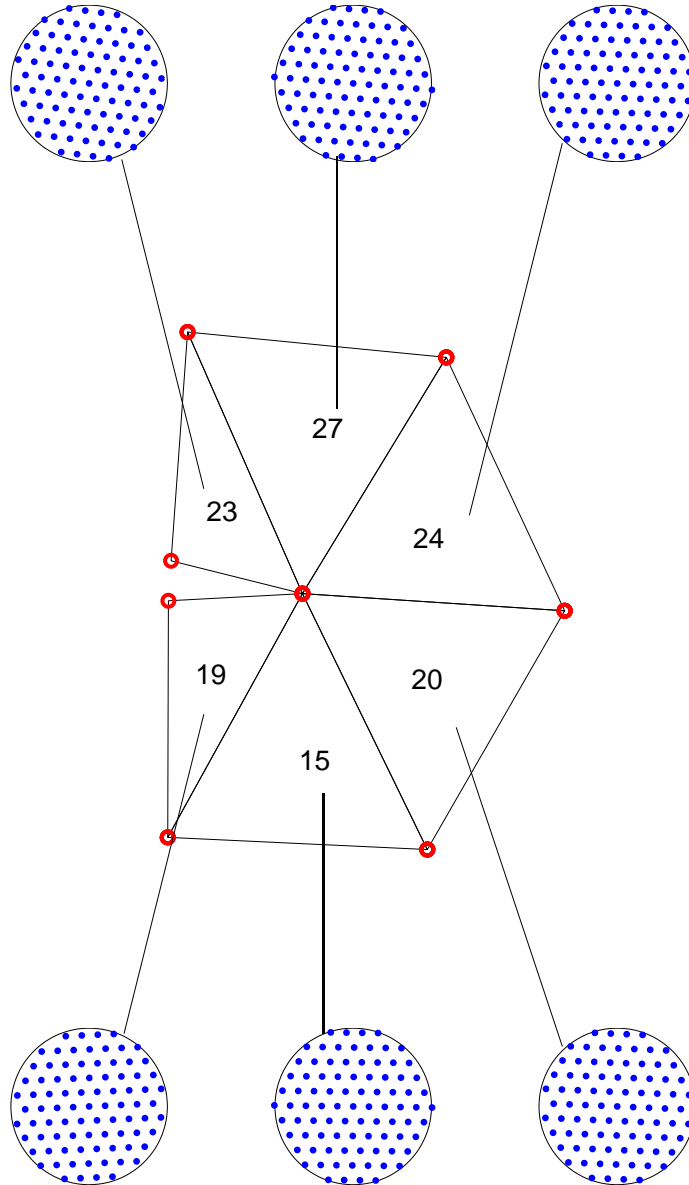

Figure 2.12: Deformed lattice and elements with node coincident with crack tip

The next figure is meant to give a perspective on the comparison of reference and deformed lattice for those elements with a node coincident with the crack tip as displayed in figure 2.12. For the atomistic based computation of energy, we attached an infinite lattice with identical atoms to the continuum. Consequently, the structure of the undeformed lattice included in the cut-off circle corresponding to each element in the discretization is the same. Based on this idea, the undeformed lattice corresponding to those elements with a common node at the crack tip is displayed at the center in figure 2.13. The non-center lattices visualized in the figure are the deformed lattices for the elements corresponding to the numbers indicated.

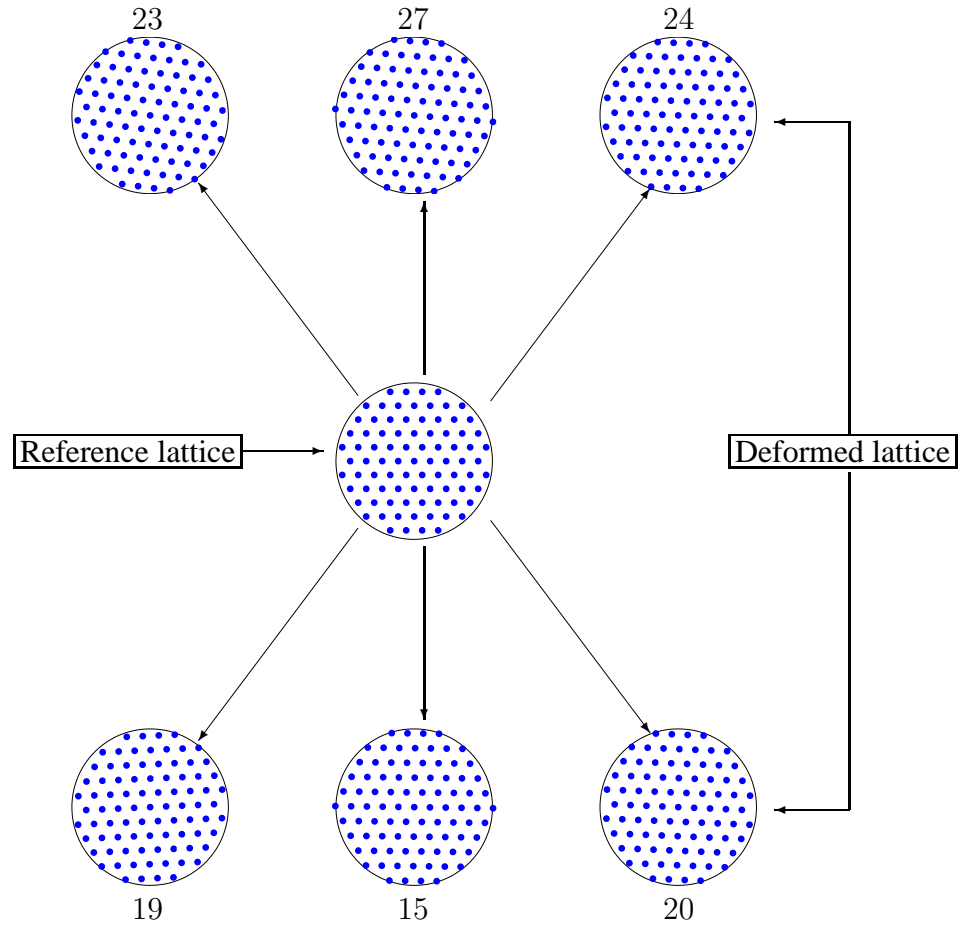Figure 2.13: Comparison of reference and deformed lattices for the six elements with the common node at the crack tip

In what follows we elaborate the results of the computation as based on the Cauchy-Born rule for different orientations of the crystallite. We considered four different orientations of the crystal lattice resulting from rotation of the original lattice counterclockwise through angles with measure

$0^0, 15^0, 30^0$ and 45^0, respectively. Each column of figure 2.14 corresponds to a rotation through a fixed angle and contains the reference and the deformed lattices computed employing the Cauchy-Born rule for each of the elements represented by the numbers indicated. Taking only one column at a time leads to comparison of the deformed lattices associated to each of the six elements and the corresponding undeformed lattice for a fixed rotation angle. Traversing along a row allows comparison of deformed lattices for different rotation angles but fixed element.
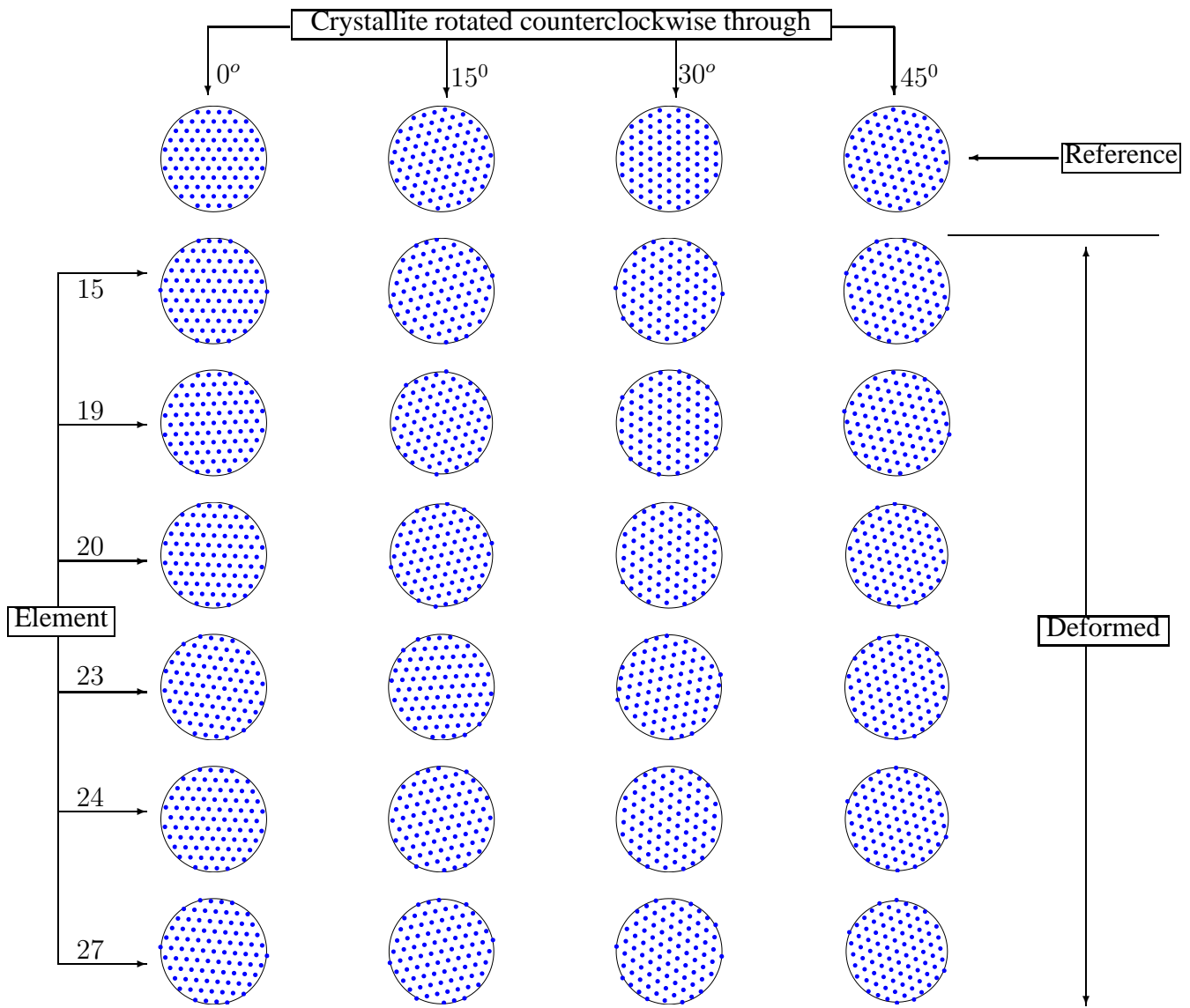

Figure 2.14: Comparison of deformed and reference lattice corresponding to rotation of a crystallite through $0^0, 15^0, 30^0$ and 45^0 angles, for the six elements with common node at the crack tip

CHAPTER 3

The Cauchy-Born rule and crystal elasticity

The Cauchy-Born rule is essentially a homogenization postulate in lattice kinematics and serves as a bridge establishing the link between atomistic process and continuum mechanics with the link to the continuum being the deformation gradient $\boldsymbol{F}$. In order to compute the strain energy density of a hyperelastic material from the interatomic potentials, a key ingredient is the Cauchy-Born rule, simply called Born rule (following Ericksen and Zanzotto). This essential but classical rule states that the crystal vectors defined by two nuclei deform in accordance with the local deformation gradient. The resulting local hyperelastic model describes the crystal behavior reasonably accurate as long as the continuum deformation is nearly homogeneous in the scale of the crystal vectors. The major restriction of the Cauchy-Born rule is that the continuum deformation needs to be homogeneous. This results from the fact that the underlying atomic system is deformed according to the continuum deformation gradient. In addition to the extraction of elastic material tensors, these models have been used in conjunction with finite element method to solve boundary value problems. In this section we will revisit the Cauchy-Born rule in a bit wider perspective.

3.1 Atomic lattice model

Consider a lattice generated by basis vectors $\{\mathbf{a}_i \mid i = 1, 2, 3\}$, the coordinates of an atom in the reference lattice is given by

$$\boldsymbol{R}(l) = \sum_i \ell^i \mathbf{a}_i \tag{3.1}$$

where $l = (\ell^1, \ell^2, \ell^3) \in \mathscr{L} \subset \mathbb{Z}^3$ is the lattice coordinate of an atom relative to this basis, $\mathbf{a}_1$, $\mathbf{a}_2$, $\mathbf{a}_3$ are linearly independent lattice elements (vectors) such that $\|\mathbf{a}_1\| = \|\mathbf{a}_2\| = \|\mathbf{a}_3\| = r_0$, lattice constant. In this model all lattice atoms are considered to be identical, i.e. we will be dealing with monatomic crystal lattice and only pairwise interaction is included in the definition of the potential energy. Furthermore, the structure is basis invariant, that is to say, the same lattice is generated by any two distinct bases

$$ B = \{\mathbf{a}_i \mid i = 1, 2, 3\} \quad \text{and} \quad \hat{B} = \{\hat{\mathbf{a}}_i \mid i = 1, 2, 3\} $$

as detailed in the Appendix **A**.
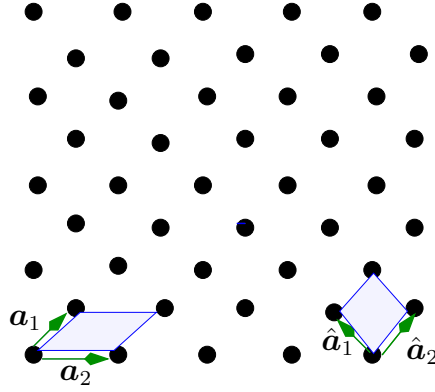
Figure 3.1: Two-dimensional lattice generated by bases $B = \{\boldsymbol{a}_1, \boldsymbol{a}_2\}$ and $\hat{B} = \{\hat{\boldsymbol{a}}_1, \hat{\boldsymbol{a}}_2\}$

If $\mathcal{L} = \{\boldsymbol{R}(l) \mid l \in \mathscr{L}\}$ is the collection of lattice sites occupied by the atoms, we specify a finite lattice in the reference configuration by

$$ \mathfrak{B}_o = \mathcal{L} \cap \Omega_L \quad \text{with} \quad \Omega \subset R^3 \text{ bounded}, \quad \Omega_L = \{L\boldsymbol{X} \mid \boldsymbol{X} \in \Omega, L \text{ a positive constant}\}. $$
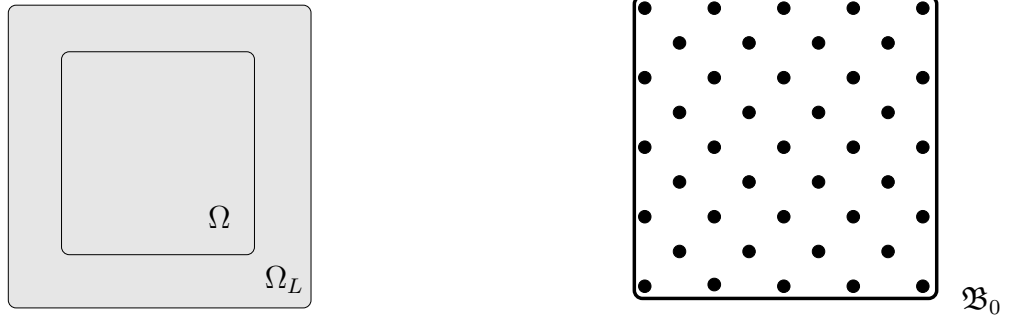
Figure 3.2: Two-dimensional domain Ω, its stretch Ω_L and finite lattice $\mathfrak{B}_0$

The deformation of the lattice is given by a discrete nonlinear map

$$\boldsymbol{\varphi} : \mathfrak{B}_o \longmapsto R^3.$$

Consequently, the total internal energy of the deformed lattice (following a suitable labeling) is described by the expression

$$E^{int}[\{\boldsymbol{\varphi}(\boldsymbol{R}_i)\}|\boldsymbol{R}_i \in \mathfrak{B}_o] = \frac{1}{2}\sum_i \sum_{j \neq i} \phi(\|\boldsymbol{\varphi}(\boldsymbol{R}_i) - \boldsymbol{\varphi}(\boldsymbol{R}_j)\|) \tag{3.2}$$

and the corresponding volume averaged lattice energy is given by

$$\frac{E^{int}}{V_L} = \frac{1}{2\,V_L}\sum_i \sum_{j \neq i} \phi(\|\boldsymbol{\varphi}(\boldsymbol{R}_i) - \boldsymbol{\varphi}(\boldsymbol{R}_j)\|), \quad \text{where} \quad V_L = \text{volume of } \Omega_L. \tag{3.3}$$

The model satisfies the principle of material frame indifference or objectivity, i.e. for any tensor $\boldsymbol{Q} \in SO(3)$,

$$E^{int}[\{\boldsymbol{\varphi}(\boldsymbol{R}_i)\}|\boldsymbol{R}_i \in \mathfrak{B}_0] \;\; = \;\; E^{int}[\{\boldsymbol{Q} \cdot \boldsymbol{\varphi}(\boldsymbol{R}_i)\}|\boldsymbol{R}_i \in \mathfrak{B}_0] \tag{3.4}$$

where $SO(3)$ denotes the set of orthogonal rotation tensors with determinant 1.

3.1.1 Energy minimization

In this part we aim at studying the property of volume averaged total energy of the lattice given by the expression in (3.3), thus, our goal is to describe the behavior of the optimization problem

$$\frac{E^{int}}{V_L} \longmapsto \min_{\boldsymbol{\varphi}} ! \tag{3.5}$$

with appropriate boundary conditions for various values of L. Here, the problem we are facing is two fold. First, determining the configuration of minimum potential energy of a cluster of identical atoms for a characteristic lengths L and then the description of variational limits of discrete lattice systems, i.e. asymptotic analysis of the resulting optimal configurations. An optimum (a minimizing) configuration is defined as the solution of the optimization problem

$$\min_{\boldsymbol{\varphi} \in \mathscr{A}}\frac{E^{int}}{V_L} := \mathscr{W}_{\Omega_L}(\boldsymbol{F}). \tag{3.6}$$

Since prescribing a homogeneous deformation on the atomic system amounts to prescribing the average (macroscopic) deformation gradient, this is therefore nothing but extracting the continuum-mechanical stored energy function from the atomistic model. In view of this, our chief objective

in describing the optimization problem (3.6) is to study the elastostatic response of the lattice to a prescribed deformation which leads to state the principle of minimum potential energy applied to the volume averaged quantity as follows

$$\frac{E^{tot}}{V_L} = \frac{E^{int}}{V_L} + \frac{E^{ext}}{V_L} \longmapsto \min_{\boldsymbol{\varphi}}! \tag{3.7}$$

The stationary points of (3.7) can be extracted from the corresponding variational problem. Thus, given a characteristic length L, the first variation of the volume averaged total potential energy is given by

$$\delta(E^{tot}) = 0. \tag{3.8}$$

This leads to local equilibrium at lattice atoms

$$\boldsymbol{f}_i(\boldsymbol{r}_{ij} \mid \boldsymbol{R}_i, \boldsymbol{R}_j \in \mathfrak{B}_0) = \boldsymbol{0} \tag{3.9}$$

$$\boldsymbol{r}_{ij} = \boldsymbol{r}_i - \boldsymbol{r}_j, \quad \boldsymbol{r}_i = \boldsymbol{\varphi}(\boldsymbol{R}_i)$$

whereby $\boldsymbol{f}_i$, the force acting on a lattice atom i due to its interaction with the rest of the members in the aggregate is given explicitly by

$$\boldsymbol{f}_i = \sum_{j \neq i} \boldsymbol{f}_{ij} \tag{3.10}$$

and the constitutive law of classical lattice statics is provided by

$$\boldsymbol{f}_{ij} = -\frac{\phi\prime}{r_{ij}} \boldsymbol{r}_{ij}. \tag{3.11}$$

The atomic level stiffness that constitutes a symmetric system stiffness matrix is given by

$$\boldsymbol{k}_{ij} = -\frac{\partial^2 E^{tot}}{\partial \boldsymbol{r}_j \otimes \partial \boldsymbol{r}_i} \tag{3.12}$$

In the subsection that follows, this stiffness matrix is used to compute the equilibrium energy per volume of a finite lattice implemented in the framework of lattice statics.

42

3.1.2 Lattice statics and equilibrium

The local equilibrium condition at each lattice atom requires that

$$-\frac{\partial E^{tot}}{\partial \boldsymbol{r}_i} = \boldsymbol{f}_i(\boldsymbol{r}_{ij} : j \in \{1, 2, .., N\} \setminus \{i\}) = \boldsymbol{0}, \quad i = 1, 2, ..., N \tag{3.13}$$

where N is the total number of atoms that make up the finite lattice.

We want to find a configuration corresponding to (3.13), and hence we solve the equilibrium equation (3.13) in the vicinity of an initial estimate $\{\boldsymbol{r}_i^0 : i = 1, 2, ..., N\}$. To this end, linearizing (3.13) around this ansatz leads to

$$\boldsymbol{f}_i = \boldsymbol{f}_i^0 + \frac{\partial \boldsymbol{f}_i}{\partial \boldsymbol{r}_i} \cdot [\boldsymbol{r}_i - \boldsymbol{r}_i^0] + \sum_{j \neq i} \frac{\partial \boldsymbol{f}_i}{\partial \boldsymbol{r}_j} \cdot [\boldsymbol{r}_j - \boldsymbol{r}_j^0] \tag{3.14}$$

$$= \boldsymbol{f}_i^0 + \boldsymbol{k}_{ii}^0 \cdot [\boldsymbol{r}_i - \boldsymbol{r}_i^0] + \sum_{j \neq i} \boldsymbol{k}_{ij}^0 \cdot [\boldsymbol{r}_j - \boldsymbol{r}_j^0]$$

Since $\boldsymbol{k}_{ii}^0 = -\sum\limits_{j \neq i} \boldsymbol{k}_{ij}^0$ we have

$$\boldsymbol{f}_i = \boldsymbol{f}_i^0 + \sum_{j \neq i} \boldsymbol{k}_{ij}^0 \cdot [(\boldsymbol{r}_j - \boldsymbol{r}_j^0) - (\boldsymbol{r}_i - \boldsymbol{r}_i^0)] \tag{3.15}$$

where,

$$\boldsymbol{f}_i^0 = \boldsymbol{f}_i(\boldsymbol{r}_{ij}^0 : j \in \{1, 2, .., N\} \setminus \{i\})$$

$$\boldsymbol{f}_i = \boldsymbol{f}_i(\boldsymbol{r}_{ij} : j \in \{1, 2, .., N\} \setminus \{i\})$$

$$\boldsymbol{k}_{ij}^0 = \frac{\partial \boldsymbol{f}_i}{\partial \boldsymbol{r}_j} \left(\boldsymbol{r}_{ij}^0 : j \in \{1, 2, .., N\} \setminus \{i\}\right)$$

and the out-of-balance force is given by

$$\boldsymbol{f} = \{\boldsymbol{f}_i\}_{i=1}^N$$

Setting $\boldsymbol{u}_i = \boldsymbol{r}_i - \boldsymbol{r}_i^0$, the *governing equation of lattice statics* is expressed as

$$\sum_{j \neq i} \boldsymbol{k}_{ij}^0 \cdot [\boldsymbol{u}_j - \boldsymbol{u}_i] = -\boldsymbol{f}_i^0, \quad i = 1, 2, ..., N \tag{3.16}$$

The equilibrium configuration can be obtained by solving (3.16). However, from the view point of implementation it is better to solve governing equation of lattice statics that explicitly involve the diagonal component of the stiffness matrix as follows

$$\boldsymbol{k}_{ii}^0 \cdot [\boldsymbol{r}_i - \boldsymbol{r}_i^0] + \sum_{j \neq i} \boldsymbol{k}_{ij}^0 \cdot [\boldsymbol{r}_j - \boldsymbol{r}_j^0] = -\boldsymbol{f}_i^0 \tag{3.17}$$

The harmonic lattice statics equation (3.17) is evaluated with zero displacement boundary condition for a finite lattice consisting of 15 atomic rows with the first row consisting of 18 atoms the second row 19 atoms, that way alternating between 18 and 19 atoms so as to mimic the pattern of the atoms in a (111)-plane of fcc type crystal.

Optim.

CBorn
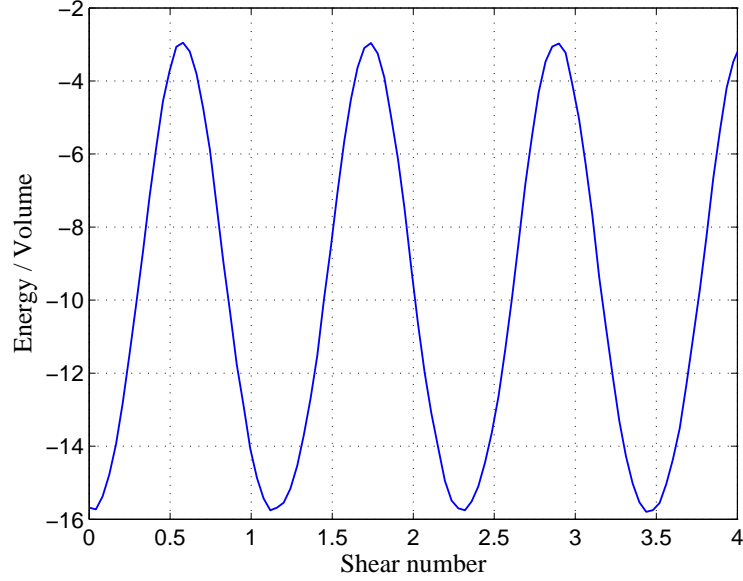
Figure 3.3: Energy per volume of the ground state

The lattice constant is taken to be 0.286nm, the values of the parameters of Lennard Jones interaction potential used are $\sigma = 0.1699$, $\epsilon = 0.2573$ and utilizing these the total internal energy per volume of the lattice at the ground state is computed. Accordingly, for simple shear deformation, figure 3.3 shows plot of the resulting energy per volume of equilibrium configuration versus shear number.

3.2 Discrete minimizers

In the preceeding subsection we solved discrete lattice statics problem and observed the behavior of the volume averaged total internal energy of the atomic system. In this part we shall investigate the behavior of such energy per volume of the ground state for increasing system size. With this in mind, we consider finite lattice of the type shown in figure 3.2 with four different sizes, i.e. we take lattice consisting different number of atoms and solve the harmonic lattice statics equation given in (3.17) for each size listed in the next table.

Lattice	Number of atomic rows	Number of atoms per row
1	9	11 resp. 10
2	11	16 resp. 17
3	15	18 resp. 19
4	17	19 resp. 20

Table 3.1: Finite lattice of different size

Since our aim is to study the effect of system size on the behavior of volume averaged energy of the lattice, we use the same lattice spacing and the same values for the parameters of the interaction potential as used in the preceeding subsection. Basically, the procedure of taking finite sized lattice might be understood as starting from the center of an infinite lattice, taking a finite portion and then proceeding from the same center to get the next finite lattice unequal to the previous. Once the lattice size and hence the number of atoms[1] in the lattice is determined, the minimum energy configuration is obtained from the solution of governing equilibrium equation (3.17) and the next task is computing energy per volume corresponding to that size. In line with this, figure 3.4 shows plot of energy per volume of the ground state against shear number for each of the four lattice sizes given in the above table 3.1.
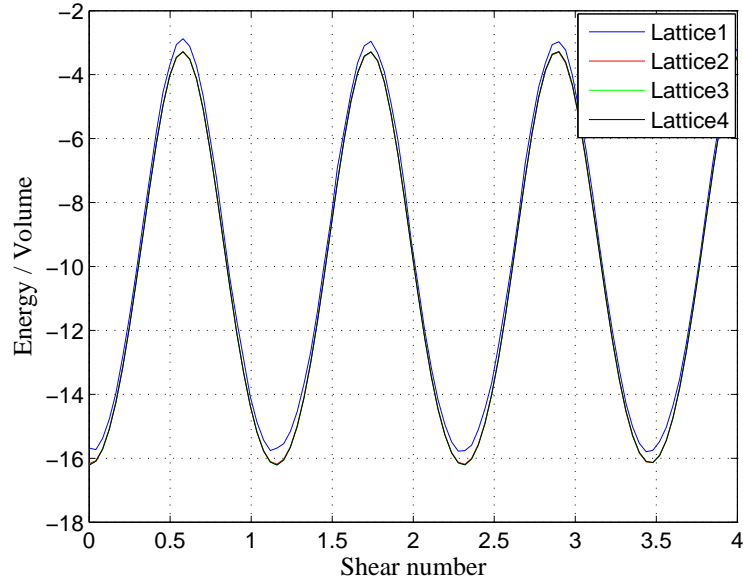
Figure 3.4: Energy per volume /vs Shear number

It can be seen from this result that, the volume averaged equilibrium energy for the different sized lattices show similar oscillatory behavior with the same period. For a better understanding of the result visualized in figure 3.4 and see the difference between energies resulting from different lat-

---

[1]11 resp.10 is meant to say 11 respectively 10 and corresponds to a row that alternates between 11 and 10 atoms

tice sizes, figure 3.5 gives a closer look at the result in the vicinity of a maximum and minimum point on the plot of energy per volume.

Figure 3.5: Comparison of energy per volume /vs Shear number at a peak and valley

3.2.1 Asymptotic behavior

In this investigation of increasing lattice size in connection with energy per volume of the ground state, the discrete minimizers tend to converge to minimizers of a limiting continuum theory defined on an appropriate space of functions, i.e. suitable Sobolev space whereby the feasible candidate for the limiting energy functional is given by

$$E_M(\boldsymbol{F}) = \int\limits_{\Omega} \mathscr{W}_0(\boldsymbol{F}; \boldsymbol{X}) d\boldsymbol{X} \tag{3.18}$$

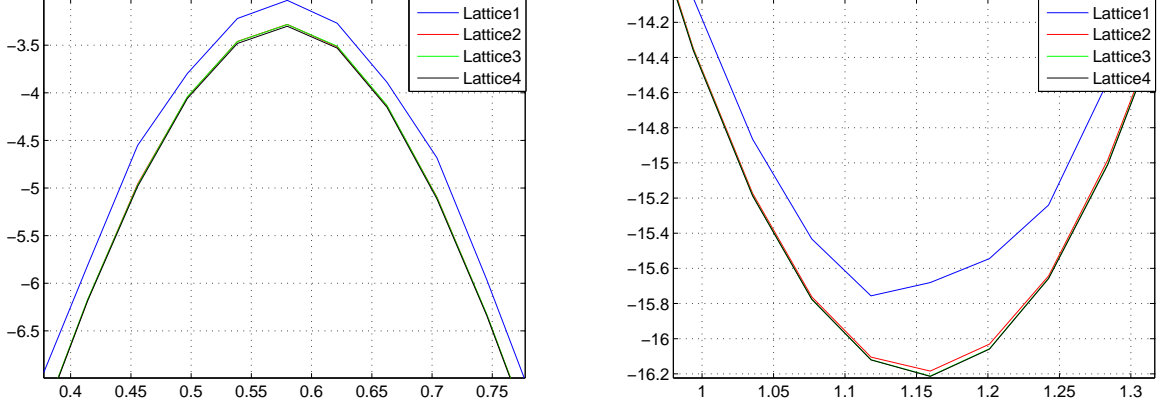with the strain energy density $\mathscr{W}_0(\boldsymbol{F}; \boldsymbol{X})$ arising from the Cauchy-Born rule and the deformation gradient $\boldsymbol{F}$ resulting from the underlying homogeneous deformation map.

A homogeneous deformation of a body from its reference configuration $\mathfrak{B}_0$ is a transformation,

$$\boldsymbol{X} \longmapsto \boldsymbol{F} \cdot \boldsymbol{X} + \boldsymbol{c}, \quad \boldsymbol{X} \in \mathfrak{B}_0 \tag{3.19}$$

where the vector **c** representing a grid translation of the whole body and the second order tensor $\boldsymbol{F}$ (the deformation gradient) are independent of the reference lattice placement $\boldsymbol{X}$.

In an effort to study the effect of system size on energetic behavior of the system, the finite lattices considered in table 3.1 and the corresponding volume averaged energy compared in figure 3.4 gave us a clear idea as to what the consequences of increasing characteristic length might be, i.e. what happens to the volume averaged energy of the ground state as the the system size gets larger. Based

46

on this observation, for the description of the asymptotic behavior of equilibrium lattice energy per volume we adopt the following notation, with $\mathscr{W}_{\Omega_L}$ as described in (3.6)

$$\lim_{L \longmapsto \infty} \mathscr{W}_{\Omega_L}(\boldsymbol{F}) := \overline{\mathscr{W}}(\boldsymbol{F}) \tag{3.20}$$

Referring to Friesecke et al.(2002) for the proof of *existence* of the above limit, in the process of linking such lattice based computation to a point of continuum, since one prescribes the atomic positions in the underlying lattice through application of the local deformation gradient following the Cauchy-Born rule, the asymptotic limit of the resulting Cauchy-Born state is given by

$$\lim_{L \longmapsto \infty} \frac{E^{int}[\{\boldsymbol{F} \cdot \boldsymbol{R}_i\}|\boldsymbol{R}_i \in \mathfrak{B}_0]}{V_L} := \mathscr{W}_{CB}(\boldsymbol{F}) \tag{3.21}$$

Thus, to determine an elastic response of a continuum with particular atomic structure based on discrete lattice statics computation, one can compute the change in the energy per volume of the crystallite by employing (3.21) where $\boldsymbol{F}$ is the deformation gradient at a given point of the continuum. In particular, if the deformation is homogeneous of the type given in (3.19), since it is an affine transformation of the whole lattice that does not affect individual interatomic distances, the asymptotic limits (3.20) and (3.21) are identical.

3.3   Energy decomposition

In what follows, we shall give an asymptotic formulation of the volume averaged internal energy based on the decomposition of energy into *bulk* and *surface* part. To this end, we shall make distinction between member atoms. A lattice atom j is said to be in the *bulk*, if the corresponding reference placement $\boldsymbol{R}_j \in \mathcal{L}_0 = \{\boldsymbol{R}_i | \boldsymbol{R}_i \in \mathcal{L} \ \& \ \boldsymbol{R}_i$ is center of a unit cell$\}$ and on the *surface* otherwise. We decompose the total internal energy of the lattice into bulk and surface part as

$$
\begin{aligned}
E^{int} &= E_b + E_s \\
&= \frac{1}{2} \sum_{\boldsymbol{R}_i \in \mathcal{L}_0}^{i} \sum_{j \neq i} \phi(\|\boldsymbol{\varphi}(\boldsymbol{R}_i) - \boldsymbol{\varphi}(\boldsymbol{R}_j)\|) + \frac{1}{2} \sum_{\boldsymbol{R}_i \in \mathcal{L} \backslash \mathcal{L}_0}^{i} \sum_{j \neq i} \phi(\|\boldsymbol{\varphi}(\boldsymbol{R}_i) - \boldsymbol{\varphi}(\boldsymbol{R}_j)\|)
\end{aligned} \tag{3.22}
$$

The volume contribution of a surface atom to the volume V_L of the region Ω_L is at most $\frac{2}{3} V_i$ where V_i is that of the ith atom in the bulk, furthermore the surface energy shows a linear relation with characteristic length L and hence doesn't contribute to the limit. Thus, for sufficiently large L expressing the volume V_L of the region Ω_L in terms of the volume of the Voronoi polyhedrons of member lattice atoms we may express the volume averaged lattice energy as a function of lattice parameter r_0 as follows,

$$\mathscr{W}_0 = \frac{1}{\sqrt{3} r_0^2} \sum_{\boldsymbol{R}_i \in \mathcal{L}_0}^{i} \sum_{j \neq i} \phi(\|\boldsymbol{\varphi}(\boldsymbol{R}_i) - \boldsymbol{\varphi}(\boldsymbol{R}_j)\|) \tag{3.23}$$

In the above formulation of energy density, the type of interaction taken into account is long-range interaction. Though it is not covered herein, it is also interesting to consider only nearest neighbor interactions, however in that case one has to introduce the notion of interfacial energy.

47

3.3.1 Validity and failure of the Cauchy-Born rule

This part is intended to visit a version of the Cauchy-Born hypothesis for monatomic crystals, which states that all atoms in a lattice consisting of identical atoms will follow a small linear displacement prescribed on the boundary. We study this hypothesis for finite lattice (as described in section 3.1) from the standpoint of energetics of the system. Since optimal energy of the atomic system will be obtained from the solution of constrained optimization problem given by

$$
\min_{\substack{\varphi \in \mathscr{A} \\ \varphi|_{\boldsymbol{R} \in \partial \mathfrak{B}_0} = \; \boldsymbol{F} \cdot \boldsymbol{R}}} \quad \frac{1}{2} \sum_i \sum_{j \neq i} \phi(\|\boldsymbol{\varphi}(\boldsymbol{R}_i) - \boldsymbol{\varphi}(\boldsymbol{R}_j)\|) \tag{3.24}
$$

and from the Cauchy-Born hypotheses, we know that minimum in (3.24) is attained when each lattice atom individually follows the prescribed deformation on the boundary, by this hypothesis therefore, the resulting optimal configuration should be unique, i.e. the corresponding deformation should be a unique minimizer. In this case, the optimal configuration (3.24) coincides with the Cauchy-Born state, consequently we have the next identity

$$
\min_{\substack{\varphi \in \mathscr{A} \\ \varphi|_{\boldsymbol{R} \in \partial \mathfrak{B}_0} = \boldsymbol{F} \cdot \boldsymbol{R}}} \quad \frac{1}{2} \sum_i \sum_{j \neq i} \phi(\|\boldsymbol{\varphi}(\boldsymbol{R}_i) - \boldsymbol{\varphi}(\boldsymbol{R}_j)\|) = \frac{1}{2} \sum_i \sum_{j \neq i} \phi(\|\boldsymbol{F} \cdot \boldsymbol{R}_i - \boldsymbol{F} \cdot \boldsymbol{R}_j\|) \tag{3.25}
$$

An obvious question that one may pose at this point is the magnitude of deformation, i.e. for how large a magnitude a given deformation satisfies the identity in (3.25). This is a question of stability where by a stable configuration we mean minimum energy configuration of the system. In what follows, we implement the optimization problem (3.24) for the first finite lattice given in table 3.1 employing this version of the Cauchy-Born hypothesis within the confines of lattice statics, i.e. we proceed to solve the harmonic lattice statics equation (3.17) for the lattice in figure 3.6 and compute the minimum energy state of the system subjected to linear deformation prescribed on boundary A, zero displacement boundary condition on boundary B, periodic boundary condition on boundaries C and D (as marked in figure 3.6) and all the non-boundary atoms are allowed to be free except for the interaction through the interatomic potential (Lennard Jones).
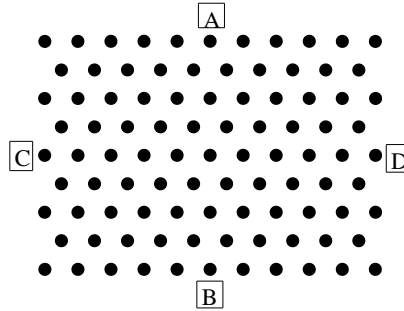

Figure 3.6: Finite lattice subject to linear deformation on boundary A

Thus, for a stereotype linear deformation simple shear applied on boundary A, the governing equation of harmonic lattice statics (3.17) solved in this context continues to render solution for some deformations and eventually the process of iteration runs into trouble after some load steps, i.e. gradually the stiffness matrix becomes rank-deficit and the method fails to solve the problem. This failure reflected in the rank of iteration matrix through deficiency can be explained in terms of the condition number. If we consider the situation before failure, the condition number of the iteration matrix as a function of shear number shows the behavior depicted in the next figure.
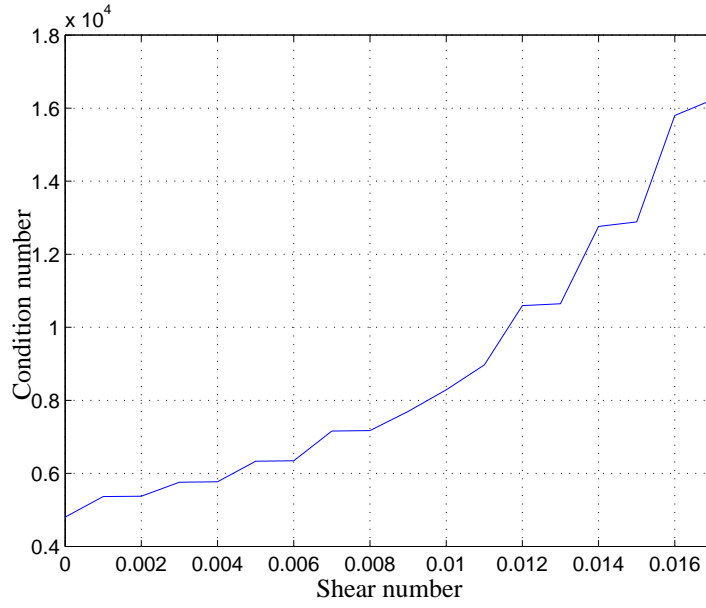
Figure 3.7: Condition number of the stiffness matrix /vs shear number before failure

This figure which shows the plot of condition number versus shear number before failure occurs in the iteration process, suggests that however we get equilibrium solution of the lattice statics equation the degree of accuracy of the solution deteriorates with increasing magnitude of deformation. In other words, one can say that the Cauchy-Born rule is valid for such small deformations in such a way that the degree of precision decreases with increasing magnitude of deformation.

Intending to see the scenario after failure we continue the iteration process, i.e. we proceed with our investigation of the condition number as a function of deformation and hence the Cauchy-Born hypothesis. In view of this, the next result gives further demonstration of the effect of increasing magnitude of deformation in the iterative solution procedure that leads to an ill-conditioned matrix beginning by a warning when using the iterative solver stating that the stiffness matrix may be rank deficient.
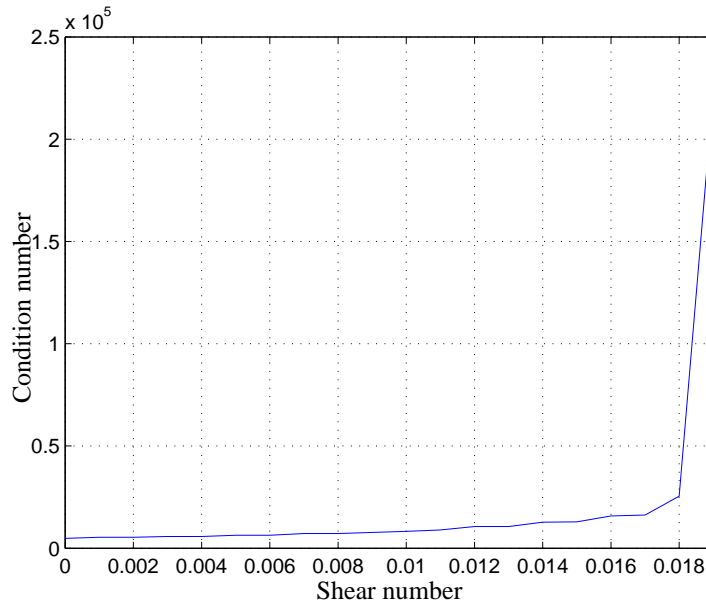
Figure 3.8: Condition number of the stiffness matrix /vs shear number

In this figure the portion of the plot until 0.018 value of the shear number corresponds to the case in which the iterative procedure provides solution with variable degree of accuracy. For a shear number a bit larger than 0.018 the solver sends warning message displaying the reciprocal condition estimator of the iteration matrix which is very close to 0, signaling that the matrix is close to singular and the result might be inaccurate. The portion of the plot beyond 0.018 shear number which shows an abrupt increase in the condition number corresponds to this situation. Thus, the value of deformation with shear number larger than 0.018 leads to instability of the system resulting in the formation of stacking fault whereby the atomic layer on the boundary that is subjected to deformation slide undeformed over the adjacent layer of atoms by non lattice translation. This failure is the effect of an overly severe deformation applied on the boundary atoms which is caused by the application of the Cauchy-Born hypothesis. Thus, models based on the Cauchy-Born rule makes sense for deformation with reasonably small magnitude such that the plastic limit won't be exceeded.

3.4   Unit cell of hexagonal lattice

In describing lattice structure one has to distinguish between the pattern of repetition (the lattice type) and what is repeated (the unit cell). Such a distinction begins with the observation that the atoms in a crystal are in a regular repeating pattern. The two important(among others) consequences of this repetition are the fundamental properties of crystal lattice, namely, symmetry and periodicity. These properties dictate the lattice to have a profound influence on the behavior of

50

a material. Based on the idea that a crystal is a repeating array, we may consider a crystal as a collection of identical unit cells stacked to fill the surface with the interatomic attractions taking the responsibility of cohesion. Indeed, interatomic forces are the reasons for the formation of crystals, since they are responsible for binding together. We consider a unit cell of hexagonal type and proceed to investigate the Cauchy-Born rule applied to the resulting lattice.

PSfrag replacements
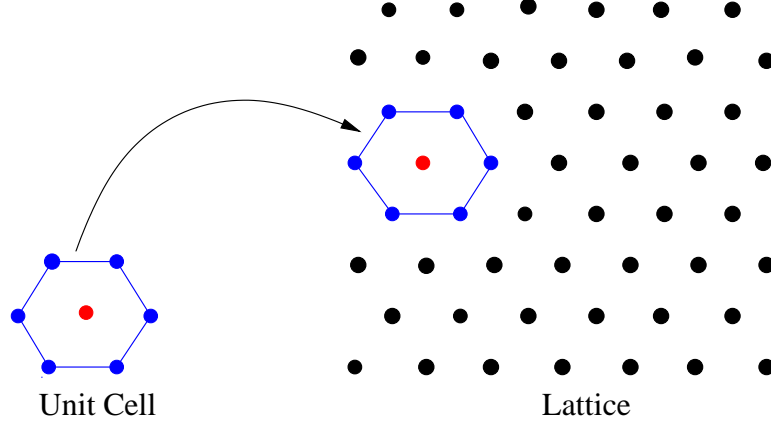
Unit Cell   Lattice

Figure 3.9: Hexagonal lattice created by stacking the unit cell

3.4.1   The Cauchy-Born rule and Lennard Jones potential

Thus far, except for examples our formulation was for any pair potential, here in this part we concentrate on the Lennard Jones potential and try to examine the Cauchy-Born rule. We commence by introducing the notion of unit cell for hexagonal lattice. Our discussion from hereon is confined to a configuration space of a lattice with a hexagonal unit cell. Here, we observe that any two unit cells have exactly two lattice atoms in common and this two atoms determine the corresponding interface.
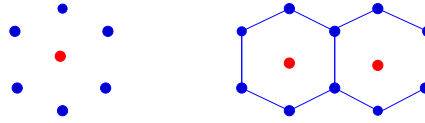
Figure 3.10: Unit cell of a hexagonal lattice and initial lattice depicting interface

The formulation in (3.25), like all lattice models makes physical sense for deformations φ whose modulus does not exceed the plastic limit. Thus, in what follows we shall show the condition under which the Cauchy-Born hypothesis holds true. To this end, we define a dimensionless parameter β as follows,

$$\beta = \frac{M}{r_o} \quad \text{where} \quad M := \max\{r_{ij} \mid j = 1, 2, ..., 6\} \tag{3.26}$$

A closer look at the graph of Lennard Jones potential reveals that there is an *inflection point* at a separation $(26/7)^{1/6}\,\sigma$ that corresponds to the maximum attractive force.
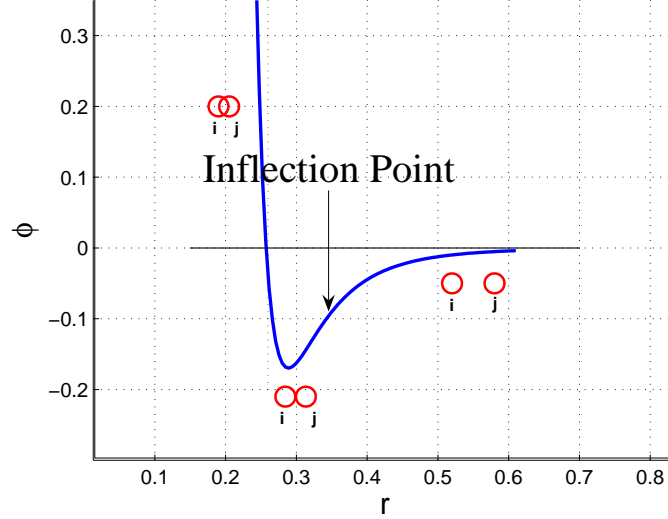
Figure 3.11: Schematic of atomic *orbitals* and Lennard Jones potential. The cohesive forces between atoms rise and fall on the scale of atomic separations with the minimum position corresponding to situation in which the orbitals are arbitrarily close while the overlap of orbitals is ruled out as impossible by Pauli exclusion principle.

Let us consider the parameter region from σ to the *inflection point*, and suppose that M lies in this region

$$\sigma < M < (26/7)^{1/6}\,\sigma$$

This leads to the following inequality

$$\frac{\sigma}{r_0} < \frac{M}{r_0} < \frac{(26/7)^{1/6}\,\sigma}{r_0}$$

and in turn this implies that

$$(1/2)^{1/6} < \beta < (13/7)^{1/6}$$

It is plain to see that in this parameter region $\mathscr{W}_0(\boldsymbol{F}) = \mathscr{W}_{CB}(\boldsymbol{F})$. Hence validity of the Cauchy-Born rule, i.e. the minimization problem (3.6) has a unique solution for each finite lattice $\mathcal{L}$. In particular, the case $\beta = 1$ corresponds to the deformation $\boldsymbol{F} = \boldsymbol{I}$, representing the hexagonal equilibrium state. The other parameter region, $0 < \beta < (1/2)^{1/6}$ corresponds to abrupt increase of internal energy to unfavorable large positive value that leads to instability[2]. In the third parameter

---

[2]The physical origin is related to Pauli Principle

region where $\beta > (13/7)^{1/6}$, a lattice atom almost doesn't feel the presence of other atom leading to de-cohesion of the system and hence resulting in the collapse of lattice. Evidently, in this region the magnitude of deformation exceeds the plastic limit beyond which dislocations are initiated.

In what follows we shall pursue a numerical experiment pertaining to this discussion. A one parameter family of deformations, the simple shear is described by the deformation gradient

$$\boldsymbol{F} = \boldsymbol{I} + \gamma \boldsymbol{e}_1 \otimes \boldsymbol{e}_2 \tag{3.27}$$

with $\boldsymbol{I}$ the identity tensor, γ the shear number and $\boldsymbol{e}_i, i = 1, 2$ Cartesian basis vectors. Assume that the hexagonal lattice is subjected to shearing deformation characterized by the deformation gradient given in the expression (3.27). In the process of deformation, atomic planes slip relative to one another as a result of which the interatomic separation between atoms in different planes change while the distance between those on the same plane remains unchanged (see figure 3.18a-c). Furthermore, by the construction of the hexagonal lattice, i.e. from the stacking arrangements of the unit cell, the volume averaged energy $\mathscr{W}_0$ is periodic in γ with the period $p = b/d$, where the scalar "b" is the magnitude of the translation vector and the quantity d is the distance between adjacent crystallographic planes with its value given in terms of lattice parameter by $d = (\sqrt{3}/2)r_0$. Our aim is to keep track of the interaction between lattice atoms, in particular we consider the interaction between atoms of a unit cell residing in different planes. To this end, we consider a lattice-angle[3] formed by lattice atoms of a unit cell in the model case of 2D as visualized in the next figure
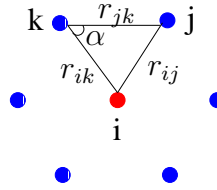
Figure 3.12: Bond-angle of a hexagonal unit cell in 2D

and consider an angle θ given by the expression

$$\theta = \Pi - \alpha. \tag{3.28}$$

where Π is the measure of a straight angle in units of radians. Since α can be expressed in terms of interatomic distances,

$$\alpha = acos \left(\frac{\boldsymbol{r}_{ik} \cdot \boldsymbol{r}_{ik} + \boldsymbol{r}_{jk} \cdot \boldsymbol{r}_{jk} - \boldsymbol{r}_{ij} \cdot \boldsymbol{r}_{ij}}{\|\boldsymbol{r}_{ik}\| \|\boldsymbol{r}_{jk}\|} \right) \tag{3.29}$$

---

[3]A hexagonal lattice also called an equilateral triangular lattice in 2D is described by either $\|\boldsymbol{a}_1\| = \|\boldsymbol{a}_2\|, \theta = 120^0$ or $\|\boldsymbol{a}_1\| = \|\boldsymbol{a}_2\|, \theta = 60^0$ where $\boldsymbol{a}_1$ and $\boldsymbol{a}_2$ are lattice basis vectors and θ is lattice angle.

therefore, it is a function of the associated deformation gradient through the relation given in (2.26). Thus, in particular for shear deformation the angle θ is a function of the shear number γ. Finally, implementing the governing equation (3.17) for the finite lattice with 9 atomic rows composed of 13/12/13... atoms per row, the computation of the secondary variable θ is made for the atom which is at the center of the lattice and the next result is obtained.
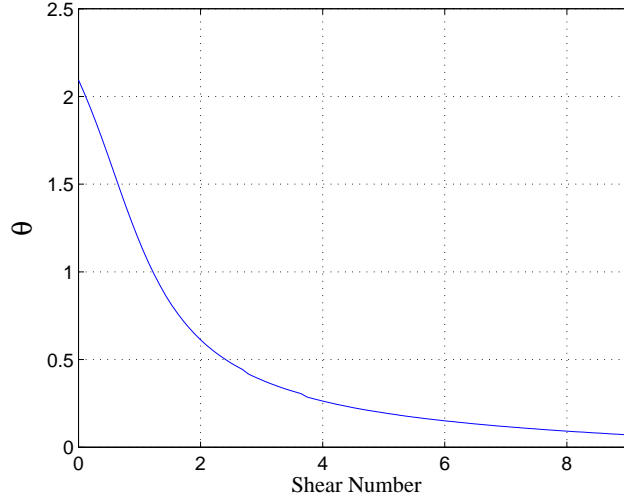
Figure 3.13: Measure of angle θ /vs shear number

The computational result in figure 3.13 shows that for large values of γ the measure of angle θ is getting closer to 0 radians implying that α is approaching *straight angle* which will be the case only if either the three lattice atoms are collinear or two of the lattice atoms residing on the same slip plane can no more be seen as distinct from the position of the third lattice atom. But since the lattice atoms forming vertices of *lattice-angles* lie in parallel slip planes, they can not be collinear and hence it means that the lattice atom at the center of the unit cell does not distinguish between the two atoms on the neighboring plane for large values of shear number. The interpretation associated with this is that the deformation is getting overly severe, from which we infer that the Cauchy-Born rule is not valid for large deformations.

3.5   Convex approximation of the potential

Central interaction potentials (Morse, Stillinger-Weber, Buckingham, Harmonic, Lennard Jones, etc) used to simulate atomic potential energy for a cluster of atoms and interaction forces between atoms have common features. A property common to all models based on these analytic potentials is the resemblance of the series(Taylor) expansion of the energy as a function of atomic positions. Pair potentials specially those defined by analytic formulae share common cut-off radii. Due to this, there are circumstances whereby such potentials can suitably be switched from one to another or even be combined within the confines of the range in which they are active. Since the harmonic potential is active for any pair of atom types for which both the cut-off radius r_c and the spring

constant k are positive, it can then replace any other pair potential that might be active in the same sense, but then only the spring constant k has to be specified. The Lennard-Jones potential is active for any pair of atom types for which both the cut-off radius r_c and the parameter ϵ are positive. Therefore, it is eligible for switching to harmonic potential.

3.5.1 Harmonic approximation of the interaction potential

In the Cauchy-Born parameter region it is often useful to approximate the Lennard Jones potential by a shifted Harmonic potential

$$\bar{\phi}(r_{ij}) = \bar{\phi}_0 + \frac{1}{2}k(r_{ij} - r_0)^2 \tag{3.30}$$

PSfrag replacements
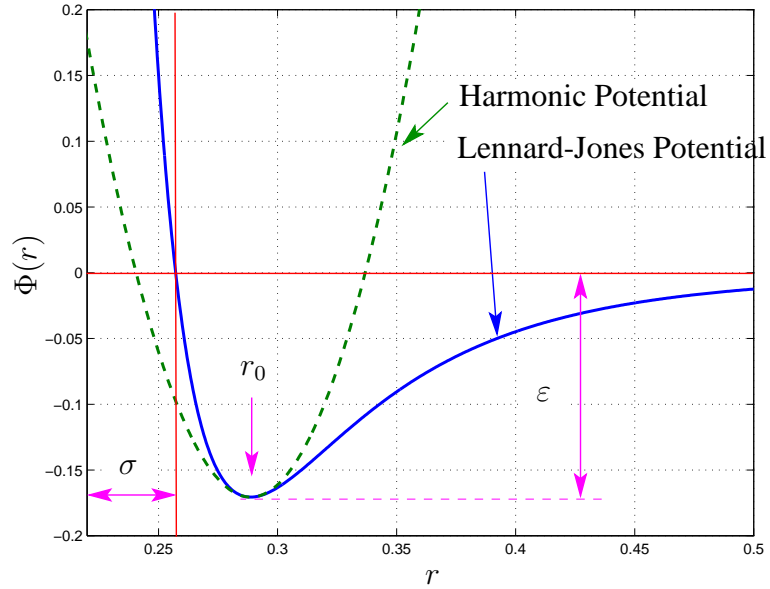
Figure 3.14: Lennard Jones potential and the Harmonic potential

The function given by the expression in (3.30) is the simplest convex approximation to the Lennard Jones potential and the fact that its minimum coincides with the potential well allows $\bar{\phi}_0$ to take-on the value $-\epsilon$. Furthermore, second order Taylor expansion of Lennard Jones potential around the equilibrium separation r_0 and subsequent comparison of the resulting expression with the one in (3.30) yields the value of the constant k which is $\frac{72\epsilon}{r_0^2}$. Recalling the relation between lattice constant r_0 and the Lennard Jones parameter σ, that is, $r_0 = 2^{\frac{1}{6}}\sigma$ leads to further simplification, $k = \frac{72\epsilon}{\sigma^2 2^{1/3}} = 57.15\frac{\epsilon}{\sigma^2}$, thereby rendering the force constant of the harmonic potential in terms of the parameters ϵ and σ of the Lennard Jones potential.

Having established this relation between the parameters of the two potentials, our objective is to solve the harmonic lattice statics equation (3.17) in the parameter region where switching between

Lennard Jones and harmonic potential is possible. To this end, we take a finite lattice consisting of 9 atomic rows with the rows consisting of either 13 or 12 atoms that follows the alternating pattern 13/12/13/12/13/12/13/12/13 between 13 and 12 atoms per row. With the focus on qualitative behavior, for the Lennard Jones potential the parameter values were taken to be $\sigma = 0.1699$, $\epsilon = 0.2573$ and the corresponding parameter of harmonic potential is computed from this values. Load and boundary conditions are applied to the specified finite lattice in the same spirit as in section 3.3.1, accordingly for simple shear deformation, the deformed positions of atomic nuclei obtained by employing the two potentials one after the other are visualized and compared in figure 3.16.
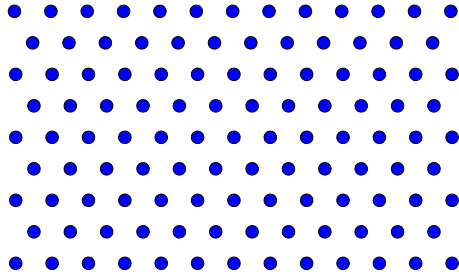
Figure 3.15: Reference configuration
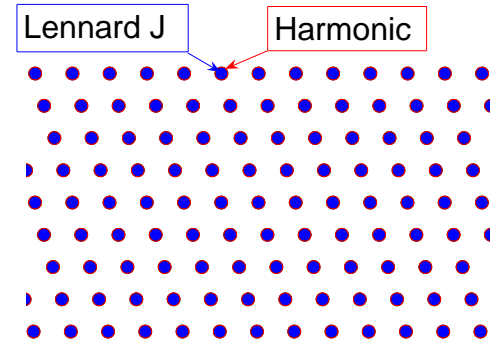
Figure 3.16: Deformed configuration

3.6 From unit cell to lattice

As mentioned in section 3.5, lattice structures can be considered as stacking arrangements[4] (nets) of unit cells. In view of this, the honeycomb like structure shown in figure 3.17 represents lattice generated by a hexagonal unit cell. Henceforth we refer to such lattice as hexagonal lattice.

3.6.1 Hexagonal lattice and the Cauchy-Born rule

Here, we revisit the Cauchy-Born rule as applied to hexagonal lattice structure. By the hypotheses of Cauchy-Born (2.26) each atom in the system follows the prescribed homogeneous deformation and hence each unit cell is individually expected to follow the average deformation encountered. Once again, implementing the harmonic lattice statics equation (3.17) for this structure with periodic boundary conditions so that the crystal lattice is reproducible throughout space, we compute the coordinates of the atomic nuclei that makeup the cells in the deformed lattice, with the main focus resting on the periodic property of the structure.

---

[4] **Atomistic hypotheses**:- A solid is not a continuum, but is rather built up from discrete subunits in a regular repetitive pattern
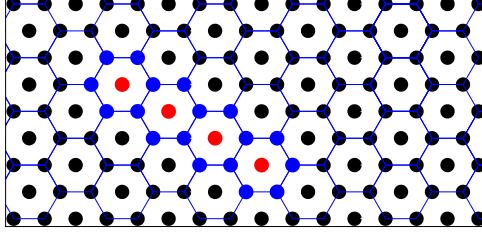
Figure 3.17: Reference Configuration

(a)

The above (figure 3.17) on the left represents the reference lattice and each of those on the right (figures 3.18a–c) depicts deformed (sheared) lattice corresponding to different deformation states. We used simple shear deformation, i.e. the structure is subjected to deformation of the type given by the expression in (3.27) and hence these results are obtained for different shear numbers each of which is less than one period where the period is as mentioned in section 3.5.1

To keep the model as simple as it could be, Lennard Jones pair potential is chosen for the description of the interaction. From the computation it can be seen that the unit cells which resemble Eulerian strain polygons of the continuum theory deform, smoothly stretching in one direction across a slip plane (line), closely obeying continuum elasticity until the shear number reaches one period. The change in the shape of the unit cells of the structure is due to the sliding of atomic planes past one another. Furthermore, all the unit cells in the lattice deform likewise, showing that the deformed structure is again periodic and thus, suggesting that one may concentrate only on the unit cell to study the behavior of the whole lattice.
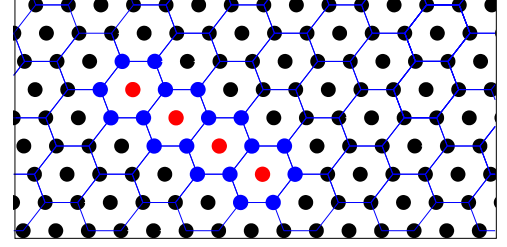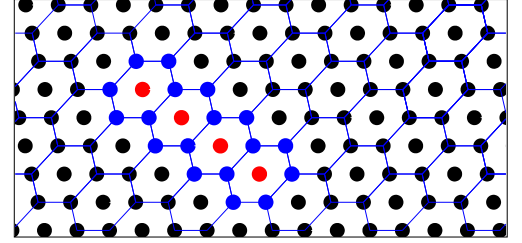
(b)
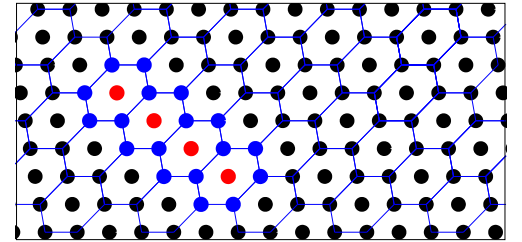
(c)

Figure 3.18: Current configurations corresponding to shear deformation

3.7 Atomic level stress

Stress at the atomic level can be seen from the standpoint of the interatomic forces arising from interactions between neighboring atoms in the collection(for an overview on stress computation at atomistic level see e.g. Cheung et al.(1991) and Cormier et al.(2001) or see the contribution by Herman et al.(1963) for a self-consistent atomic structure calculations and related problems). For the quantitative description of the stress locally at a given atom, one can consider an element of volume surrounding the atom and compute the force across each face of the element(In some cases Hellmann-Feynman theorem is helpful for the description and computation of forces at the atomic level see e.g. recent work by Nerbrant et al.(2004) or the contribution by Sorbello et al.(1980)). This procedure which is often called mechanical approach, despite the fact that it is conceptually plain, it is quite tedious in practice. Instead of this, the virial theorem, developed by Clausius and Maxwell used to determine the stress field applied on the surface of a fixed volume containing interacting particles (see Zimermann et al.(2004)) appears to be efficient. Indeed, the virial stress expression has become an invaluable computational diagnostic tool for simulations of phenomenon such as internal stress fields due to inhomogeneous precipitates (Zimermann et al.(2004)) and finite deformations leading to atomic scale plasticity. The virial stress is the most commonly used definition of stress in discrete particle systems and it depends not only on the interatomic forces but also on the atomic positions. Although the expression developed in the generalized virial theorem is both a time and spatial average, in the framework of lattice statics it reduces only to spatial average that relates stress to expected values. Here and hereafter, by the average stress theorem we mean the generalized virial theorem. Thus in what follows, the stress theorem which is known to be computationally effective and widely used in simulations is employed to describe the state of stress of a system of atoms, i.e. for the lattice generated by the hexagonal unit cell (see figure 3.17).

3.7.1 The average stress

The total stress of a stationary system can be derived by applying the variational principle(Nielsen et al.(1983, 1985)). Since the stress theorem is applicable to general systems with interactions which are differentiable functions of the particle coordinates, it can be employed in the case of particles interacting via pair potential leading to description of internal energy in the following form

$$E^{int} = \frac{1}{2} \sum_i \sum_{j \neq i} \phi(r_{ij}) \tag{3.31}$$

For such system, the symmetric form of the stress theorem is given by

$$t_{\alpha\beta} = - \sum_i \left\langle \frac{P_{i\alpha} P_{i\beta}}{m_i} \right\rangle - \frac{1}{2} \sum_i \sum_{j \neq i} \left\langle \frac{(\boldsymbol{r}_i - \boldsymbol{r}_j)_\alpha (\boldsymbol{r}_i - \boldsymbol{r}_j)_\beta}{|\boldsymbol{r}_i - \boldsymbol{r}_j|} \phi'(|\boldsymbol{r}_i - \boldsymbol{r}_j|) \right\rangle \tag{3.32}$$

where $\boldsymbol{P}_i$ is momentum tensor and $\boldsymbol{r}_i$ is the corresponding nuclear coordinate, $t_{\alpha\beta}$ is the component of stress intrinsic to the system due to bonded interactions and the angular bracket $\langle\cdot\rangle$ represents the expected value, i.e. averaging over all replicas.

For stationary system (Lattice statics) the momentum term is identically zero and hence (3.32) reduces to

$$t_{\alpha\beta} = -\frac{1}{2}\sum_i\sum_{j\neq i}\left\langle\frac{(\boldsymbol{r}_i-\boldsymbol{r}_j)_\alpha(\boldsymbol{r}_i-\boldsymbol{r}_j)_\beta}{|\boldsymbol{r}_i-\boldsymbol{r}_j|}\phi'(|\boldsymbol{r}_i-\boldsymbol{r}_j|)\right\rangle \tag{3.33}$$

For the periodic system under consideration, i.e. for the lattice built up from unit cells , the stress density is defined as

$$\sigma_{\alpha\beta} = -\frac{1}{2V}\sum_i\sum_{j\neq i}\left\langle\frac{(\boldsymbol{r}_i-\boldsymbol{r}_j)_\alpha(\boldsymbol{r}_i-\boldsymbol{r}_j)_\beta}{|\boldsymbol{r}_i-\boldsymbol{r}_j|}\phi'(|\boldsymbol{r}_i-\boldsymbol{r}_j|)\right\rangle \tag{3.34}$$

where V is the volume of the bounded domain corresponding to the finite lattice(see figure 3.2).

For a homogeneous stress field, the average stress(3.34) takes the format

$$\sigma_{\alpha\beta} = -\frac{1}{2V}\sum_i\sum_{j\neq i}\frac{(\boldsymbol{r}_i-\boldsymbol{r}_j)_\alpha(\boldsymbol{r}_i-\boldsymbol{r}_j)_\beta}{|\boldsymbol{r}_i-\boldsymbol{r}_j|}\phi'(|\boldsymbol{r}_i-\boldsymbol{r}_j|) \tag{3.35}$$

Consequently, the stress contribution of a representative atom is given by

$$\sigma_{\alpha\beta}^i = \frac{1}{2V_i}\sum_{j\neq i}\frac{(\boldsymbol{r}_i-\boldsymbol{r}_j)_\alpha(\boldsymbol{r}_i-\boldsymbol{r}_j)_\beta}{|\boldsymbol{r}_i-\boldsymbol{r}_j|}\phi'(|\boldsymbol{r}_i-\boldsymbol{r}_j|) \tag{3.36}$$

where V_i is the volume of the unit cell.

The next (figure 3.19) shows computation of the shear component of the atomic level stress and the volume averaged total energy for a cluster of atoms (a lattice generated by the unit cell), furthermore, makes comparison of the result. An important issue in multiscale mechanical modelling is the link between the effective(macroscopic) behavior observed at the continuum scale and the

phenomenon beneath the surface down to atomic scale. In this model, such a link is established by recourse to the Cauchy-Born rule(Ericksen(1984)) which connects the continuum variables to the atomistic quantities through the macroscopic deformation gradient.

Physically this stress can be interpreted as a quantity corresponding to the *pointwise* Cauchy stress[5], the continuum level stress at a quadrature point, the correspondence being established by the Cauchy-Born rule.
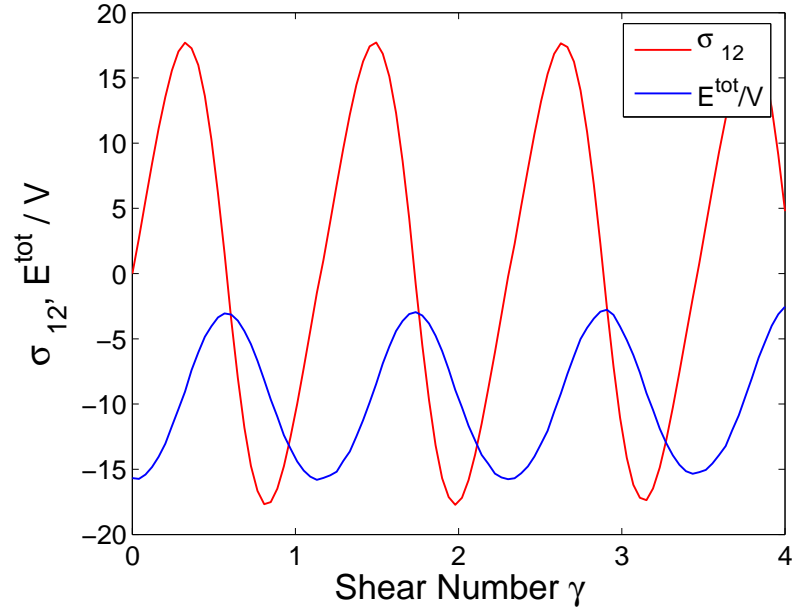
Figure 3.19: Average stress and volume averaged energy /vs Shear number

---

[5]$\boldsymbol{\sigma} = \frac{1}{V} \sum_i \left[m_i \boldsymbol{v}_i \otimes \boldsymbol{v}_i + \frac{1}{2} \sum_{j \neq i} \boldsymbol{r}_{ij} \otimes \boldsymbol{f}_{ij} \right]$ average virial stress over an effective volume[theorem of Clausius]

CHAPTER 4

Minimum energy state and feature of crystals

W*e must avoid here two complementary errors: on the one hand that the world has a unique, intrinsic, pre-existing structure awaiting our grasp; and on the other hand that the world is in utter chaos*

R. Abel,
Man is the Measure, New York: Free Press, 1976

In modelling materials within the confines of nonlinear elasticity, in particular from the standpoint of energetics one can come across different phases reflecting the diversity of internal structures of materials associated with different equilibrium states of elastic stored energy (see Dolzmann, Müller(1995)). In most cases, the appearance of these various phases is directly connected to the behavior of the strain energy density $\mathscr{W}_0$, such as its symmetry property which is inherited from the underlying crystal lattice. In connection with energy optimization, this leads to a non quasiconvex[1] variational problem and hence to the failure of the associated energy functional to be weakly lower semicontinuous, which is often the case for variational problems describing phase transforming materials particularly near the transformation temperature(for variational models in elasticity see Müller(1998) or Pedregal(1996) among others). Thus, emanating from symmetry invariance of the strain energy density that leads to multiple energy wells in general, the appearance of various phases in crystalline solids has a considerable impact on the elastic property of materials, and hence it is a centerpiece of study in materials research(see e.g. Luskin(1996) for the computation of crystalline microstructure or Bhattacharya et al.(1999) for phase transformation from cubic to orthorhombic in martensitic microstructures). In situations where there are several phases which are energetically feasible, variational problems dealing with energy minimization problems inevitably lead to the development of microstructure (fine inner structures) the relative stability of

---

[1]Ball(1977) introduced the notion of polyconvexity as a tool for characterizing strain energy density $\mathscr{W}_0$ as Morrey(1952) introduced earlier the notion of quasiconvexity for similar purpose.

which depends on the state of stress and other factors. These microstructures which are basically exhibited in an attempt to achieve the lowest possible energy are observed to influence the response of materials to different loading conditions(see e.g. Li(2002) for martensitic microstructure with homogeneous boundary condition) . Aluminum and steel are examples of materials that are capable of developing microstructures as observed in laboratory and also witnessed by simulation. If we consider the case of steel especially stainless steel, the relevant microstructure may be grouped into four major classes associated to different types, namely, Austenite, Ferrite, Martensite and Duplex.

Ferrite stainless steels have basically a bcc type crystal structure but with a change of temperature and some additional conditions of stabilization related to alloying content it transforms to austenite phase that is generally known to exhibit a single phase which is fcc type and is relatively stable over a wider range of temperature.

PSfrag replacements

bcc

fcc
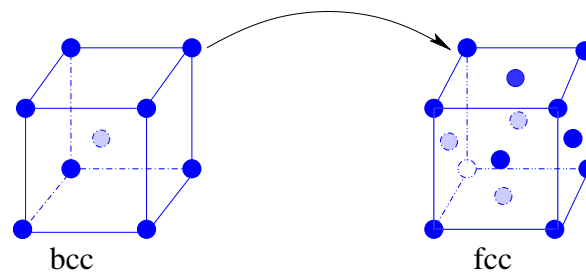
Figure 4.1: Crystallographic structure of steel, transition from ferrite(bcc) to austenite(fcc)

Motivated by problems from material science with tight focus on energetics, a central problem of interest in mechanics is concerned with the formation of microstructure and investigation of subsequent effects on the macroscopic behavior of materials(see e.g. Miehe et al.(2004) for microstructures in finite plasticity). In practice, where there is an obvious separation between length scales, for numerical computations one uses a suitably relaxed energy density that best approximates the configuration which can be achieved by the material via the development of microstructure. Here, the term relaxation is used in the spirit of the fundamental theorem of relaxation which one may roughly interpret as stating, *the energy functional resulting from the relaxed density gives the same infimum as the one obtained from the original density* (see e.g. Bhattacharya, Dolzmann(2000) for an overview on relaxed constitutive relation pertaining to phase transforming materials or Bouchitté et al.(1998) for a method of relaxation). In view of this, the formulation and use of relaxed energy density requires examination of all possible microstructures compatible with a prescribed macroscopic deformation(cf. Ball et al.(1987)). Thus, the central problem in this regard is devising an efficient technique of determining the relaxed energy density and integrating it into macroscopic computations(see e.g. Lambrecht et al.(1998) or Miehe et al.(2003) for

energy relaxation of incremental stress potentials). Unfortunately, no general algorithm as such to determine a relaxed energy of an arbitrary energy density is known thus far. Hence one way to circumvent this difficulty consists of considering a special class of microstructures that necessarily results in a partial relaxation of a given energy density. This naturally leads to restrict our attention to microstructures in the form of sequential laminate, i.e. resolving the development of several of the competing microstructures through successive branching process, laminate within laminate(see e.g. Pedregal(1993) Luskin(1997) or Kružík et al.(2003)). Such a procedure which captures the lowest energy density attainable by the material through sequential lamination is known as *rank-one convexification*. In the process of laminate construction, all microstructures generated by sequential lamination procedure should be in both static and configurational equilibrium(for a numerical approach to compatible phase transition see Carstensen et al.(2000)) and it is also required that the evolution of the microstructure during a deformation process satisfy the continuity constraint usually called rank-one compatibility condition in the sense that every new microstructure be reachable from the preceeding one along an admissible deformation path.

4.1   Lowest energy configuration

In this part we encounter problems of the type

$$\mathscr{I}(\boldsymbol{\varphi}) \longrightarrow \inf \ !$$

$$\text{where} \quad \mathscr{I}(\boldsymbol{\varphi}) = \int_{\mathcal{B}_0} \mathscr{W}_0(\boldsymbol{F}, \boldsymbol{\varphi}; \boldsymbol{X}) d\boldsymbol{X}, \ \ \boldsymbol{\varphi} \in \mathscr{A}_0 \tag{4.1}$$

$$\boldsymbol{F} = \nabla_{\boldsymbol{X}} \otimes \boldsymbol{\varphi}$$

$$\text{and} \quad \mathscr{A}_0 = \{\boldsymbol{\varphi} | \boldsymbol{\varphi} \in H^1(\mathcal{B}_0, \mathbb{R}^3), \boldsymbol{\varphi} = \boldsymbol{\varphi}_0 \text{ on } \partial \mathcal{B}_0\}$$

with $\mathcal{B}_0 \subset \mathbb{R}^3$ a bounded Lipschitz domain[2] and $\mathscr{W}_0 : \mathcal{B}_0 \times \mathbb{R}^3 \times \mathbb{R}^{3 \times 3} \to \mathbb{R}$ a continuous function satisfying the principle of material frame indifference, $\mathscr{W}_0(\boldsymbol{Q} \cdot \boldsymbol{F}) = \mathscr{W}_0(\boldsymbol{F})$ for all proper orthogonal tensors $\boldsymbol{Q} \in SO(3)$ and orientation preserving deformations $\boldsymbol{F} \in \mathbb{M}_+^{3 \times 3}$.

The case of primary interest right here is that the elastic stored energy density function $\mathscr{W}_0$ is not quasiconvex and hence nonconvex. An oft cited example of a non quasiconvex energy density is

$$\mathscr{W}_0(\boldsymbol{F}) = \min\{\mathscr{W}_0^i(\boldsymbol{F}) : i = 1, 2, \dots, N\} \tag{4.2}$$

---

[2]A bounded domain $\Omega \subset \mathbb{R}^n$ with boundary $\partial\Omega$ is said to be Lipschitz domain, if there exists constants $\alpha > 0, \beta > 0$, and a finite number of local coordinates $(x_1^r, x_2^r, ..., x_n^r)$, $1 \le r \le N$, and local Lipschitz continuous maps $f_r : \{\hat{x}^r = (x_2^r, ..., x_n^r) \in \mathbb{R}^{n-1} | \|x_i^r\| \le \alpha, 2 \le i \le n\} \to \mathbb{R}$ such that
$\partial\Omega = \cup_{r=1}^N \{(x_1^r, x^r) | x_1^r = f_r(\hat{x}^r), \|\hat{x}^r\| < \alpha\}$
$\{(x_1^r, \hat{x}^r) | f_r(\hat{x}^r) < x_1^r < f_r(\hat{x}^r) + \beta, \|x_i^r\| \le \alpha\} \subset \Omega, 1 \le r \le N,$
$\{(x_1^r, \hat{x}^r) | f_r(\hat{x}^r) < x_1^r - \beta < f_r(\hat{x}^r), \|x_i^r\| \le \alpha\} \subset \Omega^c, 1 \le r \le N,$ where $\Omega^c = \mathbb{R}^n \setminus \overline{\Omega}, \ \overline{\Omega}$ is the closure of Ω

such that for each i, $\mathscr{W}_0^i$ is a quasiconvex density representing the energy wells of the potential and $\mathscr{W}_0$ is the lower envelop, see Kohn(1991) for an overview or Carstensen et al.(1997) for the scalar double well problem.

For if, in (4.1) we impose the constitutive requirement that $\mathscr{W}_0(\cdot, \boldsymbol{\varphi}(\boldsymbol{X}); \boldsymbol{X}) : \mathbb{R}^{3\times3} \to \mathbb{R}$ be convex with respect to the deformation gradient $\boldsymbol{F}$, this hypothesis in conjunction with suitable smoothness and growth assumptions ensures the existence of a minimizer for (4.1). Indeed, existence theorems under this assumption have been provided by a number of authors, see e.g. the contribution by Beju(1971) the monograph by Oden(1973) or among others for abstract existence theorem and application to differential inclusion problems see the work of Dacorogna et al.(2002) and references therein. However, since the strain energy density $\mathscr{W}_0$ is required to be material frame indifferent,

$$\mathscr{W}_0(\boldsymbol{F}) = \mathscr{W}_0(\boldsymbol{Q} \cdot \boldsymbol{F}), \quad \forall \boldsymbol{Q} \in SO(3) \text{ and } \boldsymbol{F} \in \mathbb{R}_+^{3\times3} \tag{4.3}$$

this objectivity[3] requirement conflicts with the imposed convexity condition,

$$\mathscr{W}_0(\xi \boldsymbol{F}_1 + [1-\xi]\boldsymbol{F}_2) \leq \xi \mathscr{W}_0(\boldsymbol{F}_1) + [1-\xi]\mathscr{W}_0(\boldsymbol{F}_2), \quad \forall \boldsymbol{F}_1, \boldsymbol{F}_2 \in \mathbb{R}^{3\times3}, \, \xi \in [0,1]. \tag{4.4}$$

For the truth of this, $\mathscr{W}_0$ need not be convex and hence some less restrictive condition on $\mathscr{W}_0$ are therefore required. A suitable condition, quasiconvexity introduced by Morrey(1952) is then in place as the next candidate.

A continuous function [4] $\mathscr{W}_0 : U \to \mathbb{R}$ ($U \subset \mathbb{R}^{3\times3}$ an open set) is said to be *quasiconvex* if for any tensor $\boldsymbol{F} \in U$ and any sufficiently smooth test field $\boldsymbol{\eta} \in \mathcal{W}_0^{1,\infty}(\mathcal{B}_0, \mathbb{R}^3)$ compactly[5] supported on $\mathcal{B}_0$ it holds that

$$\int_{\mathcal{B}_0} \{\mathscr{W}_0(\boldsymbol{F} + \nabla\boldsymbol{\eta}(\boldsymbol{X}); \boldsymbol{X}) - \mathscr{W}_0(\boldsymbol{F}; \boldsymbol{X})\}d\boldsymbol{X} \geq 0 \tag{4.5}$$

for every open bounded subset $\mathcal{B}_0 \subseteq \mathbb{R}^3$, and *strongly quasiconvex* if there is a scalar $C > 0$ such that

$$\int_{\mathcal{B}_0} \{\mathscr{W}_0(\boldsymbol{F} + \nabla\boldsymbol{\eta}(\boldsymbol{X}); \boldsymbol{X}) - \mathscr{W}_0(\boldsymbol{F}; \boldsymbol{X})\}d\boldsymbol{X} \geq C \int_{\mathcal{B}_0} |\nabla\boldsymbol{\eta}(\boldsymbol{X})|^2 d\boldsymbol{X} \tag{4.6}$$

---

[3] A rigid rotation of the crystal should not change its stored energy.

[4] A mapping f: $\mathbb{R}^n \to R$ is said to be Lipschitz continuous if and only if there is a finite constant C such that $|f(\boldsymbol{X}_1) - f(\boldsymbol{X}_2)| < C\|\boldsymbol{X}_1 - \boldsymbol{X}_2\|$. Lipschitz continuity is a stronger condition than regular continuity

[5] If $U \subset \mathbb{R}^n$ is open, the support of a function $f : U \to R$ is a set $S = \{\boldsymbol{X} : f(\boldsymbol{X}) \neq 0\}$ and its compact support is the set $S_0 = \overline{S} \subseteq U$. An important consequence of compactness is that S_0 is bounded.

The condition (4.5) states that for all fluctuations $\boldsymbol{\eta}$ on $\mathcal{B}_0$ with support on $\partial \mathcal{B}_0$ the deformation $\boldsymbol{F}$ provides an absolute minimizer of the potential on the domain $\mathcal{B}_0$.

Morrey has shown that if $\mathscr{W}_0(\cdot, \boldsymbol{\varphi}; \boldsymbol{X})$ is quasiconvex for every deformation $\boldsymbol{\varphi}$, and on top of this if some continuity and growth[6] assumptions are satisfied then for various boundary value problems there exist a minimizer for the optimization problem (4.1) (see Morrey(1952, 1966)). However, the quasiconvexity condition which one may view as a constitutive restriction on the elastic stored energy density $\mathscr{W}_0$ may fail to hold.

In the event that $\mathscr{W}_0$ fails to be quasiconvex, the energy functional $\mathscr{I}$ in (4.1) is not sequentially weakly lower semicontinuous and therefore the optimization problem

$$M = \inf_{\boldsymbol{\varphi}} \{\mathscr{I}(\boldsymbol{\varphi}) : \boldsymbol{\varphi} \in \mathscr{A}_0\} \tag{4.7}$$

generally does not have any solution in $\mathscr{A}_0$.

The standard remedy in this case is, introducing the quasiconvex envelop[7] which is formally defined as the largest quasiconvex function not exceeding the given function, i.e.

$$\mathscr{W}_o^Q(\cdot, \boldsymbol{\varphi}; \boldsymbol{X}) = \sup\{\tilde{\mathscr{W}}_0 \mid \tilde{\mathscr{W}}_0 \leq \mathscr{W}_0(\cdot, \boldsymbol{\varphi}; \boldsymbol{X}) \text{ and } \tilde{\mathscr{W}}_0 \text{ is quasiconvex}\} \tag{4.8}$$

for all $\boldsymbol{X} \in \mathcal{B}_0$ and $\boldsymbol{\varphi} : \mathcal{B}_0 \rightarrow \mathbb{R}^3$, where we use standard function ordering in defining the inequality

$$\tilde{\mathscr{W}}_0 \leq \mathscr{W}_0(\cdot, \boldsymbol{\varphi}; \boldsymbol{X}) \tag{4.9}$$

to mean that

$$\tilde{\mathscr{W}}_0(\boldsymbol{F}) \leq \mathscr{W}_0(\boldsymbol{F}, \boldsymbol{\varphi}; \boldsymbol{X}), \quad \forall \boldsymbol{F} \in \mathbb{R}^{3 \times 3} \tag{4.10}$$

With the introduction of the quasiconvex envelop, the resulting functional

$$\mathscr{I}_Q(\boldsymbol{\varphi}) = \int_{\mathcal{B}_0} \mathscr{W}_0^Q(\nabla \boldsymbol{\varphi}) d\boldsymbol{X} \tag{4.11}$$

is sequentially weakly lower semicontinuous and the corresponding relaxed problem

$$\int_{\mathcal{B}_0} \mathscr{W}_0^Q(\nabla \boldsymbol{\varphi}) d\boldsymbol{X} \longrightarrow \quad \min ! \tag{4.12}$$

---

[6]The growth condition on $\mathscr{W}_0$ is usually given by $C_1 \|\boldsymbol{F}\|^p - C_0 \leq \mathscr{W}_0(\boldsymbol{F}), \forall \boldsymbol{F} \in \mathbb{R}^{3 \times 3}$ with C_0, C_1 positive constants and $1 < p < \infty$. Such a condition is convenient for theoretical justification of the approximation.

[7]An alternative and equivalent definition of the quasiconvex envelop of a function is given by

$$\mathscr{W}_0^Q = \frac{1}{V(\mathcal{B}_0)} \inf_{\boldsymbol{\eta} \in \mathcal{W}_0^{1,\infty}(\mathcal{B}_0, \mathbb{R}^3)} \int_{\mathcal{B}_0} \mathscr{W}_0(\boldsymbol{F} + \nabla \boldsymbol{\eta}) d\boldsymbol{X}$$

where $V(\mathcal{B}_0)$ is volume of the Lipschitz domain $\mathcal{B}_0$ and $\boldsymbol{\eta}$ is a test field.

has a solution $\tilde{\varphi} \in \mathscr{A}_0$ such that

$$\mathscr{I}_Q(\tilde{\varphi}) = \min_{\varphi \in \mathscr{A}_0} \mathscr{I}_Q(\varphi) \tag{4.13}$$

Eventually, following the relaxation theorem (see Dacorogna(1989) section 1), for such $\tilde{\varphi} \in \mathscr{A}_0$ which is a solution of (4.12), there exists a sequence of admissible elastic deformations

$$\{\varphi_k\}_{k \in \mathbb{N}} \subset \mathscr{A}_0 \tag{4.14}$$

which weakly converges to $\tilde{\varphi}$ in the Sobolev space $H^1(\mathcal{B}_0, \mathbb{R}^3)$ such that

$$\lim_{k \to \infty} \mathscr{I}(\varphi_k) = \mathscr{I}_Q(\tilde{\varphi}). \tag{4.15}$$

Henceforth, we call such a sequence of functions an infimizing sequence. The physical meaning of the envelop $\mathscr{W}_0^Q$ is that it represents the lowest energy density achievable by the material through the development of microstructures.

4.1.1 Loss of rank-one convexity

The notion of quasiconvexity which is based on integral condition (4.5) is not a pointwise condition on a function $\mathscr{W}_0$ and therefore, on the one hand verifying this condition as a nonlocal property is very difficult (Bartels, Carstensen, Hackel and Hoppe(2004) or Ball(1977)) in practice except for some specific cases, and on the other hand we almost never can find an analytical expression for a quasiconvex envelop of a particular function (Dolzmann(2000)). Hence, it is desirable to work with more accessible conditions which are closely related to the quasiconvex envelop.

A function $\mathscr{W}_0 : U \to R$ (with $U \subset \mathbb{R}^{3 \times 3}$ an open set) is said to be rank-one convex on U, if it is convex on all closed line segments in U with end-points differing by a tensor of rank 1, i.e.

$$\mathscr{W}_0(\xi \boldsymbol{F}_1 + [1 - \xi]\boldsymbol{F}_2) \leq \xi \mathscr{W}_0(\boldsymbol{F}_1) + [1 - \xi]\mathscr{W}_0(\boldsymbol{F}_2) \tag{4.16}$$

for any pair of tensors $\boldsymbol{F}_1$ and $\boldsymbol{F}_2$ in U satisfying the averaging constraint

$$\boldsymbol{F} = \xi \boldsymbol{F}_1 + [1 - \xi]\boldsymbol{F}_2, \quad \forall \xi \in [0, 1] \tag{4.17}$$

such that

$$\text{rank}(\boldsymbol{F}_1 - \boldsymbol{F}_2) \leq 1$$

Here and subsequently, we call $\boldsymbol{F}_1$ and $\boldsymbol{F}_2$ laminate deformations and ξ the volume fraction. In treating laminate deformations a property that one needs to pay due attention is stability(for some examples and further note on stability see e.g. DeSimone et al.(2000) or Efendiev et al.(2000)). Subject to the deformation $\boldsymbol{F}$, the material is said to be *stable* if the convex combination $\xi \boldsymbol{F}_1 + [1 - \xi]\boldsymbol{F}_2$ of the gradients $\boldsymbol{F}_1$ and $\boldsymbol{F}_2$ renders a higher energy level than the parent deformation gradient $\boldsymbol{F}$.

In the same spirit as in (4.8) one can define the corresponding envelop, the rank-one convex envelop $\mathscr{W}_0^R$ of the density function $\mathscr{W}_0$ as

$$\mathscr{W}_0^R(\cdot, \boldsymbol{\varphi}; \boldsymbol{X}) = \sup\{\tilde{\mathscr{W}}_0 \mid \tilde{\mathscr{W}}_0 \leq \mathscr{W}_0(\cdot, \boldsymbol{\varphi}; \boldsymbol{X}) \text{ and } \tilde{\mathscr{W}}_0 \text{ is rank-one convex}\} \quad (4.18)$$

Since quasiconvexity is a sufficient condition for rank-one convexity(see Dacorogna(1989) Chapter 4,Section 1), we have the inclusion relation

$$\mathscr{W}_0^Q \leq \mathscr{W}_0^R \leq \mathscr{W}_0 \quad (4.19)$$

from which one can see that $\mathscr{W}_0^R$ comprises the upper(outer) bounds of $\mathscr{W}_0^Q$. "*Indeed, this slightly weaker condition, the notion of rank-one convexity traces back to the work of Corall and Graves*"(Miehe et al.(2003)) see also Šilhavý(1997) for further details. A consequence of the relation (4.19) is that, by appeal to the fundamental theorem of relaxation we have the equalities

$$\min_{\boldsymbol{\varphi} \in \mathscr{A}} \int_{\mathcal{B}_0} \mathscr{W}_0^Q(\boldsymbol{F})d\boldsymbol{X} = \inf_{\boldsymbol{\varphi} \in \mathscr{A}} \int_{\mathcal{B}_0} \mathscr{W}_0(\boldsymbol{F})d\boldsymbol{X} = \inf_{\boldsymbol{\varphi} \in \mathscr{A}} \int_{\mathcal{B}_0} \mathscr{W}_0^R(\boldsymbol{F})d\boldsymbol{X} \quad (4.20)$$

where the set

$$\mathscr{A} = \{\boldsymbol{\varphi} \in \mathcal{W}^{1,\infty} : \boldsymbol{\varphi} = \boldsymbol{F} \cdot \boldsymbol{X} \text{ for } \boldsymbol{X} \in \partial\mathcal{B}_0\} \quad (4.21)$$

is the relevant space of admissible deformations.

However its detailed treatment is beyond the scope of this work, a closely related problem concerns the computation of generalized convex hulls of sets $K \subset \mathbb{R}^{3\times3}$. To mention a few, the quasiconvex hull K^{qh} of a given set K is defined by

$$K^{qh} = \{\boldsymbol{X} \in \mathbb{R}^{3\times3} : f(\boldsymbol{X}) \leq \sup_{\boldsymbol{Y} \in K} f(\boldsymbol{Y}), \text{ for all } f : \mathbb{R}^{3\times3} \to \mathbb{R}, f \text{ is quasiconvex}\} \quad (4.22)$$

and the rank-one convex hull K^{rh} of K is analogously defined. From their respective definitions, the relation between the aforementioned convex hulls and the set K itself leads to the following chain of inclusions, compare e.g. the contribution by Dolzmann et al.(2000).

$$K \subseteq K^{rh} \subseteq K^{qh} \quad (4.23)$$

Thus, in particular if K is the zero set of the elastic stored energy density

$$K = \{\boldsymbol{F} : \mathscr{W}_0(\boldsymbol{F}) = 0\} \quad (4.24)$$

then K^{rh} is closely related to the set of affine boundary conditions of the type mentioned in (4.21) for the variational problem (4.20) for which there exists a Lipschitz continuous function $\boldsymbol{\varphi}$ with $\mathscr{I}(\boldsymbol{\varphi}) = 0$, specifically, from (4.23) it follows that the rank-one convex hull of K gives an *inner bound* of the corresponding quasiconvex hull of the zero set *K*.

4.2   Infinitesimal rank-one convexity

In the definition (4.16) of rank-one convexity, we assumed $\mathscr{W}_0$ to be independent of the placement $\boldsymbol{X}$ and the elastic deformation map $\boldsymbol{\varphi}$. This is so because $\mathscr{W}_0$ is required to be rank-one convex only with respect to the third variable, the deformation gradient $\boldsymbol{F}$. Indeed, such an assumption of independence on $\boldsymbol{X}$ is possible for a locally isotropic continuum. Isotropy is a typical property of polycrystalline materials where there are no preferred directions in the material regarding its mechanical response and its meaning in mathematical terms requires that the energy density $\mathscr{W}_0$ satisfies

$$\mathscr{W}_0(\boldsymbol{F}) = \mathscr{W}_0(\boldsymbol{Q} \cdot \boldsymbol{F} \cdot \boldsymbol{Q}^t) \tag{4.25}$$

for all rotations $\boldsymbol{Q} \in SO(3)$ and tensors $\boldsymbol{F} \in \mathbb{R}^{3\times 3}$

Something one possibly notices here is that, verifying rank-one convexity directly from definition (4.16) is generally difficult. However, for the local version of the problem there is a way out. We recall that, for a twice differentiable stored energy density $\mathscr{W}_0$, the rank-one convexity definition (4.16) of the preceeding subsection is related to the strong ellipticity condition (2.69). The weak form of condition (2.70) also called the classical Legendre-Hadamard condition, given by the expression

$$\boldsymbol{m} \otimes \boldsymbol{N} : \frac{\partial^2 \mathscr{W}_0}{\partial \boldsymbol{F} \otimes \partial \boldsymbol{F}} : \boldsymbol{m} \otimes \boldsymbol{N} \geq 0 \tag{4.26}$$

where $\boldsymbol{m}, \boldsymbol{N} \in \mathbb{R}^3$ are first order tensors and $\boldsymbol{F}$ is a second order tensor, is employed in many situations to check the uniqueness of a minimizer.

The expression in (4.26) alternatively called infinitesimal rank-one convexity condition is used to assess such a uniqueness of solution only in the local sense, that is to say in a small neighborhood of a given deformation as the name itself imply. Referring to Ball(1977) for a general survey and further details, we however mention that the degree of regularity required for condition (4.26) is fairly severe, namely, $\mathscr{W}_0$ needs to be twice continuously differentiable and this by itself is imposing a constitutive restriction on the strain energy density $\mathscr{W}_0$ thereby making the condition somewhat expensive to be employed in as many situations as one needs. Intending to circumvent this difficulty at least for a certain class of problems, we visit dead load boundary value problems.

4.2.1   Dead loads and sufficient condition for uniqueness

In an effort to formulate a less restrictive condition we proceed by making a choice between the class of admissible deformations. We consider a class of deformations with dead loading on the boundary. Thus, if $\boldsymbol{\varphi}_1$ is a given solution of (2.63) and $\boldsymbol{\varphi}_2$ is an arbitrary kinematically admissible

68

deformation which is also a solution of (2.63) satisfying the boundary condition with corresponding deformation gradients $\boldsymbol{F}_1$ and $\boldsymbol{F}_2$, Piola-Kirchhoff stresses $\boldsymbol{\Pi}_1^t$ and $\boldsymbol{\Pi}_2^t$ and body force fields per unit mass $\boldsymbol{b}_1$ and $\boldsymbol{b}_2$ respectively then setting

$$\boldsymbol{\Psi} = \boldsymbol{\varphi}_1 - \boldsymbol{\varphi}_2 \tag{4.27}$$

we have

$$\boldsymbol{F} := \frac{\partial \boldsymbol{\Psi}}{\partial \boldsymbol{X}} = \frac{\partial \boldsymbol{\varphi}_1}{\partial \boldsymbol{X}} - \frac{\partial \boldsymbol{\varphi}_2}{\partial \boldsymbol{X}} = \boldsymbol{F}_1 - \boldsymbol{F}_2 \tag{4.28}$$

The superposed deformation $\boldsymbol{\Psi}$ satisfies the pointwise equation (2.63) and hence it should also satisfy the homogeneous equation

$$\boldsymbol{\Psi} \cdot \mathrm{Div}\boldsymbol{\Pi}^t + \rho_0 \boldsymbol{\Psi} \cdot \boldsymbol{b} = 0 \tag{4.29}$$

Since this is true $\forall \, \boldsymbol{X} \in \mathcal{B}_0$, it follows that

$$\int_{\mathcal{B}_0} [\boldsymbol{\Psi} \cdot \mathrm{Div}\boldsymbol{\Pi}^t + \rho_0 \boldsymbol{\Psi} \cdot \boldsymbol{b}]d\boldsymbol{X} = 0 \tag{4.30}$$

Obviously, the body force and the stress accompanying the superposed deformation $\boldsymbol{\Psi}$ follow directly from their definitions and are given respectively by

$$\boldsymbol{b} = \boldsymbol{b}_1 - \boldsymbol{b}_2, \text{ and } \boldsymbol{\sigma} = \boldsymbol{\sigma}_1 - \boldsymbol{\sigma}_2 \tag{4.31}$$

From the version of the product rule of divergence operator we have

$$\boldsymbol{\Psi} \cdot \mathrm{Div}\boldsymbol{\Pi}^t = \mathrm{Div}(\boldsymbol{\Psi} \cdot \boldsymbol{\Pi}^t) - \boldsymbol{\Pi}^t : \nabla_X \otimes \boldsymbol{\Psi} \tag{4.32}$$

This allow us to rewrite the expression in (4.30) as

$$\int_{\mathcal{B}_0} \mathrm{Div}(\boldsymbol{\Psi} \cdot \boldsymbol{\Pi}^t)d\boldsymbol{X} - \int_{\mathcal{B}_0} \boldsymbol{\Pi}^t : \nabla_X \otimes \boldsymbol{\Psi}d\boldsymbol{X} + \int_{\mathcal{B}_0} \rho_0 \boldsymbol{\Psi} \cdot \boldsymbol{b}d\boldsymbol{X} = 0 \tag{4.33}$$

This in turn implies that

$$\int_{\mathcal{B}_0} \boldsymbol{\Pi}^t : \nabla_X \otimes \boldsymbol{\Psi}d\boldsymbol{X} = \int_{\mathcal{B}_0} \mathrm{Div}(\boldsymbol{\Psi} \cdot \boldsymbol{\Pi}^t)d\boldsymbol{X} + \int_{\mathcal{B}_0} \rho_0 \boldsymbol{\Psi} \cdot \boldsymbol{b}d\boldsymbol{X} \tag{4.34}$$

Recalling that $\boldsymbol{\Psi} = \boldsymbol{\varphi}_1 - \boldsymbol{\varphi}_2$ and using (4.28) the above expression (4.34) reduces to

$$\int_{\mathcal{B}_0} [\boldsymbol{\Pi}_1^t - \boldsymbol{\Pi}_2^t] : [\boldsymbol{F}_1 - \boldsymbol{F}_2]d\boldsymbol{X} = \int_{\mathcal{B}_0} \mathrm{Div}([\boldsymbol{\varphi}_1 - \boldsymbol{\varphi}_2] \cdot \boldsymbol{\Pi}^t)d\boldsymbol{X} + \int_{\mathcal{B}_0} \rho_0[\boldsymbol{\varphi}_1 - \boldsymbol{\varphi}_2] \cdot \boldsymbol{b}d\boldsymbol{X}$$

By the divergence theorem

$$
\begin{aligned}
\mathrm{Div}([\boldsymbol{\varphi}_1 - \boldsymbol{\varphi}_2] \cdot \boldsymbol{\Pi}^t) &= \int\limits_{\mathcal{B}_0} \mathrm{Div}(\boldsymbol{\Psi} \cdot \boldsymbol{\Pi}^t) d\boldsymbol{X} \\
&= \int\limits_{\partial\mathcal{B}_0} \boldsymbol{\Psi} \cdot \boldsymbol{\Pi}^t \cdot \boldsymbol{N} dA \\
&= \int\limits_{\partial\mathcal{B}_0} \boldsymbol{\Psi} \cdot \boldsymbol{\sigma}^t \cdot \boldsymbol{n} dA \\
&= \int\limits_{\partial\mathcal{B}_0} \boldsymbol{\Psi} \cdot [\boldsymbol{\sigma}_1 - \boldsymbol{\sigma}_2] \cdot \boldsymbol{n} dA \quad = \int\limits_{\partial\mathcal{B}_0} [\boldsymbol{\varphi}_1 - \boldsymbol{\varphi}_2] \cdot [\boldsymbol{\sigma}_1 - \boldsymbol{\sigma}_2] \cdot \boldsymbol{n} dA
\end{aligned}
$$

Consequently,

$$
\int\limits_{\mathcal{B}_0} [\boldsymbol{\Pi}_1^t - \boldsymbol{\Pi}_2^t] : [\boldsymbol{F}_1 - \boldsymbol{F}_2] d\boldsymbol{X} = \int\limits_{\partial\mathcal{B}_0} [\boldsymbol{\varphi}_1 - \boldsymbol{\varphi}_2] \cdot [\boldsymbol{\sigma}_1 - \boldsymbol{\sigma}_2] \cdot \boldsymbol{n} dA \\
+ \int\limits_{\mathcal{B}_0} \rho_0 [\boldsymbol{\varphi}_1 - \boldsymbol{\varphi}_2] \cdot [\boldsymbol{b}_1 - \boldsymbol{b}_2] d\boldsymbol{X}
$$

For dead loading $\boldsymbol{b}_1 = \boldsymbol{b}_2$ and $\boldsymbol{\sigma}_1 \cdot \boldsymbol{n} = \boldsymbol{\sigma}_2 \cdot \boldsymbol{n}$, and hence for such a load

$$
\int\limits_{\mathcal{B}_0} [\boldsymbol{\Pi}_1^t - \boldsymbol{\Pi}_2^t] : [\boldsymbol{F}_1 - \boldsymbol{F}_2] d\boldsymbol{X} = 0 \tag{4.35}
$$

and the corresponding pointwise(local) form is

$$
[\boldsymbol{\Pi}_1^t - \boldsymbol{\Pi}_2^t] : [\boldsymbol{F}_1 - \boldsymbol{F}_2] = 0 \tag{4.36}
$$

Comparison of (4.36) and (4.32) results in

$$
\mathrm{Div}\{[\boldsymbol{\varphi}_1 - \boldsymbol{\varphi}_2] \cdot [\boldsymbol{\Pi}_1^t - \boldsymbol{\Pi}_2^t]\} = [\boldsymbol{\varphi}_1 - \boldsymbol{\varphi}_2] \cdot \mathrm{Div}(\boldsymbol{\Pi}_1^t - \boldsymbol{\Pi}_2^t), \;\; \forall \boldsymbol{X} \in \mathcal{B}_0 \tag{4.37}
$$

which implies that

$$
\boldsymbol{\varphi}_1 - \boldsymbol{\varphi}_2 = \boldsymbol{0} \tag{4.38}
$$

leading to equality of the two deformations, $\boldsymbol{\varphi}_1$ and $\boldsymbol{\varphi}_2$ and then arbitrariness of $\boldsymbol{\varphi}_2$ establishes the uniqueness we claimed. Thus, for two kinematically admissible deformations $\boldsymbol{\varphi}_1$ and $\boldsymbol{\varphi}_2$ which are distinct, we have

$$
\int\limits_{\mathcal{B}_0} [\boldsymbol{\Pi}_1^t - \boldsymbol{\Pi}_2^t] : [\boldsymbol{F}_1 - \boldsymbol{F}_2] dX \neq 0 \tag{4.39}
$$

Because of stability concern ignoring the case

$$
\int\limits_{\mathcal{B}_0} [\boldsymbol{\Pi}_1^t - \boldsymbol{\Pi}_2^t] : [\boldsymbol{F}_1 - \boldsymbol{F}_2] dX < 0 \tag{4.40}
$$

70

and employing only

$$\int\limits_{\mathcal{B}_0} [\boldsymbol{\Pi}_1{}^t - \boldsymbol{\Pi}_2^t] : [\boldsymbol{F}_1 - \boldsymbol{F}_2] d\boldsymbol{X} > 0 \tag{4.41}$$

the pointwise form of which is

$$[\boldsymbol{\Pi}_1{}^t - \boldsymbol{\Pi}_2^t] : [\boldsymbol{F}_1 - \boldsymbol{F}_2] > 0. \tag{4.42}$$

We state the sufficient condition for uniqueness of a minimizer(in the local sense) as follows,

> **A kinematically admissible deformation φ is a unique (an absolute) minimizer of (4.1) in an infinitesimal neighborhood provided that, for any other kinematically admissible deformation φ' the inequality $[\boldsymbol{\Pi}^t - \boldsymbol{\Pi}'^t] : [\nabla_X \varphi - \nabla_X \varphi'] > 0$ holds.**

In this proposition of infinitesimal uniqueness, the derivatives involved are only first-order, i.e. one order less than that needed in (4.26), as desired. Furthermore, the characterization is given in terms of the first Piola-Kirchhoff stress tensor and hence it is directly connected to the underlying elastic constitutive law. Indeed, the statement of infinitesimal rank-one convexity (4.26) is stated for the constitutive equation, however the characterization involves the tangent operator.

One merit of working with the expression in (4.26) is the direct interpretation it allows and the physical meaning it renders. Under the assumption of continuity of the tangent operator $\mathbb{L}$, referring to (4.26) we paraphrase the corresponding proposition which might be stated as, *the constitutive relation (2.29) is said to be infinitesimally rank-one convex if the fourth order tensor, the tangent operator (2.30) satisfies the relation*

$$[\boldsymbol{m} \otimes \boldsymbol{N}] : \mathbb{L} : [\boldsymbol{m} \otimes \boldsymbol{N}] \geq 0, \quad \forall \boldsymbol{m} \otimes \boldsymbol{N}. \tag{4.43}$$

We introduce, the second-order tensor $\boldsymbol{q}(\boldsymbol{N})$ with expression

$$\boldsymbol{q}(\boldsymbol{N}) = [\mathbb{I} \otimes \boldsymbol{N}] : \mathbb{L} \cdot \boldsymbol{N} \tag{4.44}$$

But then, (4.43) reduces to

$$\boldsymbol{m} \cdot \boldsymbol{q}(\boldsymbol{N}) \cdot \boldsymbol{m} \geq 0, \quad \forall \boldsymbol{m}, \boldsymbol{N} \neq \boldsymbol{0} \tag{4.45}$$

The tensor $\boldsymbol{q}(\boldsymbol{N})$ which is symmetric for hyperelastic materials, is connected to the propagation of infinitesimal plane waves from which it derives the name *acoustic tensor* whereby $\boldsymbol{N}$ represents the direction of propagation of the wave, see e.g. Šilhavy(1997) or Ogden(1984) for details.

Expression (4.43) which basically results from the incremental stability condition can be replaced by a stronger version. To this end, replacing $\geq$ by $>$ leads to an ellipticity condition which, in view of the monograph by Ogden(1984), assures that the underlying equilibrium equations are elliptic

systems in accordance with the usual terminology of the theory of partial differential equations.

Thus, with strict inequality (4.43) yields the strong ellipticity condition

$$[\,\boldsymbol{m} \otimes \boldsymbol{N}\,] : \mathbb{L} : [\,\boldsymbol{m} \otimes \boldsymbol{N}\,] > 0. \quad \forall \boldsymbol{m}, \boldsymbol{N} \neq \boldsymbol{0} \tag{4.46}$$

and consequently, (4.45) takes the format

$$\boldsymbol{m} \cdot \boldsymbol{q}(\boldsymbol{N}) \cdot \boldsymbol{m} > 0 \tag{4.47}$$

which is equivalent to saying that $\boldsymbol{q}(\boldsymbol{N})$ is positive definite for each $\boldsymbol{N} \neq \boldsymbol{0}$.

Consider a path of deformation along which the strong ellipticity condition (4.46) holds only up to some critical configuration, i.e. there is a configuration at which it fails in the sense that (4.43) holds with equality '=' for some tensor $\boldsymbol{m} \otimes \boldsymbol{N} \neq \boldsymbol{0}$. In this critical configuration for each such non-zero $\boldsymbol{N}$ there exists a vector $\boldsymbol{m} \neq \boldsymbol{0}$ such that

$$\boldsymbol{q}(\boldsymbol{N}) \cdot \boldsymbol{m} = \boldsymbol{0} \tag{4.48}$$

Thus, in configurations where strong ellipticity just fails there exists a tensor $\boldsymbol{N}$ such that $\boldsymbol{q}(\boldsymbol{N})$ is singular, and therefore

$$\det \boldsymbol{q}(\boldsymbol{N}) = 0. \tag{4.49}$$

Computation of the determinant of acoustic tensor yields crucial information as to whether the problem remains well-posed or not. Particularly, in the incremental loading procedure the singularity of the acoustic tensor is taken as part of useful arsenals that might be used to detect the critical configuration that can be interpreted in anyone of the following possible ways, 1) *the onset of instability*, 2) *emergence of bifurcation of the underlying deformation path* or 3) *loss of ellipticity of the associated boundary value problem*. An engineering terminology that sums up all these interpretations is, perhaps '*onset of material failure*'. This critical configuration is of primary interest in this part of study and therefore in what follows, we shall employ an acoustic tensor for the investigation of *material failure*. We present results from the computation of a mode I crack problem with a priori known crack path(along the plane of symmetry) for a fcc type crystalline material. The computation is performed within a finite element context whereby simple triangular elements with one integration point are adopted and the load is applied incrementally such that failure occurs at different time steps for different elements. Practically speaking, $\det \boldsymbol{q}(\boldsymbol{N})$ is computed for each element on every load step thereby monitoring for those elements where $\det \boldsymbol{q}(\boldsymbol{N})$ becomes non-positive. Consequently, the result in figure 4.2 highlights elements where failure occurred and displays the corresponding curve of the determinant of the acoustic tensor versus load step. In this process element 44 failed at the 33rd step while elements 15, 24 and 31 failed at the 36th step and element 29 failed at the 37th load step.
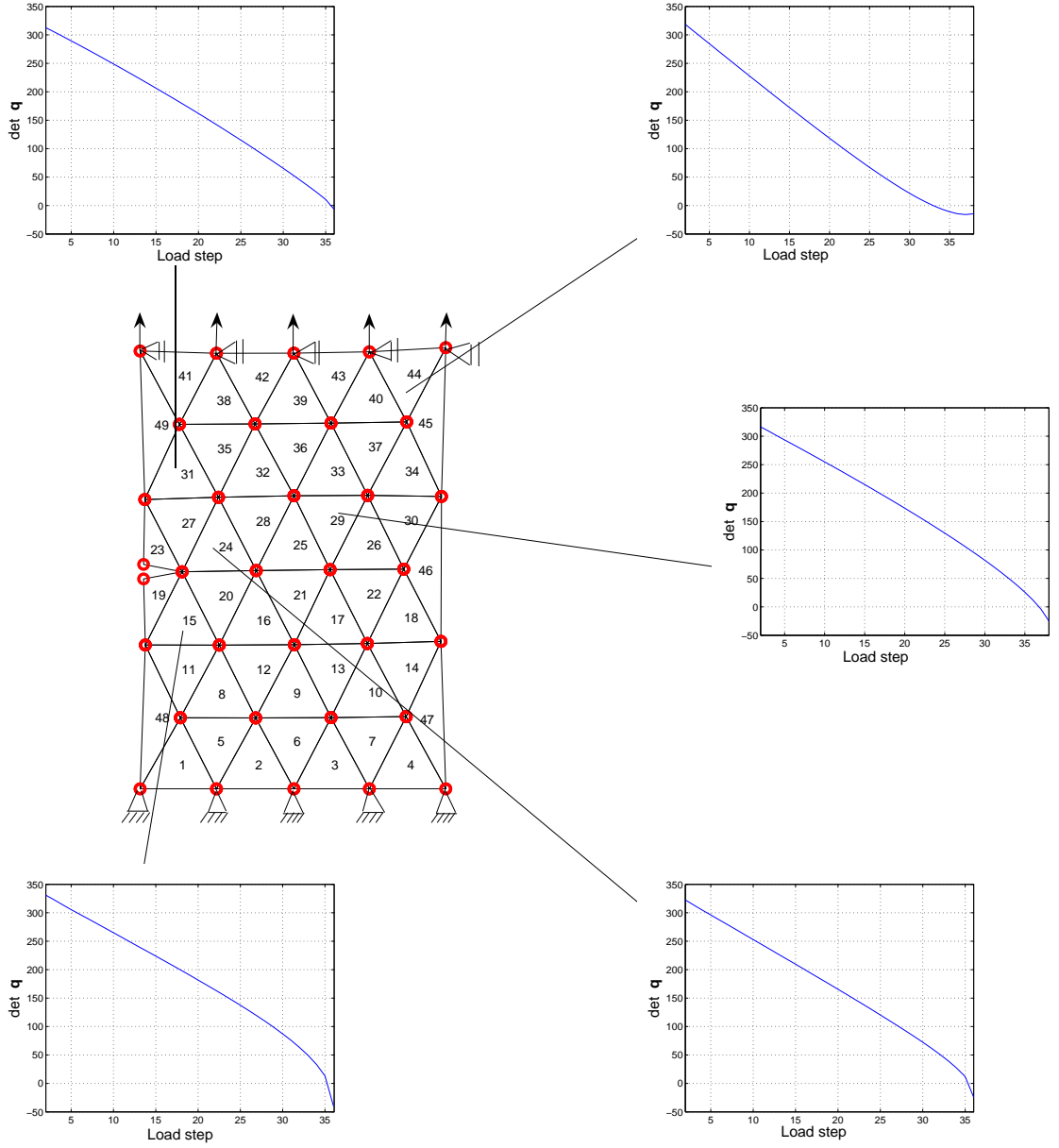
Figure 4.2: Investigation of material failure by means of the acoustic tensor

We have seen that positive definiteness of the acoustic tensor $\boldsymbol{q}$ is connected to strong ellipticity and hence to the stability of the underlying homogeneous deformation whereby the singularity of

this tensor is identified with the onset of material failure. Since the acoustic tensor is a function of the spatial direction vector $\boldsymbol{N}$, in what follows we study the effect of this dependence on the behavior of the tensor $\boldsymbol{q}$ in the planar case where the vector $\boldsymbol{N}$ is explicitely expressed as a function of planar inclination angle θ as

$$\boldsymbol{N}(\theta) = cos(\theta)\boldsymbol{e}_1 + sin(\theta)\boldsymbol{e}_2. \qquad (4.50)$$

The next result is obtained from the computation of minimum of the determinant of acoustic tensor as a function of direction vector in terms of inclination angle θ for a complete rotation. The numerical computation is performed for simple shear deformation(see figure 4.3) and uniaxial extension, tension test(figure 4.4) in the context of incremental loading procedures.

For the sake of demonstration a structure with two elements is employed. Since we apply a homogeneous deformation, we concentrate on anyone of the two elements during an incremental deformation process for both simple shear deformation and tension test.
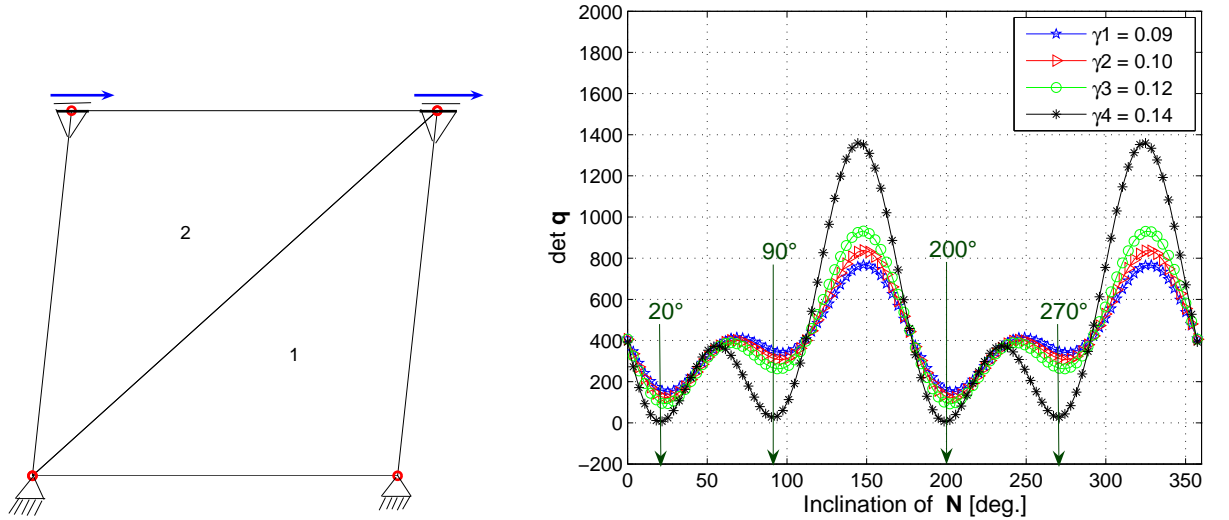
Figure 4.3: Determinant of $\boldsymbol{q}$ versus inclination angle of planar direction vector $\boldsymbol{N}$ (simple shear)

For simple shear deformation as visualized in figure 4.3, the determinant of acoustic tensor manifests oscillatory behavior with peaks at different heights and wells with different depths on its graph. Moreover, for increasing load steps the height of some of the peaks gets higher while the depth of all the wells is getting further deep. The determinant of $\boldsymbol{q}$ is periodic with period π. and
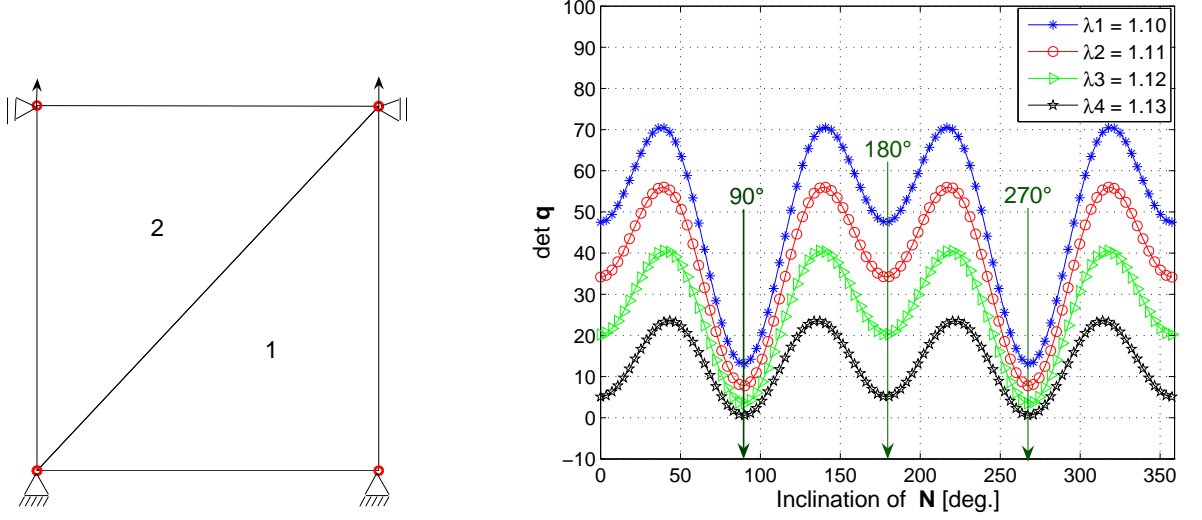
74

the above plot corresponds to 2 periods.

Figure 4.4: Determinant of q versus inclination angle of planar direction vector N (tension test)

The determinant of q is again oscillatory and periodic for tension test with the same period as in simple shear deformation. Here, for this type of deformations each load step gives rise to translation of the entire graph obtained in the preceeding step.

4.3 Rank-one convexification

In the preceeding sections we reviewed the formulation of rank-one convexity and characterization of infinitesimal rank-one convexity. Loss of rank-one convexity indicates instability of the homogeneous deformation state F (the acoustic tensor is used to detect the onset) and the development of microstructures in the form of such a pattern as laminate that can either be first- or higher-order formed by a material in order to lower its energy so as to accommodate the deformation encountered. The determination of these evolving energy minimizing microstructures leads to rank-one convexification of the energy density $\mathscr{W}_0$ through the construction of its rank-one convex envelop $\mathscr{W}_0^R$. Referring to the monographs and articles by Dacorogna et al.(1999, 1989, 1982) for a rigorous mathematical basis, or the contributions by Müller(1998) Kohn et al.(1986) Kohn (1983) Rockafellar(1970) and references therein for further survey, we intend to have a closer look at the notion of rank-one convexification as applied to phase decomposition deformation problems. For such class of deformations, the rank-one convexified stored energy density, i.e. the relevant rank-one convex envelop as a function of the homogeneous deformation is given by(Dacorogna(1989), Section 5.1.1) the optimization problem

$$\mathscr{W}_0^R(\boldsymbol{F}) = \inf_{\xi_i, \boldsymbol{F}_i} \left\{ \sum_{i=1}^{N} \xi_i \mathscr{W}_0(\boldsymbol{F}_i) \right\} \tag{4.51}$$

with the weighted average of the phases $\boldsymbol{F}_i$ rendering the homogeneous deformation $\boldsymbol{F}$

$$\boldsymbol{F} = \sum_{i=1}^{N} \xi_i \boldsymbol{F}_i \tag{4.52}$$

and the global volume fractions satisfying

$$0 < \xi_i < 1, \quad \text{such that} \quad \sum_{i=1}^{N} \xi_i = 1 \tag{4.53}$$

where N is the number of phases(cf. Pedregal(1993)).

In this context therefore, the case $N = 2$ corresponds to an occurrence of only two phases, a layered mixture of two deformation gradients $\boldsymbol{F}_1$ and $\boldsymbol{F}_2$ and hence the development of level-1 laminate with the additional requirement that the difference between the two phases be a rank-1 tensor

$$\boldsymbol{F}_1 - \boldsymbol{F}_2 = \boldsymbol{a} \otimes \boldsymbol{N} \tag{4.54}$$

For a concrete example on compatible phases(rank-one connectivity) in phase transforming materials and minimizing sequences see Ball et al.(1987).

The constraint (4.54) called the rank-one compatibility condition is required to enforce the continuity of deformation across the interface separating the twin variants (see Appendix B for the derivation). The physical origin and the geometric interpretation is related to the interfacial plane(surface) such that whether one approach the plane from below or above, when one reach the plane, prescription for displacing the atoms on that plane will be the same. From energetic point of view, the continuity constraint is needed to insure that the new microstructure is reachable from the preceeding one by a combination of branching[8] and pruning process under conditions that several phases are energetically favorable(compare the work of Knowles et al.(1978) for the emergence of discontinuous deformation gradients).

The vector '$\boldsymbol{N}$' is normal to the interfacial plane in the reference configuration and '$\boldsymbol{a}$' is a vector to be determined. If the vectors $\boldsymbol{a}$, $\boldsymbol{N}$ and the volume fraction ξ are already known then for a given parent deformation the deformations in the variants are given by

$$\boldsymbol{F}_1 = \boldsymbol{F} + [1 - \xi]\boldsymbol{a} \otimes \boldsymbol{N} \tag{4.55}$$
$$\boldsymbol{F}_2 = \boldsymbol{F} - \xi\boldsymbol{a} \otimes \boldsymbol{N}$$

From this, one can say that the aggregate $\{\boldsymbol{F}, \boldsymbol{a}, \boldsymbol{N}, \xi\}$ constitute a complete set of degrees of freedom for the laminate. Following Kohn(1991) a laminate of level-k is taken to be a phase mixture of two level-$(k-1)$ laminate and the generation of level-k laminate contains 2^k laminate. For the sake of completeness, uniform deformations might be labeled as level-0 laminate.

---

[8]By **branching** we mean the splitting of a variant into a rank-one laminate and by **pruning** we are referring to the elimination of variants with volume fraction reducing to zero. Thus, branching and pruning are mechanisms by which microstructures are allowed to effect topological(structural) transitions
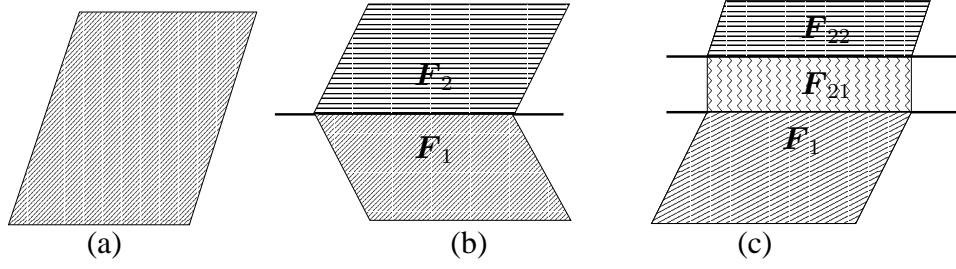
Figure 4.5: Schematic of microstructure corresponding to level-1 laminate (b) and level-2 laminate (c). Two phases emerge corresponding to the homogeneous deformations $\boldsymbol{F}_1$ and $\boldsymbol{F}_2$ developing as a result of shear bifurcation (figure (b)) and further bifurcation of $\boldsymbol{F}_2$ (figure (c))

4.3.1 Approximate rank-one convex envelop

The approximation of rank-one convex envelop can be considered as the first step towards the simulation of nonlinear behavior of materials with either affine or non-affine boundary conditions (Roubícek(1996)). Following the description (4.51) of rank-one convex envelop, the next step is the investigation of the resulting relaxed energy functional which is given by

$$\mathscr{I}_R(\boldsymbol{\varphi}) = \int_{\mathcal{B}_0} \mathscr{W}_0^R(\boldsymbol{F}) d\boldsymbol{X}. \tag{4.56}$$

In the event that $N > 2$, which corresponds to a decay of homogeneous deformation state into more than two phases, the rank-one convexification procedure (4.51) has a serious drawback, mainly, for it is not possible to bound the cardinal number N, i.e. one can not a priori prescribe the number of evolving phases, consequently evaluating the infimum becomes difficult. An alternative procedure which is a sort of algorithmic approach and that provides a recursion formula for sequential rank-one convexification was suggested by Kohn(1986) and is described as follows (see e.g. Miehe et al.(2003) and citations therein for algorithmic solution of constrained minimization problem).

We start with

$$\mathscr{W}_0^{R_0} = \mathscr{W}_0 \tag{4.57}$$

and for each integer $k \geq 1$ define recursively

$$\mathscr{W}_0^{R_k}(\boldsymbol{F}) = \inf_{\xi_k, \boldsymbol{F}_1, \boldsymbol{F}_2} \left\{ \xi_k \mathscr{W}_0^{R_{k-1}}(\boldsymbol{F}_1) + [1 - \xi_k] \mathscr{W}_0^{R_{k-1}}(\boldsymbol{F}_2) \right\} \tag{4.58}$$

with the local volume fraction $0 < \xi_k < 1$ and the average deformation

$$\boldsymbol{F} = \xi_k \boldsymbol{F}_1 + [1 - \xi_k] \boldsymbol{F}_2 \tag{4.59}$$

such that

$$\text{rank}(\boldsymbol{F}_1 - \boldsymbol{F}_2) \leq 1.$$

77

Using (4.55) the variational problem (4.58) reduces to

$$\mathscr{W}_0^{R_k}(\boldsymbol{F}) = \inf_{\xi_k, \boldsymbol{a}, \boldsymbol{N}} \left\{ \xi_k \mathscr{W}_0^{R_{k-1}}(\boldsymbol{F}_1) + [1 - \xi_k] \mathscr{W}_0^{R_{k-1}}(\boldsymbol{F}_2) \right\} \tag{4.60}$$

The exact rank-one convex envelop is then obtained in the long run from the limit of the sequence of envelops $\{\mathscr{W}_0^{R_k}\}_{k=0}^{\infty}$, i.e.

$$\mathscr{W}_0^R = \lim_{k \to \infty} \mathscr{W}_0^{R_k}.$$

The expression in (4.58) implies that any phase of level-$(k-1)$ decomposes into two phases of level-k with the anticipation that they minimize the average of the corresponding stored energy. In this fashion, we have laminate within laminate, or more precisely sequential laminate. Directly from the recursion relation (4.60) we have the following relation between successive rank-one convex envelops at various levels

$$\mathscr{W}_0^R \leq \ldots \leq \mathscr{W}_0^{R_{k+1}} \leq \mathscr{W}_0^{R_k} \leq \ldots \leq \mathscr{W}_0^{R_1} \leq \mathscr{W}_0^{R_0} = \mathscr{W}_0 \tag{4.61}$$

An observation of the order relation (4.61) reveals that, for phase decomposition deformations, the level-k envelop (rank-one convex envelop) constitutes the lower bounds of the corresponding level-$(k-1)$ envelop, indeed it comprises *lower bounds* of all corresponding lower level rank-one convex envelops. The use of the term lower level here, refers to indices smaller than the given index.

4.3.2 Continuum-atomistics and rank-one convexification

Once we have the algorithm for approximating the rank-one convex envelop, the next step is description of the corresponding ground state configuration, i.e. computation of the optimal energy configuration resulting from minimization of the relaxed energy functional arising from optimal density function as described in (4.60). The energy obtained from atomistic level computation is incorporated to the optimized density function based on the description (2.28).

Variable optimization

For a solution of (4.60) to be an optimal density, it is required that the stationarity condition with respect to all the variables $(\xi_k, \boldsymbol{a}, \boldsymbol{N})$ be satisfied, i.e.

$$\frac{\partial \hat{\mathscr{W}_0}}{\partial \xi_k}(\xi_k, \boldsymbol{a}, \boldsymbol{N}; \boldsymbol{F}) = 0$$

$$\frac{\partial \hat{\mathscr{W}_0}}{\partial \boldsymbol{a}}(\xi_k, \boldsymbol{a}, \boldsymbol{N}; \boldsymbol{F}) = \boldsymbol{0}$$

$$\frac{\partial \hat{\mathscr{W}_0}}{\partial \boldsymbol{N}}(\xi_k, \boldsymbol{a}, \boldsymbol{N}; \boldsymbol{F}) = \boldsymbol{0}$$

where $\quad \hat{\mathscr{W}_0}(\xi_k, \boldsymbol{a}, \boldsymbol{N}; \boldsymbol{F}) := \xi_k \mathscr{W}_0^{R_{k-1}}(\boldsymbol{F}_1) + [1 - \xi_k] \mathscr{W}_0^{R_{k-1}}(\boldsymbol{F}_2)$.

Since the optimal interface orientation $\mathbf{N}$ can readily be obtained from the determinant of acoustic tensor, all we need to determine is the remaining two variables ξ_k and $\boldsymbol{a}$ which can be obtained from the solution of

$$\left.\begin{array}{rll} \dfrac{\partial \hat{\mathscr{W}_0}}{\partial \xi_k}(\xi_k, \boldsymbol{a}, \boldsymbol{N}; \boldsymbol{F}) = & [\![\mathscr{W}_0^{R_{k-1}}]\!] - \boldsymbol{a} \cdot \langle \boldsymbol{\Pi}^t \rangle \cdot \boldsymbol{N} & = 0 \\[2ex] \dfrac{\partial \hat{\mathscr{W}_0}}{\partial \boldsymbol{a}}(\xi_k, \boldsymbol{a}, \boldsymbol{N}; \boldsymbol{F}) = & [\![\boldsymbol{\Pi}^t]\!] \cdot \boldsymbol{N} & = \boldsymbol{0} \end{array}\right\} \text{Nonlinear system}$$

We keep on computing these variables at each level except level-0. At level-0, the only task is incorporating the atomistic level information to the continuum through energetic means, i.e. the energy extracted from atomistics is absorbed to the strain energy density $\mathscr{W}_0^{R_0}$ as described in (2.28). Proceeding to level-1 where the computation of optimal variables start, we treat the above nonlinear system of equations. Thus, for a given ξ_k the traction equilibrium equation

$$[\![\boldsymbol{\Pi}^t]\!] \cdot \boldsymbol{N} = \boldsymbol{0} \tag{4.62}$$

is solved iteratively with the tangent stiffness matrix given in terms of the acoustic tensor

$$\boldsymbol{K}_T = \boldsymbol{q}_1 - \xi_k [\![\boldsymbol{q}]\!]. \tag{4.63}$$

The resulting pair $\{\xi_k, \boldsymbol{a}\}$ comprises the requisite optimal volume fraction and optimal amplitude, if it satisfies the configurational equilibrium equation(compare Maxwell relation, Gurtin(1983) or Fosdick et al.(1989))

$$[\![\mathscr{W}_0^{R_0}]\!] - \boldsymbol{a} \cdot \langle \boldsymbol{\Pi}^t \rangle \cdot \boldsymbol{N} = 0 \tag{4.64}$$

The index attached to the acoustic tensor (4.63) arises from the dependence on the associated twin deformation, i.e.

$$\mathbb{L}_1 = \frac{\partial^2 \mathscr{W}_0^{R_0}(\boldsymbol{F}_1; \boldsymbol{X})}{\partial \boldsymbol{F}_1 \otimes \partial \boldsymbol{F}_1} \tag{4.65}$$

and the definition (4.44).

Iteration strategy

The method of solving the coupled nonlinear system has two steps, namely, *prediction* and *correction* steps. The prediction step is characterized by picking a $\xi_k \in [0, 1]$ and solving (4.62) for the amplitude '$\boldsymbol{a}$' using Newton-Raphson method(For the Newton method we refer to Bonet et al.(1997) Burden et al.(2005) or any standard reference on numerical analysis). At the correction step we plug the values of the pair $\{\xi_k, \boldsymbol{a}\}$ in (4.64) and see if it satisfies the equation. In this computation $\xi_k = 0.5$ is taken to be the initial volume fraction and the corresponding initial amplitude is $\boldsymbol{a}_0 = -0.3420 \boldsymbol{e}_1 + 0.9397 \boldsymbol{e}_2$. From the plot of the determinant of the acoustic tensor as a function of $\boldsymbol{N}$(see figure 4.3) we have two directions over one period, namely one corresponding to $\theta = 20^0$ and the other to 90^0. Here, we consider only one direction $\boldsymbol{N}(20^0)$. The optimal variables obtained in this prediction-correction method are summarized in the next table.

79

θ	20^0
$\boldsymbol{N}$	$0.9397\boldsymbol{e}_1 + 0.3420\boldsymbol{e}_2$
ξ	0.264
$\boldsymbol{a}$	$-0.024\boldsymbol{e}_1 + 0.015\boldsymbol{e}_2$

In the end, for the description of energy functional at level-1 the rank-one convexified density $\mathscr{W}_0^{R_1}$ is made to incorporate the atomistic level energy as described in (2.28). Ultimately, in the context of sequential lamination procedures with $\mathscr{W}_0^{R_1}$ at hand the next step is computing $\mathscr{W}_0^{R_2}$, which is essentially nothing but repeating all the steps performed to get $\mathscr{W}_0^{R_1}$ with the only change that $\mathscr{W}_0^{R_1}$ this time plays the role of $\mathscr{W}_0^{R_0}$. In general, any work to get level-k envelop with $k \geq 2$ is a repetition of the variables optimization procedures conducted at the preceeding level-$(k-1)$ step followed by incorporating the crystal based computation of energy as stated in (2.28).

Finite elements and minimization of relaxed energy

Eventually the level-k envelop $\mathscr{W}_0^{R_k}$ with the atomistic input already incorporated renders the relaxed energy functional of this level

$$\mathscr{I}_{R_k}(\boldsymbol{\varphi}) = \int_{\mathcal{B}_0} \mathscr{W}_0^{R_k}(\boldsymbol{F})d\boldsymbol{X} \tag{4.66}$$

and the next step is solving the variational problem

$$\mathscr{I}_{R_k}(\boldsymbol{\varphi}) \longmapsto \min! \tag{4.67}$$

To find a minimizing configuration one may tackle directly (4.67) by employing one of the known iterative schemes such as conjugate gradient or Newton-Raphson method. However, this equilibrium configuration can alternatively be extracted from the stationarity condition in terms of the vanishing first order variation which renders

$$\int_{\mathcal{B}_0} \frac{\partial \mathscr{W}_0^{R_k}}{\partial \boldsymbol{F}} : \nabla_{\boldsymbol{X}} \delta\boldsymbol{\varphi}(\boldsymbol{X})d\boldsymbol{X} = \boldsymbol{0}. \tag{4.68}$$

Substituting the stress function $\boldsymbol{\Pi}_k^t$ for the derivative of the envelop with respect to $\boldsymbol{F}$ leads to

$$\int_{\mathcal{B}_0} \boldsymbol{\Pi}_k^t : \nabla_{\boldsymbol{X}} \delta\boldsymbol{\varphi}(\boldsymbol{X})d\boldsymbol{X} = \boldsymbol{0}. \tag{4.69}$$

In the context of standard finite element procedures, discretizing the reference domain $\mathcal{B}_0$ into elements $\{\mathcal{B}_0^e : e = 1, 2, ..., n_{el}\}$ and assembly of the resulting integrals over the elements yields

$$\mathop{A}_{e=1}^{n_{el}} \int_{\mathcal{B}_0^e} \boldsymbol{\Pi}_{ke}^t : \nabla_{\boldsymbol{X}} \delta\boldsymbol{\varphi}(\boldsymbol{X}) d\boldsymbol{X} = \boldsymbol{0} \ \text{ with } \ \underset{e}{\cup} \mathcal{B}_0^e = \mathcal{B}_0 \tag{4.70}$$

Using the trial deformation interpolated from the shape functions leads to the equilibrium equation

$$\mathop{A}_{e=1}^{n_{el}} \sum_{\ell} \int_{\mathcal{B}_0^e} \boldsymbol{\Pi}_{ke}^t : \delta\boldsymbol{\varphi}_\ell \otimes \nabla_{\boldsymbol{X}} \boldsymbol{N}_\ell(\boldsymbol{X}) d\boldsymbol{X} = \boldsymbol{0} \tag{4.71}$$

where $\boldsymbol{\varphi}_\ell$ is an element nodal coordinate.

The system (4.71) is nonlinear where the nonlinearity lies in the stress function $\boldsymbol{\Pi}_{ke}^t$ emanating from its connection to the atomistics through (2.29). Consequently, its solution involves an iterative procedure that leads to linearization thereby necessitating the introduction of the fourth order tensor, the tangent operator $\mathbb{L}_{ke}$ computed from atomistic data as described in (2.30). For a force controlled simulation, in the finite element procedures the expression on the left hand side of (4.71) constitutes the internal force vector while the same procedure leads to the corresponding discretization of the external force which is given by

$$\mathop{A}_{e=1}^{n_{el}} \sum_{\ell} \int_{\partial\mathcal{B}_0^e} \boldsymbol{T}_{ke} \cdot \delta\boldsymbol{\varphi}_\ell \boldsymbol{N}_\ell(\boldsymbol{X}) dA \tag{4.72}$$

and the relevant equilibrium equation in the absence of body force is given by

$$\mathop{A}_{e=1}^{n_{el}} \sum_{\ell} \left[\int_{\mathcal{B}_0^e} \boldsymbol{\Pi}_{ke}^t : \delta\boldsymbol{\varphi}_\ell \otimes \nabla_{\boldsymbol{X}} \boldsymbol{N}_\ell(\boldsymbol{X}) d\boldsymbol{X} - \int_{\partial\mathcal{B}_0^e} \boldsymbol{T}_{ke} \cdot \delta\boldsymbol{\varphi}_\ell \boldsymbol{N}_\ell(\boldsymbol{X}) dA \right] = \boldsymbol{0} \tag{4.73}$$

As indicated in the order relation (4.61) for each $k \geq 0$ the envelop $\mathscr{W}_0^{R_{k+1}}$ renders a lower energy level than its predecessor $\mathscr{W}_0^{R_k}$ and hence the configuration at each level-k laminate is a metastable configuration lowering the energy in the local sense. The next result, figure 4.6 is the element energy density for level-0 and level-1 lamination computed for the structure with two elements (see figure 4.3) subjected to simple shear deformation.
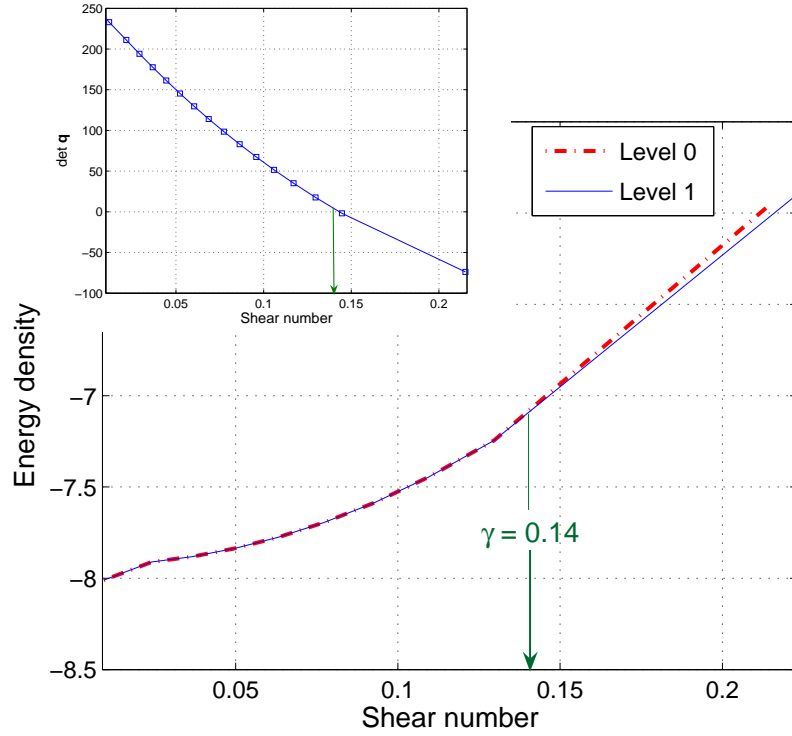
Figure 4.6: Determinant of acoustic tensor/energy density versus shear number

The level-1 density agrees with the homogeneous density(level-0) until the shear number reaches 0.14 and gives strictly lower value for shear number beyond that. The shear number 0.14 corresponds to critical deformation associated with the onset of failure as detected by the determinant of the acoustic tensor.
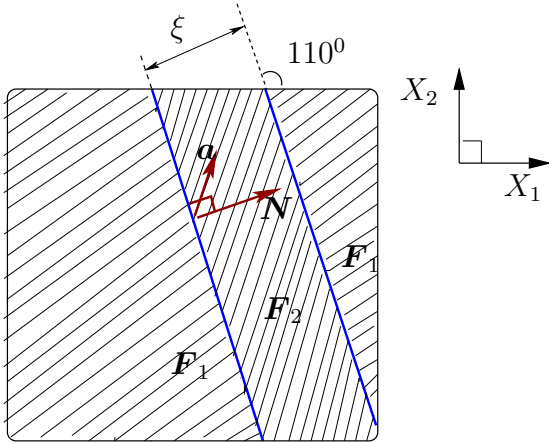

Figure 4.7: Schematic of evolving microstructure for phase decomposition deformation as determined by the vector **N**, model case of 2D.

The direction vector $\boldsymbol{N}$ which is orthogonal to an interface plane determines the optimal orientation of the splitting plane, and hence for a phase decomposition deformation the alignment of these planes relative to each other. In figure 4.7, for the unit normal $\boldsymbol{N}$ $= [\cos(\theta) \quad \sin(\theta)]$ that makes an angle of 20^0 with the horizontal the corresponding splitting plane(2D case) and the associated angle 110^0 is shown. We recall that $\boldsymbol{N}$ is obtained from the determinant of the acoustic tensor, thus the angle 20^0 corresponds to a minima on the graph of acoustic tensor $\boldsymbol{q}$ as a function of the direction vector $\boldsymbol{N}$ (see figure 4.3).

Referring to the expression in (4.73), the first Piola-Kirchhoff stress tensor $\boldsymbol{\Pi}_{ke}^t$ represents the stress at level-k in the element e. The Frobenius[9] norm of this stress can be evaluated and might be used as a measure of sensitivity to instability, i.e. it helps assess the relative stability of the structure. The next result is computation of the push-forward of $\boldsymbol{\Pi}_{ke}^t$, the spatial Cauchy stress. The computation is made for simple shear deformation and tension test at level-0 and the components of the symmetric Cauchy stress against the displacement of a point on the top margin of the two-element structure (as in figure 4.3 and figure 4.4) are displayed.
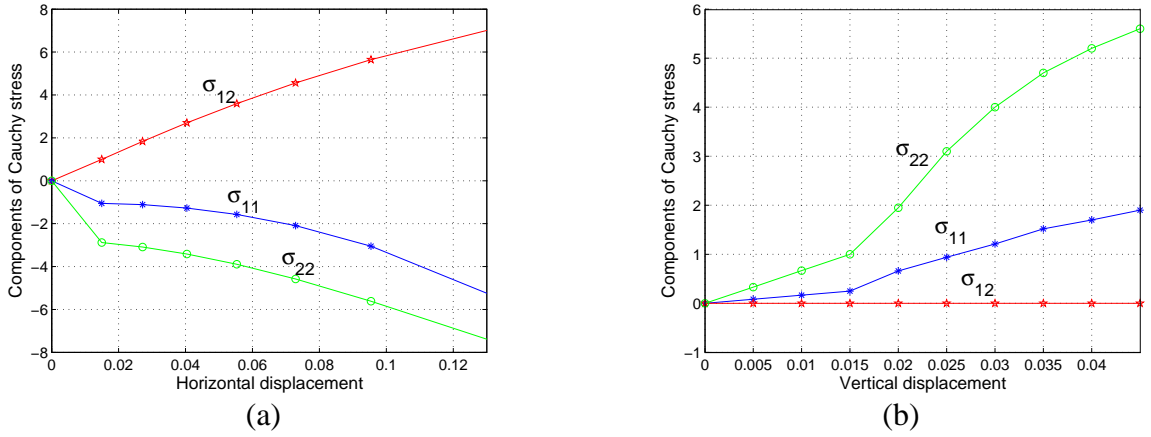

Figure 4.8: Components of the Cauchy stress tensor /vs displacement of a point on top margin, for simple shear deformation(a) and tension test(b)

4.4 Phase decomposition deformation and oscillation

Within the confines of rank-one convexification procedures, this section focuses on a minimizing deformation of phase splitting problems(for phase mixing associated with energy minimizers see Ball(1987)). For a phase decomposition problem, the macroscopic deformation state $\boldsymbol{F}$ is unstable and therefore decomposes into two phases $\boldsymbol{F}_1$ and $\boldsymbol{F}_2$ each of which may further split into pairs of phases $\boldsymbol{F}_{11}$, $\boldsymbol{F}_{12}$ and $\boldsymbol{F}_{21}$, $\boldsymbol{F}_{22}$ respectively(compare Pedregal(1993)). The average deformation is then the superposition of these phases, in other words, it is the weighted average of all the variants with the weight coming from the global volume fractions with the restriction that the rank-one compatibility condition (4.54) is satisfied for each splitting at each level.

---

[9]The Frobenius norm also called the Euclidean norm of a square matrix $\boldsymbol{A}$ is given by $\| \boldsymbol{A} \| = \sum\limits_{i,j} A_{ij}^2$
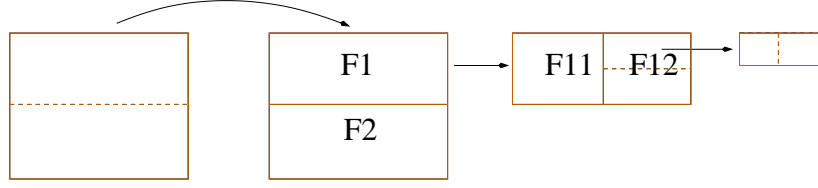
Figure 4.9: Schematic of phase decomposition deformation

To figure out this process, we start with level-1 splitting. At this level, since the homogeneous deformation splits exactly into two deformations that lower the energy, we write a convex combination

$$\boldsymbol{F} = \xi_1 \boldsymbol{F}_1 + [1 - \xi_1] \boldsymbol{F}_2 \tag{4.74}$$

According to the rank-one compatibility condition (4.54), we demand that

$$\boldsymbol{F}_1 - \boldsymbol{F}_2 = \boldsymbol{a}_1 \otimes \boldsymbol{N}_1 \tag{4.75}$$

such that $(\boldsymbol{F}_1 - \boldsymbol{F}_2) \leq 1$.

Based on the assumption that each of the level-1 variant further splits, repeating the procedure in (4.74) for the pair $\{\boldsymbol{F}_1, \boldsymbol{F}_2\}$, the deformation of the variants ($\boldsymbol{F}_1$ and $\boldsymbol{F}_2$) is recovered from the respective twins as,

$$\boldsymbol{F}_1 = \xi_2 \boldsymbol{F}_{11} + [1 - \xi_2] \boldsymbol{F}_{12} \text{ and } \boldsymbol{F}_2 = \tilde{\xi}_2 \boldsymbol{F}_{21} + [1 - \tilde{\xi}_2] \boldsymbol{F}_{22} \tag{4.76}$$

with the local volume fractions

$$0 < \xi_2, \tilde{\xi}_2 < 1$$

such that

$$\boldsymbol{F}_{11} - \boldsymbol{F}_{12} = \boldsymbol{a}_2 \otimes \boldsymbol{N}_2 \text{ and } \boldsymbol{F}_{21} - \boldsymbol{F}_{22} = \tilde{\boldsymbol{a}}_2 \otimes \tilde{\boldsymbol{N}}_2 \tag{4.77}$$

As a result, the original average deformation is described by

$$\boldsymbol{F} = \xi_1 \xi_2 \boldsymbol{F}_{11} + \xi_1 [1 - \xi_2] \boldsymbol{F}_{12} + [1 - \xi_1] \tilde{\xi}_2 \boldsymbol{F}_{21} + [1 - \xi_1][1 - \tilde{\xi}_2] \boldsymbol{F}_{22} \tag{4.78}$$

We refer to the ensemble

$$\mathcal{G}_2 = \{\boldsymbol{F}_{ij} | i, j \in \{1, 2\}\} \tag{4.79}$$

the *generation* of level-2 laminate deformations(see figure 4.9). Roughly speaking, the description (4.78) represents a deformation with gradients oscillating among the members of $\mathcal{G}_2$, i.e.

$$\boldsymbol{F}_{11}, \ \boldsymbol{F}_{12}, \ \boldsymbol{F}_{21} \ \text{ and } \ \boldsymbol{F}_{22}$$

and with the respective volume fractions

$$\xi_1 \xi_2, \ \xi_1 [1 - \xi_2], \ [1 - \xi_1] \tilde{\xi}_2 \ \text{ and } \ [1 - \xi_1][1 - \tilde{\xi}_2].$$

The determinant of acoustic tensor which is used to check the onset of instability of the homogeneous deformation is computed at each level of the rank-one convexification procedures so as to detect the critical configuration for splitting. In view of this, minimum of the determinant of the acoustic tensor for the onset of failure at two consecutive levels, level-0 and level-1 is computed and the results are compared in figure 4.10. Since the twins $\boldsymbol{F}_1$ and $\boldsymbol{F}_2$ are piecewise homogeneous, the failure at level-1 is detected for $\boldsymbol{F}_1$ and is compared with that of $\boldsymbol{F}$ (failure occurs for $\boldsymbol{F}$ at $\gamma = 0.14$ while it is at $\gamma = 0.15$ for $\boldsymbol{F}_1$)
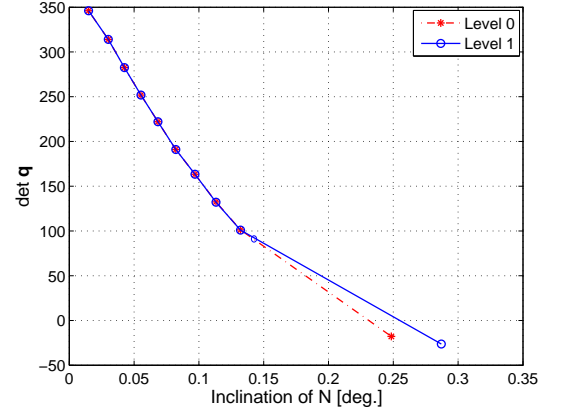
Figure 4.10: Comparison of minimum of det$\boldsymbol{q}$ for splitting of $\boldsymbol{F}$ and further splitting of $\boldsymbol{F}_1$.

For an overview on the numerical treatment of oscillation especially those arising in the context of nonconvex problems, see Chipot(1991). The vectors $\boldsymbol{N}_1$, $\boldsymbol{N}_2$ and $\tilde{\boldsymbol{N}}_2$ normal to the interfaces, that give optimal spatial orientation of the layers and the vectors $\boldsymbol{a}_1$ $\boldsymbol{a}_2$ and $\tilde{\boldsymbol{a}}_2$ that denote the relevant amplitudes of jump of the deformation gradient across the interfaces are computed from stationarity condition as described in the previous subsection. Then the original deformation $\boldsymbol{F}$ is expressed as a convex combination of the generation of level-2 variants (4.78) and the corresponding effective rank-one convexified density which by abuse of notation we write $\mathscr{W}_0^{R_2}$ follows from the infimum of the weighted average of the initial level density $\mathscr{W}_0^{R_0}$ evaluated at each of these gradients and is given by

$$\mathscr{W}_0^{R_2}(\boldsymbol{F}) = \inf\{\xi_1\xi_2\mathscr{W}_0^{R_0}(\boldsymbol{F}_{11}) + \xi_1[1-\xi_2]\mathscr{W}_0^{R_0}(\boldsymbol{F}_{12})+$$
$$[1-\xi_1]\tilde{\xi}_2\mathscr{W}_0^{R_0}(\boldsymbol{F}_{21}) + [1-\xi_1][1-\tilde{\xi}_2]\mathscr{W}_0^{R_0}(\boldsymbol{F}_{22})\}. \tag{4.80}$$

The rank-one compatibility(connectivity) constraint (4.77) and the convex combinations (4.74) together with the expression (4.76) renders an explicit formula for the computation of each of the laminate deformations from the original homogeneous deformation $\boldsymbol{F}$, the vectors and the local volume fractions as,

$$\boldsymbol{F}_{11} = \boldsymbol{F} + [1-\xi_1]\boldsymbol{a}_1 \otimes \boldsymbol{N}_1 + [1-\xi_2]\boldsymbol{a}_2 \otimes \boldsymbol{N}_2, \quad \boldsymbol{F}_{12} = \boldsymbol{F} + [1-\xi_1]\boldsymbol{a}_1 \otimes \boldsymbol{N}_1 - \xi_2\boldsymbol{a}_2 \otimes \boldsymbol{N}_2$$
$$\boldsymbol{F}_{21} = \boldsymbol{F} - \xi_1\boldsymbol{a}_1 \otimes \boldsymbol{N}_1 + [1-\tilde{\xi}_2]\tilde{\boldsymbol{a}}_2 \otimes \tilde{\boldsymbol{N}}_2, \quad\quad \boldsymbol{F}_{22} = \boldsymbol{F} - \xi_1\boldsymbol{a}_1 \otimes \boldsymbol{N}_1 - \tilde{\xi}_2\tilde{\boldsymbol{a}}_2 \otimes \tilde{\boldsymbol{N}}_2.$$

Nonetheless, for a deformation that further decays, this way of writing the average deformation appears to be inconvenient. This necessitates the introduction of global volume fraction and leads to a much more convenient and suitable relabeling of the variants that suggests the use of consecutive

indices which then ushers to express (4.78) as

$$\boldsymbol{F} = \sum_{i=1}^{4} \nu_i \boldsymbol{F}_i \tag{4.81}$$

A global volume fraction ν_ℓ is computed from the local volume fraction ξ_i as

$$\nu_1 = \xi_1 \xi_2, \qquad \nu_3 = [1 - \xi_1]\tilde{\xi}_2$$
$$\nu_2 = \xi_1[1 - \xi_2], \quad \nu_4 = [1 - \xi_1][1 - \tilde{\xi}_2]$$

and then the re-indexing of the deformation gradients follows the same pattern as the volume fractions, namely,

$$\boldsymbol{F}_1 = \boldsymbol{F}_{11}, \ \boldsymbol{F}_2 = \boldsymbol{F}_{12}, \ \boldsymbol{F}_3 = \boldsymbol{F}_{21} \ \text{and} \ \boldsymbol{F}_4 = \boldsymbol{F}_{22}. \tag{4.82}$$

For a phase decomposition deformation the level-2 solution represents metastable state. Thus, with the anticipation that the next level can lower the energy further, if the variants of level-2 undergo phase split, we then have the generation of level-3 laminate deformations

$$\mathcal{G}_3 = \{\boldsymbol{F}_i | \ i = 1, 2, ..., 8\} \tag{4.83}$$

consisting of eight members with a consequent oscillation of the original deformation gradient between these members of $\mathcal{G}_3$ in an attempt to lower the energy. At every level of splitting the interface plane is identified with the normal vector $\mathbf{N}$ where $\mathbf{N}$ is obtained from the minimum of determinant of acoustic tensor.

Material force method coupled with continuum–atomistics

*W*e used to think that if we knew one, we knew two, because one and one are two. We are finding that we must learn a great deal more about 'and'.

Sir Arthur Eddington,
The Harvest of a Quiet Eye (A. L. Mackay),
1977

Material forces govern the behavior and evolution of defects in solids. In hyperelastic materials these forces which are connected to the Eshelby stress tensor are especially well suited to describe the sensitivity of cracks to propagate.Thereby the question of appropriate growth criteria, i.e. how far and in which direction a crack will glide under a certain loading condition is implied by the material force. Since crack propagation begins with a variety of fundamental processes which occur within a highly localized ultra–fine volume of material that constitute the fracture process zone surrounding a crack tip where a marked deformation of the crystal lattice including the breaking of atomic bonds occur, this section is aimed at imbuing the material force method with atomistic content.

5.1   Spatial interaction forces

The notion of material forces that dates back to the works of Eshelby deals with the mechanics of defects and singularities, and is concerned with the response to variations of material placements with respect to the material manifold and represent the tendency of defects to move relative to the ambient material, as detailed in Steinmann(2000). The translation of defects on the macroscale is accompanied by significant deformation across several widely different length scales starting from the rapture of cohesive bonds at the atomic scale, see e.g. Kohlhoff et al.(1991), Friesecke et

al.(2002) Klein et al.(1998). Since continuum models basically deal with average material properties on the dominant scale, specific details of the process on the finer scales can not be emphasized. Atomistic models provide significant information down to the level of lattice and allow us to probe the detailed crystalline and defect structures, see e.g. the contribution by Lilleodden et al.(2003) and the overview by Ortiz and Philips(1999). In view of this, for the appreciation of the macro(micro)scopic process, a continuum-atomistic framework which is based on energetic formulations is proposed. To this end therefore, we recall essentials of atomistic modelling in the context of currently available approximations to the total energy and the use of empirical potentials, compare e.g. Sunyk and Steinmann(2001), Tadmor et al.(1999) and Ortiz and Phillips(1999). Thus, with the crystallite body in mind, we begin with quantitative description of the total energy

$$E^{tot} = \sum_i \sum_{j>i} \phi(r_{ij}) \tag{5.1}$$

where the inner series represents the energy contribution of individual atoms due to interaction with every other atom in the collection, see e.g. the contribution by Ortiz and Phillips(1999). The quantity $\phi(r_{ij})$ is an empirical potential, the Lennard-Jones pair-potential. The equilibrium separation denoted r_0 is attained when the repulsive core balances the attractive tail of the potential and it is plain to see that the parameter σ which is the value of the separation at which $\phi = 0$ is a function of r_0. Thus, σ is responsible for setting the length scale of interaction while the other parameter ϵ being related to the well-depth of the potential, determines the energy scale. Furthermore, the spatial interaction force between individual pairs results from the negative gradient of the potential and is given by

$$\mathfrak{f}_{ij} = -\frac{\partial E_{ij}}{\partial \boldsymbol{r}_{ij}} = -\frac{\phi'}{r_{ij}} \boldsymbol{r}_{ij} \tag{5.2}$$

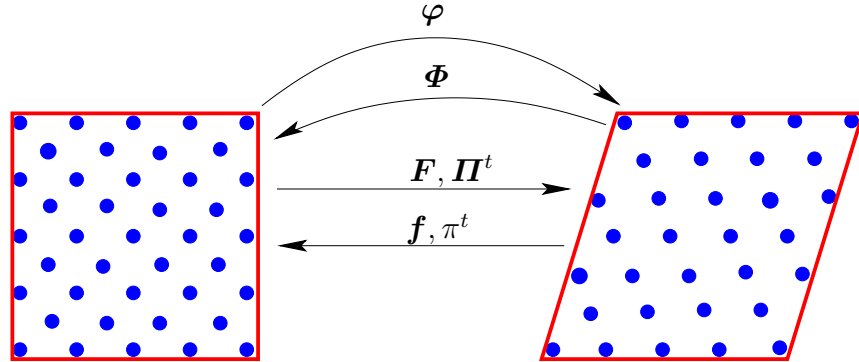## 5.2 Material and spatial motion problems

PSfrag replacements

Figure 5.1: Material motion and spatial motion

We proceed by a review of basic geometrically nonlinear kinematics of the quasistatic spatial (forward), and material (backward) motion problems, see figure 5.1. Thus, if $\mathcal{B}_0$ denotes the material

configuration occupied by a body of interest then the nonlinear deformation map φ links a material placement $\boldsymbol{X} \in \mathcal{B}_0$ to the corresponding spatial placement $\boldsymbol{x} = \varphi(\boldsymbol{X}) \in \mathcal{B}_t$ and the associated deformation gradient

$$\boldsymbol{F} = \nabla_{\boldsymbol{X}} \otimes \varphi(\boldsymbol{X}) \tag{5.3}$$

renders the spatial motion linear tangent map. Furthermore, the two-point spatial stress tensor is furnished by

$$\boldsymbol{\Pi}^t = \partial_{\boldsymbol{F}} \mathcal{W}_0 \tag{5.4}$$

with $\mathcal{W}_0$ the strain energy per unit volume in the undeformed configuration for hyperelastic material response, and the push forward of the stress tensor yields the spatial Cauchy stress $\boldsymbol{\sigma}$. Likewise, in the material motion problem $\mathcal{B}_t$ denotes the spatial configuration, $\boldsymbol{\Phi}$ is the nonlinear deformation map assigning a spatial placement $\boldsymbol{x} \in \mathcal{B}_t$ to a material placement $\boldsymbol{X} = \boldsymbol{\Phi}(\boldsymbol{x}) \in \mathcal{B}_0$ and the corresponding deformation gradient

$$\boldsymbol{f} = \nabla_{\boldsymbol{x}} \otimes \boldsymbol{\Phi}(\boldsymbol{x}) \tag{5.5}$$

leads to the material linear tangent map. The material two-point stress tensor is given by

$$\boldsymbol{\pi}^t = \partial_{\boldsymbol{f}} \mathcal{W}_t \tag{5.6}$$

and the pull back of this to the material configuration results in the well-known Eshelby (configurational) stress tensor

$$\boldsymbol{\Sigma}^t = \frac{1}{\det \boldsymbol{f}} \boldsymbol{\pi}^t \cdot \boldsymbol{f}^t \tag{5.7}$$

5.3 The Eshelby stress tensor and material interaction forces

For the description of the underlying kinematics by recourse to the Cauchy-Born rule (as explained in Ericksen(1984)) we shall relate changes in atomic positions to macroscopic deformation. In view of this, for an infinite crystal subject to homogeneous deformation, since lattice vectors are assumed to deform as would material line elements, it follows that the lattice vector $\boldsymbol{r}_{ij}$ in the spatial configuration is obtained from its counter part $\boldsymbol{R}_{ij}$ in the material configuration through the local deformation gradient $\boldsymbol{F}$ as

$$\boldsymbol{r}_{ij} = \boldsymbol{F} \cdot \boldsymbol{R}_{ij} \tag{5.8}$$

Consequently, with the assumption that the energy of each atom is uniformly distributed over the volume V_0 of its Voronoi polyhedron, the strain energy density per unit volume in the material configuration which eventually allows us to compute the energy directly from the atomistic model takes the format

$$\mathcal{W}_0 = \frac{1}{2V_0} \sum_{j \neq i} \phi(\|\boldsymbol{F} \cdot \boldsymbol{R}_{ij}\|) \tag{5.9}$$

89

and the continuum (macroscale) level spatial motion two-point stress tensor also reduces to

$$\boldsymbol{\Pi}^t = \frac{1}{2V_0} \sum_{j \neq i} \mathfrak{f}_{ji} \otimes \boldsymbol{R}_{ij}. \tag{5.10}$$

Furthermore, its push-forward results in the spatial Cauchy stress tensor which in terms of atomistic features is expressed as

$$\boldsymbol{\sigma}^t = \frac{1}{2V_t} \sum_{j \neq i} \mathfrak{f}_{ji} \otimes \boldsymbol{r}_{ij}. \tag{5.11}$$

and the material motion two-point stress tensor transforms to

$$\boldsymbol{\pi}^t = \frac{1}{2V_t} \sum_{j \neq i} [\, \phi(r_{ij}) \boldsymbol{I} - \mathfrak{F}_{ji} \otimes \boldsymbol{R}_{ij} \,] \cdot \boldsymbol{F}^t \tag{5.12}$$

where the material interaction force is given by

$$\mathfrak{F}_{ji} = \frac{\phi'}{r_{ij}} \boldsymbol{C} \cdot \boldsymbol{R}_{ij} = -\mathfrak{F}_{ij} \quad \text{with} \quad \boldsymbol{C} = \boldsymbol{F}^t \cdot \boldsymbol{F} \tag{5.13}$$

the right Cauchy–Green tensor. Ultimately,the Eshelby stress tensor is given by

$$\boldsymbol{\Sigma}^t = \frac{1}{2V_0} \sum_{j \neq i} [\, \phi(r_{ij}) \boldsymbol{I} - \mathfrak{F}_{ji} \otimes \boldsymbol{R}_{ij} \,] \tag{5.14}$$
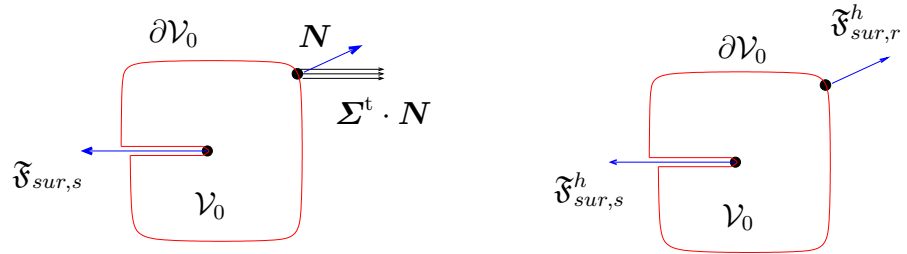
5.4   Material node-point forces

Figure 5.2: Subdomain with regular and singular boundary, material node point forces

Consider a homogeneous subdomain $\mathcal{V}_0 \subset \mathcal{B}_0$ of a continuum material body with crack which is loaded along the boundary $\partial \mathcal{V}_0$ by material surface tractions in terms of the Eshelby stress $\boldsymbol{\Sigma}^t$ with the reference normal $\boldsymbol{N}$ (see Figure 5.2). Following the definition employed by Steinmann(2000), the resultant material surface force $\mathfrak{F}_{sur}$ acting on $\mathcal{V}_0$ is given by

$$\mathfrak{F}_{sur} = \int_{\partial \mathcal{V}_0} \boldsymbol{\Sigma}^t \cdot \boldsymbol{N} \mathrm{d}A \tag{5.15}$$

Decomposing the boundary into a regular(smooth) and a singular part, with the singular part denoting a crack tip

$$\partial\mathcal{V}_0 = \partial\mathcal{V}_0^r \cup \partial\mathcal{V}_0^s \quad \text{such that} \quad \partial\mathcal{V}_0^r \cap \partial\mathcal{V}_0^s = \emptyset,$$

the material surface force on the continuum can then be given by

$$\mathfrak{F}_{sur} = \int_{\partial\mathcal{V}_0^r} \boldsymbol{\Sigma}^t \cdot \boldsymbol{N} \mathrm{d}A + \int_{\partial\mathcal{V}_0^s} \boldsymbol{\Sigma}^t \cdot \boldsymbol{N} \mathrm{d}A \tag{5.16}$$

consequently, the quasi-static equilibrium of surface forces renders

$$\int_{\partial\mathcal{V}_0^r} \boldsymbol{\Sigma}^t \cdot \boldsymbol{N} \mathrm{d}A + \int_{\partial\mathcal{V}_0^s} \boldsymbol{\Sigma}^t \cdot \boldsymbol{N} \mathrm{d}A = \boldsymbol{0} \tag{5.17}$$

and the resulting expression in the framework of continuum–atomistics is

$$\mathfrak{F}_{sur} = \frac{1}{2V_0} \sum_{j \neq i} \int_{\partial\mathcal{V}_0^r} [\, \phi(r_{ij})\boldsymbol{I} - \mathfrak{F}_{ji} \otimes \boldsymbol{R}_{ij} \,] \cdot \boldsymbol{N} \mathrm{d}A + \mathfrak{F}_{sur,s} = \boldsymbol{0} \tag{5.18}$$

where the last equality results from the statement of quasistatic equilibrium of material forces for the subdomain and the first equality is the consequence of disjoint union of the boundary. Taking into account the decomposition of $\mathcal{V}_0$ into disjoint union, the resulting material force acting on the singular boundary is given by

$$\mathfrak{F}_{sur,s} = -\frac{1}{2V_0} \sum_{j \neq i} \int_{\partial\mathcal{V}_0^r} [\, \phi(r_{ij})\boldsymbol{I} - \mathfrak{F}_{ji} \otimes \boldsymbol{R}_{ij} \,] \cdot \boldsymbol{N} \mathrm{d}A \tag{5.19}$$

Subsequently, the versatile vectorial J-integral which coincides in the limiting case with the above material force appears as

$$\mathfrak{J} = \lim_{\partial\mathcal{V}_0^r \to 0} \frac{1}{2V_0} \sum_{j \neq i} \int_{\partial\mathcal{V}_0^r} [\, \phi(r_{ij})\boldsymbol{I} - \mathfrak{F}_{ji} \otimes \boldsymbol{R}_{ij} \,] \cdot \boldsymbol{N} \mathrm{d}A = -\mathfrak{F}_{sur,s} \tag{5.20}$$

Eventually, following the standard Galerkin type discretization procedure (see Steinmann et al.(2001)) for a comprehensive overview), the discrete material node-point force is given by

$$\mathfrak{F}_{sur,K}^h = \overset{n_{el}}{\underset{e=1}{\mathsf{A}}} \{ \frac{1}{2V_0} \sum_{j \neq i} \int_{\mathcal{V}_0^e} [\, \phi(r_{ij})\boldsymbol{I} - \mathfrak{F}_{ji} \otimes \boldsymbol{R}_{ij} \,] \cdot \nabla_X N^k \mathrm{d}V \} \tag{5.21}$$

91

5.5 Numerical examples

This section offers a perspective on the applications which have been made possible by our coupled continuum atomistic model. Thus, for illustrative purposes first we present computations regarding crack extention i.e. a cracked disk in tension and a central crack in rectangular sheet under tension, next to these illustrations we present investigations concerning the evolution of morphology of an inclusion in the context of finite elements. Finally, with the intention to establish a connection between defect mechanics and constitutive microstructures, we shall consider microscopic processes and their evolution that are taking place beneath the observed macroscopic phenomenology. Evidently, one of the areas in which such observation seems to be important is the cohesive zone in front of the crack tip in which a conventional continuum mechanics statement of the boundary value problem of interest is supplemented by constitutive laws governing the decohesion. In view of this, a computation relating stress to bond stretching deformations based directly on atomistics is presented.

5.5.1 Crack extension

We consider a fracture mechanics specimen with initial crack. The stress state and the corresponding computed discrete material node point force is depicted in the adjacent figure pointing opposite to the direction of potential energy decrease i.e. in other words, it points opposite to the direction of crack growth and its magnitude is proportional to the energy release in the process of gliding.

Figure 5.3: Stress and material force

Next, we consider a center cracked fracture mechanics specimen in tension i.e. a central crack in a rectangular sheet under tension. Because of symmetry focusing only on one of the tips, the adjacent figure shows the computed discrete material node point force associated with the crack-tip on the right side. Thus, the growth of the crack is in the direction opposite to the material force, in other words, the replacement of the material position of the crack-tip node point that enlarges the crack length corresponds to a decrease of the potential energy.
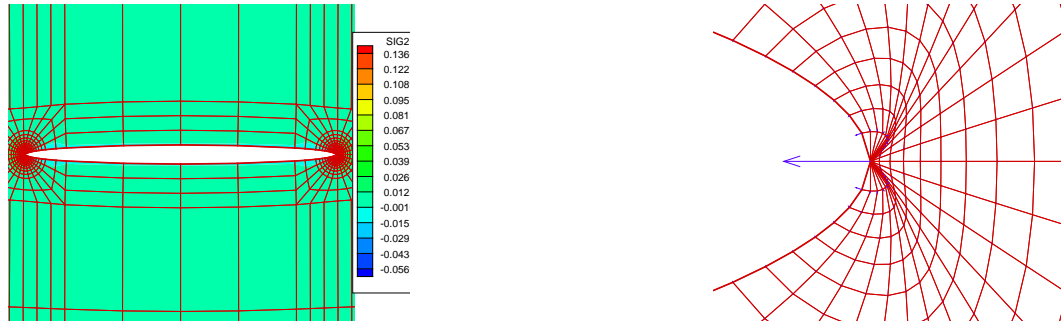
Figure 5.4: Stress depicted in the first figure and material force seen in the second figure

5.5.2 Morphology of a void

Now, we consider a specimen with a circular void in tension. Here, the computed discrete material node point forces mark the interface between the inclusion and the bulk material, furthermore, these forces point in the direction of a potential energy increase upon replacement of the material node point position. Thus, indicating the growth of the inclusion into an ellipse with major axis coinciding with the dominant discrete material forces thereby suggesting the morphological change of the specimen in the direction opposite to the material forces and hence the shape of the resulting new surface.
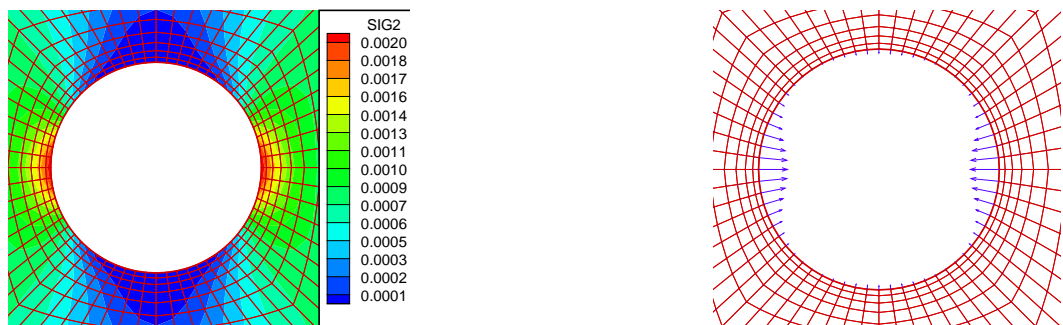

Figure 5.5: Stress depicted in the first figure and material force seen in the second figure corresponding to morphology of a void

5.5.3 Effect of length scale of interaction

As has already been mentioned, the parameters σ and ϵ of the Lennard Jones potential being connected to the length and energy scale respectively, are responsible for the nature and strength of interactions and hence determine the properties of the crystal under consideration. In what follows, the length scale is allowed to vary while the energy scale is kept fixed. Evidently, stresses are shown to be significantly elevated with the increase in length scale, that is, varying σ. But since the stress is restraining type, one can view the effect as hardening/softening of the crystal.
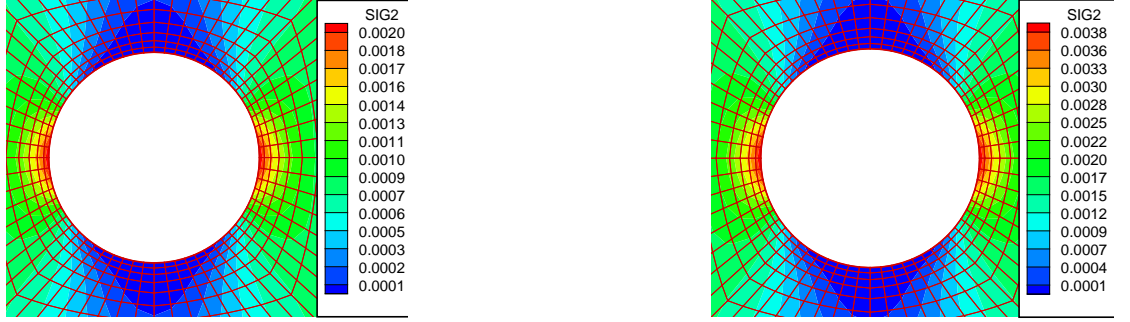

Figure 5.6: Stress corresponding to $\sigma = 0.286$ in the first figure and material force seen in the second figure corresponding to $\sigma = 0.318$

Relating the volume elements $dV_0 \subset \mathcal{B}_0$ and $dV_t \subset \mathcal{B}_t$ by appeal to the material volume ratio $J = Det\boldsymbol{F}$ and using the Piola transformation the spatial Cauchy stress is related to the Eshelby stress $\boldsymbol{\Sigma}^t$, thus affecting the integrand in the expression for Node-point forces (5.21).

The next figures show superposed material forces corresponding to the above stress comparison for crack growth and evolution of morphology of inclusion. It is revealed from the computation that the material force corresponding to higher stress has smaller magnitude compared to the one resulting from low stress state and recalling that the norm of material force is proportional to the energy release in the process of crack extension, it follows that the longer the material force the higher the energy release. To provide physical origin and render appropriate atomistic interpretation, we identify the equilibrium separation r_0 with the atomic bond length and observing that increasing σ is the same thing as enlarging such a length, it is straightforward to see that shorter bond corresponds to higher energy, which is in agreement with the fundamental theory of atomic bonds that states, shorter bonds are stronger than longer ones and hence the cost of breaking them is higher than that of the corresponding longer bond of the same atom in terms of energy.

Figure 5.7: Comparison of material force corresponding to crack extension and morphology of a void for different values of the parameter, i.e. $\sigma = 0.286 / 0.318$

Considering a cohesive zone ahead of the crack, postulating that the influence of atomic attractions is representable as a restraining stress acting on the separating surfaces and hence on the atoms, based on what is happening to the interaction forces one may investigate the nature of stress(force) when the atoms at the crack tip can be considered pulled apart, consequently out of range of their equilibrium. Thus, the next figure (figure 5.8) which depicts interaction force versus interatomic separation indicates the change(rise and fall) of force with bond length and reveals the variation of force with atomic separation.
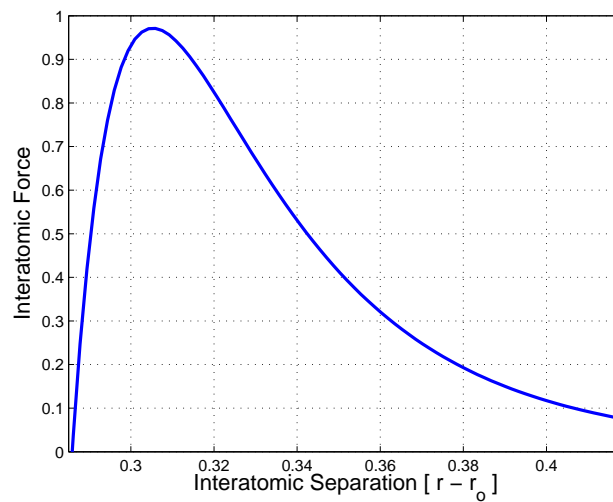

Figure 5.8: Interaction force /vs atomic separation

CHAPTER 6

Summary and Conclusions

For the truth of the conclusions of physical science, observation is the supreme Court of Appeal. It does not follow that every item which we confidently accept as physical knowledge has actually been certified by the Court; our confidence is that it would be certified by the Court if it were submitted. But it does follow that every item of physical knowledge is of a form which might be submitted to the Court. It must be such that we can specify (although it may be impracticable to carry out) an observational procedure which would decide whether it is true or not. Clearly a statement cannot be tested by observation unless it is an assertion about the results of observation. Every item of physical knowledge must therefore be an assertion of what has been or would be the result of carrying out a specified observational procedure.

Sir Arthur Eddington(1882 - 1944),
The Philosophy of Physical Science, 9–10 (1958)

The Cauchy-Born rule which serves as a bridge linking lattice to the continuum has a central place in continuum-atomistic modelling. This rule for monatomic lattice paraphrased, *all the atoms in a lattice consisting of identical atoms follow small affine deformation prescribed on the boundary*, is studied in chapter 3 in the context of lattice statics with simple shear deformation applied to a finite lattice. An elaboration of this rule as applied to a mode-I crack problem in the framework of standard Galerkin type finite elements is treated in chapter 2 whereby a homogeneous deformation $\boldsymbol{F}$ is applied to the underlying lattice at a quadrature point. The Cauchy-Born rule facilitates the incorporation of atomistic level information to the continuum which includes inheriting symmetry of the underlying lattice structure and periodicity. In this work, we reviewed a formulation of the hybrid continuum atomistic approach as based on the Cauchy–Born rule by way of substituting the phenomenological macroscopic strain energy density by the atomistic energy function emanating from direct atomistic considerations, thus, providing an overview as to how atomistics can inform

macroscopic continuum descriptions for crystalline material in the context of the mechanics of continua. In modelling material properties, nonconvex stored energy densities arise oftentimes due to either material symmetry or phase transition which inevitably leads to loss of ellipticity of the corresponding boundary value problem. If loss of ellipticity is due to symmetry, the minimizers of total energy of the continuum coincide with the natural states of the solid with different phases. Moreover, under this circumstance we can have a number of minimizers thereby violating the uniqueness of the solution in this case. On the other hand, in the event that loss of ellipticity is caused by phase transition, since during the transition process some wells associated to various phases which are usually metastable arises, the corresponding variational problem may have no solution. Physically, the nonexistence of solution is associated to microstructure formation. Which ever is the cause, i.e. be it due to symmetry or phase transition, materials energetically prefer states with minimal energy configurations and the approximation of such minimizers can be made through sequential lamination as covered in chapter 4. In this setting, in order to lower its energy a crystal adopts a mixture of phases and sequential lamination allows for separation of different phases by interfaces with suitable orientation where the requisite optimal orientation is rendered by the vector N. N is the vector normal to the interfacial plane which can be obtained from the vanishing determinant of the acoustic tensor q. Since N is associated with the equilibrium solution(minimum) it has to satisfy the stationarity equation with respect to all the variables. Thus in this regard, with the assumption of sufficient smoothness of the strain energy density function $\mathscr{W}_0$ stationarity with respect to the amplitude of the deformation jump a yields the *traction equilibrium equation*

$$\llbracket \boldsymbol{\Pi}^t \rrbracket \cdot \boldsymbol{N} = \boldsymbol{0} \tag{6.1}$$

with $\llbracket \boldsymbol{\Pi}^t \rrbracket \cdot \boldsymbol{N} =: \boldsymbol{f}(\xi, \boldsymbol{a})$ a nonlinear function of ξ and $\boldsymbol{a}$.

From a geometric standpoint, one can characterize the evolving phases beginning with the requirement of continuity across an interface. The relevant constraint often called rank-one compatibility condition rests primarily on the assumption that across the interface plane(determined by a normal N) between the phases associated to the gradients $\boldsymbol{F}_1$ and $\boldsymbol{F}_2$ whether one uses $\boldsymbol{F}_1$ or $\boldsymbol{F}_2$ to describe deformation of the points on the interfacial plane the result will be the same. Indeed, this is evident from the following observation. Since for a position vector $\boldsymbol{R}_i$ of an atom in the interface plane the contraction $\boldsymbol{N} \cdot \boldsymbol{R}_i = 0$, it follows that the contraction of the tensor $\boldsymbol{a} \otimes \boldsymbol{N}$ with $\boldsymbol{R}_i$ also gives 0. Consequently,

$$[\boldsymbol{F}_2 + \boldsymbol{a} \otimes \boldsymbol{N}] \cdot \boldsymbol{R}_i = \boldsymbol{F}_2 \cdot \boldsymbol{R}_i \tag{6.2}$$

Thus, for a deformation gradient $\boldsymbol{F}_1$ given by the expression

$$\boldsymbol{F}_1 = \boldsymbol{F}_2 + \boldsymbol{a} \otimes \boldsymbol{N} \tag{6.3}$$

we obtain

$$\boldsymbol{F}_1 \cdot \boldsymbol{R}_i = \boldsymbol{F}_2 \cdot \boldsymbol{R}_i \tag{6.4}$$

The all-important implication of the rank-one compatibility constraint is the kind of splitting plane between various phases and hence the type of twin pairs that can coexist. Supposing that a body deforms in two states specified by the deformation gradients $\boldsymbol{F}_1$ and $\boldsymbol{F}_2$, enforcing the condition of rank-one compatibility across an interface plane makes it possible to construct a continuous piecewise affine deformation consisting of a mixture of layers. In problems where various phases arise due to the underlying crystal symmetry, these gradients can be determined from the wells on the energy landscape. However, in situations such as those associated with phase transforming materials where it is not possible to construct such a deformation at ease due to local minima, the usual procedure is sequential approximation of twins until the ground state of energy is achieved. Indeed, this is the basic assumption on which sequential lamination is founded and furthermore all that one is doing with the rank-one convexification algorithm is exactly this.

The sequential lamination (rank-one convexification) algorithm which calls for rank-one compatibility constraint at each step is essentially a partial relaxing technique that provides twin deformations corresponding to metastable state each time. On top of (6.1), at each level the twins are expected to satisfy the *configurational equilibrium equation*

$$\llbracket \mathcal{W}_0 \rrbracket - \boldsymbol{a} \cdot \left\langle \boldsymbol{\Pi}^t \right\rangle \cdot \boldsymbol{N} = 0 \tag{6.5}$$

that results from the optimality condition with respect to the volume fraction ξ, where $\llbracket \mathcal{W}_0 \rrbracket$ denotes the jump in the energy density and $\left\langle \boldsymbol{\Pi}^t \right\rangle$ is the average of the stress function.

The homogeneous equations (6.1) and (6.5) constitute nonlinear systems in ξ and $\boldsymbol{a}$(the amplitude of the deformation jump). Hence, the optimal values of ξ and $\boldsymbol{a}$ are determined from these coupled system of equations iteratively. Furthermore, the computation at any level-k remembers only the most recent past, just the preceeding step and proceeding to the next step of lamination is decided based on the singularity of the acoustic tensor. However, the relative stability of the underlying structure can be judged on the basis of stress computation in the current generation of laminate, i.e. the Frobenius norm of the first Piola-Kirchhoff stress tensor can be computed and the laminate deformation is regarded as equilibrium deformation if this norm vanishes.

In chapter 5, we presented computational results of prototype examples in connection with the notion of material force applied to examination of defects at the atomic level. One of the important recognitions that stands at the foundation of this work is the process of linking the continuum and microscopic perspectives i.e. a framework that connects macroscopic response with microstructural details of a deforming crystal. Indeed, incorporation of atomistic level data so as to inform continuum descriptions of a deforming crystal for the purpose of examining defect structures is formulated and subsequent association of the insights gleaned from atomistics to assess the evolution of defects with applied deformation are emphasized through examples dealing with crack problems and evolution of morphology of a void which are typical model problems that involve multiscale systems. In all the computations an fcc type crystal is considered and the simulation is restricted to the (111)-plane.

Transformation of bases

In what follows, we shall show that lattice structure is described by a basis of lattice vectors that can be chosen in infinitely many ways. To this end, we first fix a Cartesian coordinate system with origin at one of the atoms and consider any two arbitrary bases. Thus, if we take

$$\boldsymbol{B} = \{\mathbf{a}_1, \mathbf{a}_2, \mathbf{a}_3\} \quad \text{and} \quad \hat{\boldsymbol{B}} = \{\hat{\mathbf{a}}_1, \hat{\mathbf{a}}_2, \hat{\mathbf{a}}_3\}$$

to be two distinct generators(bases) of lattice, by the hypotheses that $\boldsymbol{B}$ constitutes a basis, every member of $\hat{\boldsymbol{B}}$ can be expressed as a linear combination of elements of $\boldsymbol{B}$, and hence one can write $\hat{\boldsymbol{B}} = \boldsymbol{Q} \cdot \boldsymbol{B}$

Since $\boldsymbol{B}$ is a basis, it follows that $\boldsymbol{B}^{-1}$ exists

$$
\begin{aligned}
\text{this leads to} \quad \boldsymbol{B}^{-1} \cdot \hat{\boldsymbol{B}} &= \boldsymbol{B}^{-1} \cdot \boldsymbol{Q} \cdot \boldsymbol{B} \\
\text{consequently} \quad det(\boldsymbol{B}^{-1} \cdot \hat{\boldsymbol{B}}) &= det(\boldsymbol{B}^{-1} \cdot \boldsymbol{Q} \cdot \boldsymbol{B}) \\
&= det(\boldsymbol{B}^{-1})det(\boldsymbol{Q})det(\boldsymbol{B}) \\
&= \frac{1}{det(\boldsymbol{B})}det(\boldsymbol{Q})det(\boldsymbol{B}) \\
&= det(\boldsymbol{Q})
\end{aligned}
$$

<u>Claim !</u> $\boldsymbol{Q}$ is orthogonal
On the one hand
$\hat{\mathrm{B}} = \boldsymbol{Q} \cdot \mathrm{B}$ implies $\boldsymbol{Q} = \hat{\mathrm{B}} \cdot \mathrm{B}^t$

On the other hand

$$
\begin{aligned}
r_0^2 \boldsymbol{I} &= \hat{\mathrm{B}} \cdot \hat{\mathrm{B}}^t \\
&= \boldsymbol{Q} \cdot \mathrm{B} \cdot \mathrm{B}^t \cdot \boldsymbol{Q}^t \\
&= r_0^2 \boldsymbol{Q} \cdot \boldsymbol{Q}^t \\
\text{Hence} \quad \boldsymbol{Q} \cdot \boldsymbol{Q}^t &= \boldsymbol{I}
\end{aligned}
$$

In similar fashion

$$\boldsymbol{Q}^t \cdot \boldsymbol{Q} = \boldsymbol{I}$$

From which we get

$$\boldsymbol{Q} \cdot \boldsymbol{Q}^t = \boldsymbol{I} = \boldsymbol{Q}^t \cdot \boldsymbol{Q}$$

And hence

$$
\begin{aligned}
det(\boldsymbol{Q} \cdot \boldsymbol{Q}^T) \quad &= det(\boldsymbol{I}) = 1 \\
\text{leads to} \quad &\quad det(\boldsymbol{Q}) = \pm 1
\end{aligned}
$$

Consequently

$$det(\boldsymbol{B}^{-1} \cdot \hat{\boldsymbol{B}}) \quad = \pm 1$$

This proves that, $\boldsymbol{M} = \boldsymbol{B}^{-1} \cdot \hat{\boldsymbol{B}}$ is an isomorphism.

Showing that

$$\boldsymbol{B}^{-1} \cdot \hat{\boldsymbol{B}} \in GL(\mathbb{Z}^3)$$

Thus, $\boldsymbol{B}$ and $\hat{\boldsymbol{B}}$ generate the same lattice. In other words, the lattice is independent of the choice of basis, i.e. basis invariant.

Geometric compatibility

Phase transition in crystalline solids often leads to the development of characteristic microstructural features involving fine mixtures of phases and in some cases such feature is a plane interface that separates one homogeneous phase from another. Thus, supposing that for energetic reasons a body prefers to deform, say in two states specified by homogeneous deformation gradients $\boldsymbol{F}^+$ and $\boldsymbol{F}^-$, to make it possible to construct a continuous piecewise affine deformation consisting of layers having deformation gradients $\boldsymbol{F}^+/\boldsymbol{F}^-/\boldsymbol{F}^+/\boldsymbol{F}^-\ldots$, geometric compatibility needs to be satisfied across an interface separating regions deformed with gradients $\boldsymbol{F}^+$ and $\boldsymbol{F}^-$.
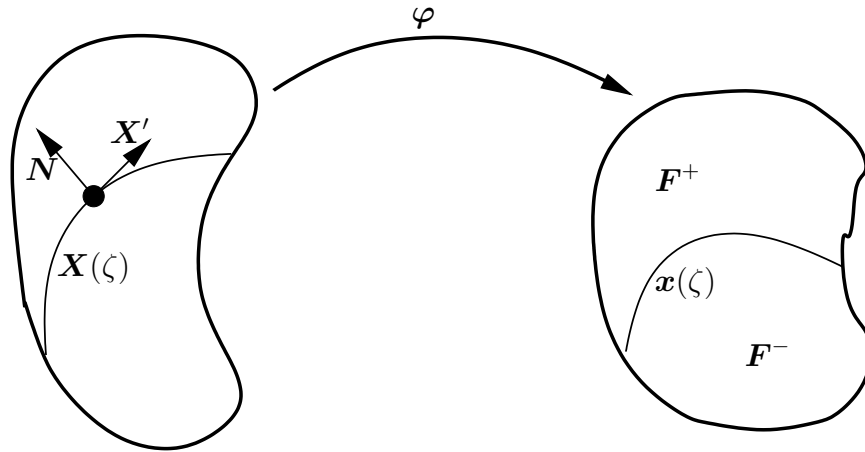

Figure B.1: Two-phase deformation

Consider a curve $\boldsymbol{X}=\boldsymbol{X}(\zeta)$ contained in the interface(surface) in the reference configuration with ζ parameterizing the curve. The image of this curve under the deformation map φ is given by

$$\boldsymbol{x} = \varphi(\boldsymbol{X}) = \varphi(\boldsymbol{X}(\zeta))$$

and a tangential vector to the curve in the current configuration is given by

$$\frac{\mathrm{d}\varphi\left(\boldsymbol{X}\left(\zeta\right)\right)}{\mathrm{d}\zeta} = \boldsymbol{F} \cdot \boldsymbol{X}'$$

where

$$\boldsymbol{X}' = \frac{d\boldsymbol{X}}{d\zeta}.$$

In order that the crystal maintain its continuity across the interface between the two transformed regions, the tangent vector $\boldsymbol{X}'$ should have one and only one image at the interface. This leads to the equality

$$\boldsymbol{F}^{+} \cdot \boldsymbol{X}' = \boldsymbol{F}^{-} \cdot \boldsymbol{X}'$$

The physical meaning of this is, whether we approach the interface(plane/surface) from the ,+' or ,-' part, when we reach there, prescription for displacing a tangent vector will be the same. This implies that

$$\left[\boldsymbol{F}^{+} - \boldsymbol{F}^{-}\right] \cdot \boldsymbol{X}' = [\![\boldsymbol{F}]\!] \cdot \boldsymbol{X}' = 0$$

Since this is true for all vectors tangent to the interface, it follows that $[\![\boldsymbol{F}]\!]$ takes the form

$$\boldsymbol{a} \otimes \boldsymbol{N}$$

where $\boldsymbol{N}$ is the unit normal conventionally pointing from the region that deforms with $\boldsymbol{F}^{-}$ to the one that deforms with $\boldsymbol{F}^{+}$ and the vector

$$\boldsymbol{a} = [\![\boldsymbol{F}]\!] \cdot \boldsymbol{N}$$

is called amplitude of the jump of the deformation gradient $\boldsymbol{F}$.

Multi-well structures of $\mathscr{W}_0$ based on Lennard Jones potential

We will show that strain energy density as a function of atomic positions can never be convex. We consider the normalized density, that is, $\mathscr{W}_0 \geq 0$.

$$
\begin{aligned}
\mathscr{W}_0(\boldsymbol{F}; \boldsymbol{R}_{ij}) \quad &= E^{int}/V = \frac{1}{2V}\sum_{j \neq i} \phi(\|\boldsymbol{r}_{ij}\|) = \frac{1}{2V}\sum_{j \neq i} \phi(\|\boldsymbol{F} \cdot \boldsymbol{R}_{ij}\|) \\
&= \frac{1}{2V}\sum_{j \neq i} 4\epsilon \left[\left(\frac{\sigma}{\|\boldsymbol{F} \cdot \boldsymbol{R}_{ij}\|} \right)^{12} - \left(\frac{\sigma}{\|\boldsymbol{F} \cdot \boldsymbol{R}_{ij}\|} \right)^{6} \right] \\
&= \frac{1}{2V}\sum_{j \neq i} 4\epsilon \left(\frac{\sigma}{\|\boldsymbol{F} \cdot \boldsymbol{R}_{ij}\|} \right)^{6} \left[\left(\frac{\sigma}{\|\boldsymbol{F} \cdot \boldsymbol{R}_{ij}\|} \right)^{6} - 1 \right] \\
&= \frac{2\epsilon}{V}\sum_{j \neq i} \frac{\sigma^6}{\|\boldsymbol{F} \cdot \boldsymbol{R}_{ij}\|^6} \left[\left(\frac{\sigma}{\|\boldsymbol{F} \cdot \boldsymbol{R}_{ij}\|} \right)^{4} + \left(\frac{\sigma}{\|\boldsymbol{F} \cdot \boldsymbol{R}_{ij}\|} \right)^{2} + 1 \right] \left[\left(\frac{\sigma}{\|\boldsymbol{F} \cdot \boldsymbol{R}_{ij}\|} \right)^{2} - 1 \right] \\
&= \frac{2\epsilon}{V}\sum_{j \neq i} \underbrace{\frac{\sigma^6}{\|\boldsymbol{F} \cdot \boldsymbol{R}_{ij}\|^6} \left[\frac{\sigma^2}{\|\boldsymbol{F} \cdot \boldsymbol{R}_{ij}\|^2} \left[\frac{\sigma^2}{\|\boldsymbol{F} \cdot \boldsymbol{R}_{ij}\|^2} + 1 \right] + 1 \right]}_{:= \, \mathscr{K}(\|\boldsymbol{F} \cdot \boldsymbol{R}_{ij}\|)} \left[\frac{\sigma^2}{\|\boldsymbol{F} \cdot \boldsymbol{R}_{ij}\|^2} - 1 \right] \\
&= \frac{2\epsilon}{V}\sum_{j \neq i} \mathscr{K}(\|\boldsymbol{F} \cdot \boldsymbol{R}_{ij}\|) \left[\left(\frac{\sigma}{\|\boldsymbol{F} \cdot \boldsymbol{R}_{ij}\|} \right)^{2} - 1 \right]
\end{aligned}
$$

Obviously, $\quad \mathscr{K}(\boldsymbol{F} \cdot \boldsymbol{R}_{ij}) > 0$ for all $\boldsymbol{F}$ and all $\boldsymbol{R}_{ij}$ and hence,

$$
\begin{aligned}
\mathscr{W}_0(\boldsymbol{F}; \boldsymbol{R}_{ij}) = 0 \quad &\Longleftrightarrow \left(\frac{\sigma}{\|\boldsymbol{F} \cdot \boldsymbol{R}_{ij}\|} \right)^{2} - 1 = 0 \\
&\Longleftrightarrow \|\boldsymbol{F} \cdot \boldsymbol{R}_{ij}\| = \sigma \\
&\Longleftrightarrow \boldsymbol{F} \cdot \boldsymbol{R}_{ij} \cdot \boldsymbol{F} \cdot \boldsymbol{R}_{ij} = \sigma^2 \\
&\Longleftrightarrow \boldsymbol{R}_{ij} \cdot \boldsymbol{F}^t \cdot \boldsymbol{F} \cdot \boldsymbol{R}_{ij} = \sigma^2 \\
&\Longleftrightarrow \boldsymbol{F}^t \cdot \boldsymbol{F} \cdot \boldsymbol{R}_{ij} = \sigma^2 \frac{\boldsymbol{R}_{ij}}{\|\boldsymbol{R}_{ij}\|^2} \\
&\Longleftrightarrow \boldsymbol{F}^t \cdot \boldsymbol{F} = \sigma^2 \frac{\boldsymbol{R}_{ij} \otimes \boldsymbol{R}_{ij}}{\|\boldsymbol{R}_{ij}\|^4}
\end{aligned}
$$

This shows that the normalized strain energy density $\mathscr{W}_0$ assumes its minimal value(which is zero in this case) for a given deformation gradient $\boldsymbol{F}$ whenever its right Cauchy-Green tensor satisfies

$$\boldsymbol{C} \;=\; \sigma^2 \frac{\boldsymbol{R}_{ij} \otimes \boldsymbol{R}_{ij}}{\|\boldsymbol{R}_{ij}\|^4}$$

From the dependence on the indices, it follows that the number of zeros in the energy landscape depends on the number of atoms that are taking part in the simulation process. Consequently $\mathscr{W}_0$ has multiple well structure.

Bibliography

[1] E. Aranda & P. Pedregal: On the computation of the Rank-One convex hull of a function, *SIAM. J. Sci. Comp.* **22**(5), 1772–1790 (2001)

[2] E. Aranda & P. Pedregal: Numerical approximation of non-homogeneous, non-convex vector variational problems, *Numer. Math.* **89**(3), 425–444 (2001)

[3] D. N. Arnold, R. Winther, : Mixed finite element for elasticity, *Numer. Math.* **92**, 401–419 (2002)

[4] M. Arroyo and T. Belytschko: An atomistic–based finite deformation membrane for single crystalline films. *J. Mech. Phys. Solids* **50**, 1941–1977 (2002).

[5] J. M. Ball : Convexity conditions and existence theorems in nonlinear elasticity, *Arch. Rat. Mech. Anal.* **63**, 337–403 (1977)

[6] J. M. Ball & R. D. James : Fine Phase Mixtures as Minimizers of Energy *Arch. Rat. Mech. Anal.* **100**, 13–52 (1987)

[7] S. Bartels, C. Carstensen, K. Hackl & U. Hoppe : Effective relaxation for microstructure simulations: algorithms and applications *Compt. Methods Appl. Mech. Engrg.* (193), 5143–5175 (2004)

[8] S. Bartels, A. Prohl: Multiscale resolution in the computation of crystalline microstructure, *Numer. Math.* **96**(4), 641-660 (2004).

[9] I. BEJU: Theorems on existence, uniqueness and stability of the solution of the place boundary-value problem, in statics, for hyperelastic materials. *Arch. Rational Mech. Anal.* **42**, 1–23 (1971)

[10] K. Bhattacharya and G. Dolzmann : Relaxed constitutive relations for phase transforming materials, *J. Mech. Phys. Solids* **48**(6/7) 1493–1517 (2000)

[11] K. Bhattacharya, B. Li, and M. Luskin : The simply laminated microstructure in martensitic crystals that undergo a cubic to orthorhombic phase transformation, *Arch. Rat. Mech. Anal.* **149**(2) 123–154 (1999)

[12] B. Brighi, M. Chipot : Approximated convex envelope of a function, *SIAM J. Numer. Anal.* **31**, 128–148 (1994)

[13] G. Bouchitté, I. Fonseca and L. Mascarenhas, "A global method for relaxation", *Arch. Rat. Mech. Anal.* **145**, 51–98 (1998)

[14] J. Bonet, R. D. Wood, Nonlinear Continuum Mechanics for Finite Element Analysis, **Cambridge**, (1997)

[15] J. Q. Broughoton, F. F. Abraham, N. Berstein and Kaxiras: Concurrent coupling of length scales: Methodology and application. *Phys. rev.* **60(4)**, 2391 (1999).

[16] B. Budiansky and J. R. Rice: Conservation laws and energy-release rates. *J. Appl. Mech.* **40**, 201–203 (1973).

[17] R.L. Burden and J. D. Faires: Numerical Analysis. **Brooks Cole**, (2005).

[18] C. Carstensen, P. Plecháč : Numerical analysis of compatible phase transitions in elastic solids. *SIAM J. Numer. Anal.* **37**(6), 2061-2081 (2000)

[19] C. Carstensen, Petr Plecháč : Numerical solution of the scalar double-well problem allowing microstructure. *Math. Comp.* **66**, 997-1026 (1997)

[20] P. Chadwick : Applications of an energy-momentum tensor in non-linear elastostatics, *J. Elas.* **5**(3–4), 249–258 (1975)

[21] M. Charlotte, L. Truskinovsky : Linear elastic chain with a hyper-pre-stress, *J. Mech. Phy. Sol.* **50** 217–251 (2002)

[22] N. Chaudhuri, S. Müller : Rank-one convexity implies quasiconvexity on certain hypersurfaces, *Pro. Roy. Soc. Edinburgh* **133A** 1263–1272 (2003)

[23] K. S. Cheung, S. Yip : Atomic-level stress in an inhomogeneous system, *J. Appl. Phys.* **70**(10), 5688–5690 (1991)

[24] M. Chipot : Numerical analysis of oscillations in nonconvex problems, *Numer. Math.* **59**, 747–767 (1991)

[25] M. Chipot : Hyperelasticity for crystals, *Euro. J. Appl. Math.* **1**, 113-129 (1990)

[26] M. Chipot, D. Kinderlehrer: Equilibrium configurations of crystals, *Arch. Rat. Mech. Anal* **103**, 237–277 (1988)

[27] J. Cormier, J. M. Rickman & T. J. Delph : Stress calculation in atomistic simulations of perfect and imperfect solids, *J. Appl. Phy.* **89**(1), 99–104 (2001)

[28] B. Dacorogna, I. Fonseca : A-B quasiconvexity and implicit partial differential equations, *Calc. Var.* **14**, 115 (2002)

[29] B. Dacorogna, I. Fonseca, J. Malý, & K. Trivisa,: Relaxation problems under constraints, *Calc. Var.* **9**, 185 (1999)

[30] B. Dacorogna : Direct Methods in the Calculus of Variations, **Springer**, (1989)

[31] B. Dacorogna : Quasiconvexity and relaxation of non convex problems in the calculus of variations, *J. Funct. Anal.* **46**, 102–118 (1982)

[32] R. Denzer, F. J. Barth and P. Steinmann: Studies in elastic fracture mechanics based on the material force method.. *Int. J. Num. Meth. Eng.* **58**, 1817–1835 (2003).

[33] A. DeSimone, G. Dolzmann : Material instabilities in nematic elastostatics, *Physica D* **136**, 175–191 (2000)

[34] A. DeSimone : Energy minimizers for large ferromagnetic bodies, *Arch. Rat. Mech. Anal.* **125**,99–143 (1993)

[35] G. Dolzmann, S. Müller : Microstructures with Finite Surface Energy: the Two-Well Problem, *Arch. Rat. Mech. Anal.* **132**, 101–141 (1995)

[36] G. Dolzmann, N. Walkington : Estimates for numerical approximations of rank-one convex envelopes, *Numer. Math.* **85**, 647–964 (2000)

[37] G. Dolzmann: Numerical computation of Rank-One convex envelopes *SIAM J. Numer. Anal.* **36**(5), 1621–1635 (1999)

[38] R. E. Dudo & J. Q. Broughton : Concurrent coupling of length scales in solid state systems, *Phys. Stat. Sol.* **217**(b), 251–291 (2000)

[39] Y. Efendiev & M. Luskin : Stability of microstructures for some martensitic transformations, *Math. Comp. Mod.* **34**, 1289–1305 (2000)

[40] J. L. Ericksen : Constitutive theory for some constrained elastic crystals, *Int. J. Solid. Struc.* **22**, 951–964 (1986)

[41] J. L. Ericksen: The Cauchy and Born Hypotheses for Crystals. *Phase Transitions and Material Instabilities in Solids*, **Academic Press**, 61–77 (1984).

[42] J. L. Ericksen: Some phase transitions in crystals, *Arch. Rat. mech. Anal.* **73** 99–124 (1980)

[43] J. D. Eshelby : The elastic energy-momentum tensor, *J. Elas.* **5**(3-4), 321–335 (1975)

[44] L. L. Fischer, G. E. Beltz : Continuum mechanics of crack blunting on the atomic scale: elastic solutions, *Modelling Simul. Mater. Sci. Eng.* **5**, 517–537 (1997)

[45] G. Francfort, C. J. Larsen : Existence and convergence for quasistatic evolution in brittle fracture, *Comm. Pure Appl. Math.* **56**(10), 1465-1500 (2003)

[46] I. Fonseca, and G. Leoni, On lower semicontinuity and relaxation, *Proc. Royal Soc. Edin.* **131** 519 (2001)

[47] I. Fonseca, S. Müller : A-quasiconvexity: a necessary and sufficient condition for lower semicontinuity under PDE constraints, *SIAM J. Math. Anal.* **30**, 1355 (1999)

[48] I. Fonseca, S. Müller, and P. Pedregal : Analysis of concentration and oscillation effects generated by gradients, *SIAM J. Math. Anal. 29* 736-756 (1998)

[49] I. Fonseca : The lower quasiconvex envelope of the stored energy function of an elastic crystal, *J. Math. Pur. Appl.*, **67**(2), 175-195 (1988)

[50] R. L. Fosdick & B. Hertog : The Maxwell relation and Eshelby's conservation law for minimizers in elasticity theory, *J. Elas.* **22**, 193–200 (1989)

[51] D. A. French : On the convergence of finite-element approximations of a relaxed variational problem, *SIAM J. Numer. Anal. 27*, 419–436 (1990)

[52] G. Friesecke and F. Theil: Validity and Failure of the Cauchy-Born Hypothesis in a Two-Dimensional Mass-Spring Lattice. *J. Nonlinear Sci.* **12**, 445–478 (2002)

[53] G. Friesecke, R. James : A scheme for the passage from atomistic to continuum theory for thin films, nanotubes and nanorods, *J. Mech. Phy. Sol.* **48**, 1519–1540 (2000)

[54] E. Fried, M.E. Gurtin : Coherent solid-state phase transitions with atomic diffusion: a thermo-mechanical treatment, *J. Statist. Phys.* **95**, 1361 (1999)

[55] N. M. Ghoniem, E. P. Busso, N. Kioussis & H. Huang : Multiscale modelling of nanomechanics and micromechanics.An overview, *Phil. Mag.* **83**(31-34), 3475–3528 (2003)

[56] M. K. Gobbert, A. Prohl : A discontinuous finite element method for solving a multiwell problem, *SIAM J. Numer. Anal.* **37**(1), 246–268 (1999)

[57] S. Grabowski, K. Kadau & P. Entel : Atomistic modelling of Diffusion in aluminum, *Phase Trans.* **75**(1-2), 265–272 (2002)

[58] M. E. Gurtin : Two-phase deformations of elastic solids, *Arch. Rat. Mech. Anal.* **84**, 1–29 (1983)

[59] M. E. Gurtin: On the nature of configurational forces. *Arch. Rot. Mech. Anal.* **131**, 67–100 (1995).

[60] M. E. Gurtin and P. Podio-Guidugli: Configurational forces and a constitutive theory for crack propagation that allows for curving and kinking. *J. Mech. Phys. Solids* **46**, 1343–1378 (1998).

[61] N.G. Hadjiconstantinou : Hybrid atomistic-continuum formulations and the moving contact-line problem. *J. Comp. Phys.* **154** 245-265, (1999)

[62] G. T. Hahn and A. R. Rosenfield: Local yielding and extension of a crack under plane stress. *Acta Met.* **13**, 293–306 (1965)

[63] F. Herman, S. Skillman : Atomic Structure Calculations, **Princeton-Hill**, (1963)

[64] K. Kadau, P. Entel : Atomistic Investigations of the Thermodynamical Stability and Martensitic Nucleation of Fe80Ni20 Nanoparticles *Phase Transitions* **75**(1-2), 59-65 (2002)

[65] K. Kadau and P. Entel : Atomistic study of the structural transformation in thin iron films on copper, *J. Magn. Magn. Mater.* **531**, 198-199 (1999)

[66] R. Kienzler, G. Herrmann : On Material Forces in Elementary Beam Theory, *J. Appl. Mech.* **53**, 561–564 (1986)

[67] P. Klein and H. Gao: Crack nucleation and growth as strain localization in a virtual internal bond continuum. *J. Eng. Frac. Mech.* **61**, 21–48 (1998).

[68] J. Knap and M. Ortiz: An analysis of the quasicontinuum method. *J. Mech. Phys. Solids* **49**, 1899–1923 (2001).

[69] J. K. Knowles & E. Sternberg : On the failure of ellipticity and the emergence of discontinuous deformation gradients in plane finite elastostatics, *J. Elas.* **8**, 329–379 (1978)

[70] S. Kohlhoff, P. Gumbsch and H.F. Fischmeister: Crack propagation in bcc crystals studied with a combined finite-element and atomistic model. *Phil. Mag.* **64**, 851–878 (1991).

[71] R.V. Kohn: The Relaxation of a double-well energy, *Contin. Mech. Thermodyn.* **3**, 193–236 (1991).

[72] R.V. Kohn, G. Strang : Optimal design and relaxation of a variational problem I, II, III. *Communications on Pure and Applied Mathematics* **39**, 113–137, 139–182, 353–377 (1986).

[73] R.V. Kohn: Explicit relaxation of a variational problem in optimal design. *Bulletin of the American Mathematical Society* **9**, 211–214 (1983).

[74] V. Kouznetsova, M. G. D. Grees :Multi-scale constitutive modelling of heterogeneous materials with a gradient-enhanced computational homogenization scheme, *Int. J. Numer. Meth. Engng.* **54**(8), 1235–1260 (2002)

[75] M. Kružík, M. Luskin : The Computation of Martensitic Microstructure with Piecewise Laminate, *J. Sci. Comp.* **19**(1-3), 293–308 (2003)

[76] M. Lambrecht, C. Miehe & J. Dettmar : Energy relaxation for non-convex incremental stress potentials in a strain-softening elastic-plastic bar, *Int. J. Sol. Str.* **35**, 3859–3897 (1998)

[77] B. Li : Approximation of martensitic microstructure with general homogeneous boundary data, *J. Math. Anal. Appl.* **266** 451-467 (2002)

[78] B. Li and M. Luskin : Finite element analysis of microstructure for the cubic to tetragonal transformation, *SIAM J. Numer. Anal.* **35**(1) 376-392 (1998)

[79] T. Liebe, R. Denzer and P. Steinmann: Application of the material force method to isotropic continuum damage. *Comp. Mech.* **30**, 171–184 (2003)

[80] E. T. Lilleodden, J. A. Zimmermann, S. M. Foiles and W. D. Nix: Atomistic simulations of elastic deformation and dislocation nucleation during nanoindentation. *J. Mech. Phys. Solids* **51**, 901–920 (2003).

[81] M. Luskin: On the computation of crystalline microstructure, *Act. Numerica* **5**, 191–258 (1996).

[82] M. Luskin: Approximation of laminated microstructure for rotationally invariant double well energy density, *Num. Math.* **75**, 2051–221 (1997).

[83] J. Marsden, T. Hughes : Mathematical Foundations of Elasticity, **Dover**, (1994)

[84] GA. Maugin: Material forces, concepts and applications. *Appl. Mech. Rev.* **48**, 213–245 (1995).

[85] GA. Maugin: Material Inhomogeneities in Elasticity. **Chapman & Hall**, (1993)

[86] C. Miehe, M. Lambrecht, E. Gürses :Analysis of material instabilities in inelastic solids by incremental energy minimization and relaxation methods: evolving deformation microstructures in finite plasticity", *J. Mech. Phys. Solids* **52**, 2725-2769 (2004).

[87] C. Miehe, M. Lambrecht : Analysis of microstructure development in shearbands by energy relaxation of incremental stress potentials: Large-strain theory for standard dissipative solids *int. J. Numer. Meth. Engng.* **58**, 1–41 (2003)

[88] C. Miehe , M. Lambrecht : "A Two-Scale Finite Element Relaxation Analysis of Shear Bands in Non-Convex Inelastic Solids: Small-Strain Theory for Standard Dissipative Materials", *Com. Meth. Appl. Mech. Engng.* (192), 473-508 (2003).

[89] J. A. Moriarty : Atomistic simulation of thermodynamic and mechanical properties of metals, *J. Comp. Matt. Desi.* **5** 109–129 (1998)

[90] C. B. Morrey: Quasiconvexity and the lower semicontinuity of multiple integrals, *Pacific J. Math.* **2**, 25–53 (1952)

[91] C. B. Morrey: Multiple integrals in the calculus of variations. **Springer**, (1966)

[92] R. Müller and G. A. Maugin: On material forces and finite element discretization. *J. Comp. Mech.* **29**, 52–60 (2002).

[93] S. Müller: Variational models for microstructure and phase transitions. In Calculus of Variations and Geometric Evolution problems. **Springer**, (1998).

[94] S. Müller, V. Šverák : Convex integration for Lipschitz mappings and counterexamples to regularity, *Ann. Math.* **157**, 715–742 (2003)

[95] P.-O. Nerbrant, B. Roos & A. J. Sadlej: First-order properties and the Hellmann-Feynman theorem in the case of a limited CI wave function *Int.J.Quant.Chem.* **15**(2), 135–145 (2004).

[96] O. H. Nielsen & Richard M. Martin: First Principles Calculation of Stress. *Phy. Rev. Let.* **50**(9), 697–700 (1983).

[97] O. H. Nielsen & Richard M. Martin: Quantum-mechanical theory of stress and force. *Phy. Rev. B* **32**(6), 3780–3791 (1985).

[98] J.T. Oden: Approximations and numerical analysis of finite deformations of elastic solids, in "Nonlinear Elasticity" **Academic press**, (1973)

[99] R. W. Ogden : Non-Linear Elastic Deformations, **Willey**, (1984)

[100] D.L. Olmsted, L. G. Hector, W.A. Curtin, R.J. Clifton, : Atomistic simulations of dislocation mobility in Aluminum, Nickel, and Al/Mg Alloys, *Modelling Simul. Mater. Sci. Eng.* **13**, 371-388 (2005)

[101] M. Ortiz and R. Philips: Nanomechanics of defects in solids. *Adv. Appl. Mech.* **36**, 1–79 (1999).

[102] M. Ortiz, E. A. Repetto & L. Stainier: A theory of subgradient dislocation structures *J. Mech. Phy. Solids* **48**, 2077–2114 (2000)

[103] M. Ortiz : Microcrack Coalescence and Macroscopic Crack-Growth Initiation in Brittle Solids, *Int. J. Solids Str.* **36**(4), 231–250 (1988)

[104] P. Pedregal : On the numerical analysis of nonconvex variational problems, *Numer. Math.* **74**, 325–336 (1996).

[105] P. Pedregal: Laminate and microstructure *E. J. Appl. Math.* **4**, 121–149 (1993)

[106] R. Phillips: Crystals, Defects and Microstructures **Cambridge**, (2001)

[107] R. Phillips, M. Dittrich, & K. Schulten : Quasicontinuum representations of atomic-scale mechanics: From proteins to dislocations, *Ann. Rev. Mater. Res.* **32**, 219-233 (2002)

[108] M. J. Puska, R. M. Nieminen & M. Manninen : Atoms embedded in an electron gas, *Phy. Rev.* **24**(B), 3037 (1981).

[109] H. Rafii-Tabar, L. Hua & M. Gross : A multi-scale atomistic-continuum modelling of crack propagation in a two-dimensional macroscopic plate, *J. Phys. Cond. Matt.* **10**, 2375-2387 (1998).

[110] J: R. Rice : A Path Independent Integral and the Approximation Analysis of Strain Concentration by Notches and Cracks, *J. Appl. Mech.* **35** 379–386 (1968).

[111] R.T. Rockafellar: Convex Analysis, *Princeton University: Princeton, NJ*, (1970)

[112] T. Roubícek : Numerical approximation of relaxed variational problems, *J. Conv. Anal.* **3**, 329–347 (1996).

[113] R. E. Rudd, J. Q. Broughton : Concurrent Coupling of Length Scales in Solid State Systems *Phys. Stat. Sol.* **217**(b) 251–291 (2000)

[114] V. B. Shenoy, R. Miller, E. B. Tadmor, D. Rodney, R. Philips & M. Ortiz : An adaptive finite element approach to atomistic-scale mechanics-the quasicontinuum method, *J. Mech. Phy. Sol.* **47** 373–642 (1999)

111

[115] J. Y. Shu, W. E. King & N. A. Fleck : Finite elements for materials with strain gradient effects, *Int. J. Numer. Meth. Engng.* **44** 373–391 (1999)

[116] M. Šilhavý: The Mechanics and Thermodynamics of Continuous Media. **Springer**, (1997)

[117] R. S. Sorbello and Baab B. Dasgupta; Force on an atom in an electric field: Feynman-Hellmann theorem and oscillator strengths *Phy. Rev. B* **21**(6), 2196–2200 (1980).

[118] P. Steinmann: Application of material forces to hyperelastic fracture mechanics. I. continuum mechanical setting. *Int. J. Solids* **37**, 7371–7391 (2000).

[119] P. Steinmann, D. Ackermann and F.J. Barth: Application of material forces to hyperelastic fracture mechanics. Part II: Computational setting. *Int. J. Solids and Structures* **38**, 5509–5526 (2001).

[120] R. Sunyk and P. Steinmann: Localization Analysis of Mixed Continuum-Atomistic Models. *J. Phys. IV France* 2001, **11**: 251–258.

[121] R. Sunyk and P. Steinmann: On higher gradients in continuum–atomistic modelling. *Int. J. Solids and Structures* **40**, 6877–6896 (2003).

[122] V. Šverák : Rank-one convexity does not imply quasi-convexity. *Proc. R. Soc. Edinb.* **120**(A), 185–189 (1992)

[123] E. B. Tadmor, G. S. Smith, N. Bernstein and E. Kaxiras: Mixed finite element and atomistic formulation for complex crystals. *Phy. Rev.* **59**, 235–245 (1999).

[124] E. B. Tadmor, M. Ortiz & R. Philips : Quasicontinuum analysis of defects in solids, *Phil. Mag. A* **73**(6), 1529–1563 (1996)

[125] C. Trimarco, GA. Maugin: Pseudomomentum and material forces in nonlinear elasticity, variational formulations and application to brittle fracture. *Act. Mech.* **94**, 1–28 (1992)

[126] G. Zanzotto : The cauchy-born hypothesis, nonlinear elasticity and mechanical twining in crystals, *Act. Cryst.* **52**(A), 839–849 (1996).

[127] J. A. Zimmermann, E. B. Webb III, J. J. Hoyt, R. E. Jones, P. A. Klein & D. J. Bammann : Calculation of stress in atomistc simulation, *Modelling Simul. Mater. Sci. Eng.* **12**, 319–332 (2004)

[128] P. Zhang, P. Klein, Y. Huang, H. Gao and P. D. Wu: Numerical simulation of cohesive fracture by the virtual internal bond method. *Comp. Mod. Eng. Sci.* **3**, 263–278 (2002).

CURRICULUM   VITAE

Name:-   Tadesse Abdi
Gender:-   Male
Nationality:-   Ethiopian
Date of Birth:-   26. Sept. 1967
Place of Birth:-   Shewa, Ethiopia

Educ. Institution	Year	Award
1. Addis Ababa University	1983 - 1987	B.Sc., Mathematics
2. Addis Ababa University	1994 - 1996	M.Sc., Mathematics
3. University of Kaiserslautern	2000 - 2002	M.Sc.nat.,Industrial Mathematics

Since 01.10.2002 Ph.D. student at the   Chair of Applied Mechanics
(Prof. Dr.-Ing. Paul Steinmann)
University of Kaiserslautern